

UNIVERSITAT POLITÈCNICA DE VALÈNCIA
DEPARTAMENTO DE MÁQUINAS Y MOTORES TÉRMICOS



UNIVERSITAT
POLITÈCNICA
DE VALÈNCIA

**ASSESSMENT AND OPTIMIZATION OF FRICTION
LOSSES AND MECHANICAL EFFICIENCY IN
INTERNAL COMBUSTION ENGINES**

DOCTORAL THESIS

PhD Candidate:

Mr. Antonio José Jiménez Reyes

Directed by:

Dr. Bernardo Tormos Martínez

Valencia, September 2022

DOCTORAL THESIS

ASSESSMENT AND OPTIMIZATION OF FRICTION LOSSES AND MECHANICAL EFFICIENCY IN INTERNAL COMBUSTION ENGINES

Presented by: Antonio José Jiménez Reyes

Directed by: Dr. Bernardo Tormos Martínez

Comittee:

President: Dr. José M. Desantes

Secretary: Dr. Francisco J. Jiménez-Espadafor

Vocal: Dr. Hannes Allmaier

External Evaluators:

Reviewer 1: Dr. Robert I. Taylor

Reviewer 2: Dr. Izabel F. Machado

Reviewer 3: Dr. Hannes Allmaier

Valencia, September 2022

Resumen.

En la actualidad, el ámbito del transporte mediante el uso de vehículo ligero sufre un gran cambio hacia la descarbonización. Cada vez más, las autoridades europeas restringen las emisiones de gases de efectos invernaderos hacia la atmósfera emitidos por estos vehículos. Soluciones alternativas a la propulsión con energía fósil, como la implementación de vehículos eléctricos o híbridos, no está lo suficientemente desarrollada para sustituir a los motores de combustión interna alternativos (MCIA), debido a su todavía alto coste de producción y baja infraestructura para abastecer la demanda de energía eléctrica.

En este contexto, la transición hacia una movilidad sostenible y renovable sigue pasando por el aumento de la eficiencia y la reducción del consumo de combustible en motores de combustión interna. Una alternativa a la mejora de la eficiencia es la reducción de las pérdidas mecánicas por fricción, o en otras palabras, optimización de la tribología. La tribología en un MCIA lleva asociada aspectos mecánicos como la optimización de los acabados superficiales de los distintos componentes que conforman el motor y la optimización de propiedades física, químicas y reológicas del aceite que lo compone. Esta última solución presenta un alto ratio beneficio/coste, ya que su implementación no lleva asociada ninguna modificación en el hardware y su implementación es directa.

Uno de los objetivos de la Tesis Doctoral, es desarrollar un modelo 1D que contenga la información tribológica de un motor de combustión interna que no se puede obtener experimentalmente, que contribuya al entendimiento y optimización de las pérdidas mecánicas por fricción y que ahorre el coste experimental asociado a entender la tribología desde el punto de vista empírico. Estos parámetros van desde el espesor de película de aceite entre los componentes de un par rozante hasta la contribución a la fricción de las componentes hidrodinámicas y de asperezas de cada elemento rozante. Además, se ha desarrollado un modelo cuasi estacionario para cuantificar la energía disipada por fricción en un ciclo de conducción real y el consumo de combustible asociado al mismo.

Así pues, a través de este modelo, se implementan soluciones que pasan desde aceites optimizados reológicamente hasta acabados superficiales de baja rugosidad, entendiendo la fenomenología asociada a cada tecnología y aportando parámetros claves para la optimización de dicha solución. Finalmente, se estima el ahorro en términos de consumo de combustible que se puede alcanzar con estas soluciones implementadas mediante el modelo cuasi estacionario en condiciones de conducción real.

Resum.

Actualment, l'àmbit del transport mitjançant l'ús de vehicles lleugers pateix un gran canvi cap a la descarbonització. Cada vegada més, les autoritats europees restringeixen les emissions de gasos d'efecte hivernacle cap a l'atmosfera emesos per aquests vehicles. Les solucions alternatives a la propulsió amb energia fòssil, com la implementació de vehicles elèctrics o híbrids, no està prou desenvolupada per substituir els motors de combustió interna alternatius (MCIA), a causa del seu encara alt cost de producció i baixa infraestructura per abastir la demanda d'energia elèctrica.

En aquest context, la transició cap a una mobilitat sostenible i renovable continua passant per l'augment de l'eficiència i la reducció del consum de combustible en motors de combustió interna. Una alternativa per a la millora de l'eficiència és la reducció de les pèrdues mecàniques per fricció, o en altres paraules, la optimització del comportament tribològic del motor. La tribologia en un MCIA porta associada aspectes mecànics com ara l'optimització dels acabats superficials dels diferents components que conformen el motor i l'optimització de propietats física, químiques i reològiques de l'oli que va a emprar. Aquesta última solució presenta una alta ràtio benefici/cost, ja que la seva implementació no porta associada cap modificació de la màquina i la seva implementació és directa.

Un dels objectius de la Tesi Doctoral és desenvolupar un model 1D que permet obtindre la informació tribològica d'un motor de combustió interna que no es pot obtenir experimentalment, que contribueixi a l'enteniment i l'optimització de les pèrdues mecàniques per fricció i que estalviï el cost experimental associat a entendre la tribologia des del punt de vista empíric. Aquests paràmetres van des de l'espessor de pel·lícula d'oli entre els components d'un parell tribològic fins a la contribució a la fricció dels components amb regim hidrodinàmic i de la rugositat de cada element. A més, s'ha desenvolupat un model gairebé estacionari per quantificar l'energia dissipada per fricció en un cicle de conducció real i el consum de combustible associat.

Així, a través d'aquest model, s'implementen solucions que passen des d'olis optimitzats reològicament fins a acabats superficials de baixa rugositat, entenent la fenomenologia associada a cada tecnologia i aportant paràmetres clau per optimitzar aquesta solució. Finalment, s'estima l'estalvi en termes de consum de combustible que es pot assolir amb aquestes solucions implementades mitjançant el model quasi estacionari en condicions de conducció real.

Abstract.

Currently, the field of light-duty vehicle transport is undergoing a major shift towards decarbonisation. Increasingly, European authorities are restricting emissions of greenhouse gases into the atmosphere from these vehicles. Alternative solutions to fossil fuel propulsion, such as the implementation of electric or hybrid vehicles, are not sufficiently developed to replace internal combustion engine alternatives (ICEs), due to their still high production cost and low infrastructure to meet the demand for electric power.

In this context, the transition towards sustainable and renewable mobility continues to be based on increasing efficiency and reducing fuel consumption in internal combustion engines. An alternative to improving efficiency is the reduction of mechanical frictional losses, or in other words, optimisation of tribology. Tribology in an MCI is associated with mechanical aspects such as the optimisation of the surface finishes of the different components that make up the engine and the optimisation of the physical, chemical and rheological properties of the oil that makes up the engine. This last solution presents a high benefit/cost ratio, as its implementation does not involve any hardware modification and its implementation is straightforward.

One of the objectives of the Doctoral Thesis is to develop a 1D model that contains the tribological information of an internal combustion engine that cannot be obtained experimentally, which contributes to the understanding and optimisation of mechanical friction losses and saves the experimental cost associated with understanding tribology from an empirical point of view. These parameters range from the oil film thickness between two tribological components to the contribution to friction of the hydrodynamic and roughness components of each friction element. In addition, a quasi-stationary model has been developed to quantify the energy dissipated by friction in a real driving cycle and the associated fuel consumption.

Thus, through this model, solutions ranging from rheologically optimised oils to low roughness surface finishes are implemented, understanding the phenomenology associated with each technology and providing key parameters for the optimisation of the solution. Finally, the savings in terms of fuel consumption that can be achieved with these solutions implemented using the quasi-stationary model in real driving conditions are estimated.

*“Cuanto más sé, más sé que no sé,
y cuanto más sé que no sé, más
incertidumbre me crea.”*

Agradecimientos

Y llegó el día. Podría añadir un capítulo más a esta tesis doctoral agradeciendo a todos y a cada una de las personas que aportaron, directa o indirectamente, a la consecución de este documento. Comencemos por el principio.

Gracias Francisco Payri por aquella llamada telefónica y la oportunidad de venir aquí por primera vez allá por el año 2016. Gracias José María Desantes por la segunda bienvenida un año más tarde. A Vicente Macián, porque todo comenzó en Fundamento en Ingeniería del Mantenimiento, siguió con innumerables correcciones de informes de resultado y acabó siendo ratos de desconexión dónde hablábamos de karting, slot, rutas de todoterreno y un sinfín de batallas. A Bernardo Tormos, por apostar, por tener paciencia y por defender las, a veces, propuestas locas que se me iban ocurriendo durante estos cuatro años.

Me gustaría agradecer al programa de Formación de Profesorado Universitario del Ministerio de Ciencia, Innovación y Universidades por soportar financieramente mis estudios doctorales (FPU18/02116) y la estancia de investigación que contribuyó a aumentar los conocimientos desarrollados en la presente tesis doctoral (EST21/00451).

A mis compañeros de línea (o en su defecto, batalla), por las risas, noches en vela, discusión de resultados, comidas juntos... Toni, Sophia, Becario, Jorge, Norma, Xavi, Mariajo, gracias. A los que compartimos edificio y no pasaron de largo.... Bare, Diego, Alba, María, Felipe, Santi, Cassio... Al que además, comparto momentos fuera y nos sigue uniendo una amistad, Iván. Mención aparte al “Sheriff”, por su sentido del humor, su compañerismo y por sus innumerables soluciones a problemas cotidianos, si solo trabajaran 1/4 de lo que él...

A Mariajo, Alex y Paola. Porque en el comienzo de esta historia, me hicieron sentir como un hijo, gran amigo y mejor pareja del mundo.

Família Tomanik, minha experiência no Brasil começou com vocês. Márcia, 1000 vezes obrigado por sua acolhida, seu sorriso, sua alegria e sua preocupação. Victor, porque com você os dias de trabalho passaram para segundo plano e os melhores momentos ficaram conosco. A Roberto Martins por sua acolhida na LFS e paciência. A Francisco Profito por sua constante disposição em ajudar. A todos e a cada um que conheci nessa experiência louca, viajando de Iguazú até o Ríó, compartilhando hobbies, sonhos e me ensinando toda a experiência que é o Brasil. Fa, com você eu vivi um dos meses mais loucos que eu já me lembro, e foi apenas no final. Muito obrigado

por sua loucura e alegria, sua maneira de viver e sua maneira de ver o mundo. E o Dr. Tomanik. Todos têm pelo menos um mentor na vida a quem admiram, respeitam e escutam. Sempre direi que a experiência com você foi como o serviço militar, mas as horas de trabalho duro valeram a pena. Graças a você, conheci as exigências, a dedicação e a perfeição no trabalho, mas também, sua maneira de ver a vida mudou a minha. Nunca terei palavras suficientes para agradecer por toda essa experiência juntos.

A la familia que se escoge y dejan el estrés en un segundo plano... Isma, Juanje, Irene, Ana, Javi, Andrea, Edith... Al hermano que toda persona querría tener a su lado en cualquier situación y momento, Adri.

Y por último, a los tres seres que mostraron su apoyo incondicional en todas y cada una de las decisiones que fui tomando en este camino. Papá, Mamá y Ade. Nos vemos en la siguiente batalla.

Table of Contents

1	Introduction	1
1.1	Overview: background and context.....	3
1.1.1	Energy Consumption in Transportation	4
1.1.2	Energy consumption in passenger cars	7
1.1.3	Mechanical losses in ICE	8
1.1.4	Modeling friction losses in ICE	9
1.2	Objectives of the thesis	10
1.2.1	Validate a steady-state friction model	10
1.2.2	Validate a transients friction model	11
1.2.3	Assessment of performance of different Low Viscosity Engine Oils in model validated	11
1.2.4	Evaluation of different cylinder surfaces in the model validated	11
1.3	Thesis document structure	12
1.4	Thesis publications	13
	Bibliography	14
2	Literature Review: Friction losses in ICE	17
2.1	Introduction	19
2.2	Lubrication in ICE	21
2.2.1	General lubrication theory	21

2.2.2	Hydrodynamic lubrication	22
2.2.3	Elastohydrodynamic lubrication	24
2.2.4	Mixed lubrication	24
2.2.5	Boundary lubrication	25
2.2.6	Engine oil properties	26
2.2.6.1	Introduction	26
2.2.6.2	Viscosity	28
2.2.6.3	Effect of temperature on viscosity	29
2.2.6.4	Effect of pressure on viscosity	30
2.2.6.5	Effect of shear rate on viscosity	31
2.2.6.6	Viscosity index	32
2.3	Mechanical losses in ICE	33
2.3.1	Piston assembly	33
2.3.1.1	Piston rings	34
2.3.1.2	Piston skirt	36
2.3.2	Crankshaft	37
2.3.2.1	Journal bearings	37
2.3.2.2	Con-rod bearings	38
2.3.3	Valvetrain	39
2.4	Numerical models applied to assess the friction in ICE	41
2.4.1	Piston-ring assembly	41
2.4.1.1	Classical Reynolds Equation and Stochastic Asperity Contact Models	42
2.4.1.2	Average Reynolds Equation (Patir and Cheng's average flow model)	43
2.4.1.3	Deterministic method - Quasistatic approximation	44
2.4.1.4	Deterministic method - Full approximation	45
2.4.1.5	Other piston ring model considerations	45

2.4.2	Piston-skirt	47
2.4.3	Bearings	48
2.4.3.1	Impedance Approach	48
2.4.3.2	Mobility Approach	49
2.4.3.3	Reynolds equation	49
2.4.4	Valvetrain	50
	Bibliography	52
3	Experimental tools and theoretical model	61
3.1	Introduction	63
3.2	Experimental tools	63
3.2.1	Steady state: Engine and test cell characteristics	63
3.2.2	Transient state: Vehicle and test cell characteristics	66
3.3	Engine friction: steady state theoretical models	68
3.3.1	Piston-ring model	68
3.3.1.1	Gas pressure force: blow-by model	70
3.3.1.2	Ring tension force	72
3.3.1.3	Piston assembly temperature	72
3.3.1.4	Hydrodynamic friction force	74
3.3.1.5	Asperity friction force	76
3.3.1.6	Coefficient of friction measurement	77
3.3.2	Piston skirt model	81
3.3.3	Bearings	82
3.3.3.1	Mobility method	83
3.3.3.2	Reynolds equation	84
3.3.4	Valvetrain	85
3.3.5	Auxiliaries	87
3.3.5.1	Coolant pump	87
3.3.5.2	Oil pump power	88

3.3.5.3	Fuel pump power	89
3.4	Engine friction: transient theoretical model	90
	Bibliography	93
4	Model results	95
4.1	Introduction	97
4.2	Steady-state model	97
4.2.1	Methodology and boundary conditions	97
4.2.2	Global results	100
4.2.3	Piston-ring assembly	103
4.2.4	Piston skirt	107
4.2.5	Bearings	109
4.2.5.1	Connecting rod bearing	110
4.2.5.2	Journal bearing	112
4.2.6	Camshaft	114
4.3	Transient model	117
4.3.1	Introduction	117
4.3.2	Methodology	117
4.3.3	Results and model validation	118
4.3.3.1	Model validation: Drive cycle fuel consumption	118
4.3.3.2	Mechanical losses and its distribution during driving cycles	124
4.4	Conclusions	132
	Bibliography	133
5	Optimization of friction losses in ICE	135
5.1	Introduction	137
5.2	Friction reduction from the point of view of lubricant ...	137
5.2.1	Lubricant matrix	137

5.2.2	Results: Total engine friction	139
5.2.3	Results: Piston-ring and skirt assembly	141
5.2.4	Results: Engine bearings	144
5.2.5	Results: camshaft	146
5.2.6	Results: Evaluation of the engine oils in a WLTC cycle	149
5.2.6.1	Methodology	149
5.2.6.2	Main cycle characteristics	151
5.2.6.3	Fuel savings produced	152
5.2.6.4	Results: Total energy balance	155
5.3	Friction reduction from the point of view of surface finishing	157
5.3.1	Boundary conditions	158
5.3.2	Simulation results	158
5.3.2.1	Piston rings	158
5.3.2.2	Piston skirt	160
5.3.2.3	Journal bearings	161
5.3.2.4	Camshaft	163
5.3.2.5	Friction saving in the engine	165
5.4	Conclusions	168
	Bibliography	170
6	Conclusions and future works	171
6.1	Introduction	173
6.2	Conclusions	173
6.3	Future works	175
	Bibliography	177

Index of Figures

- 1.1 World total final consumption by sector [10] 5
- 1.2 Energy used in transport scenarios [12] 5
- 1.3 World Greenhouse Gas Emissions in 2016 [13]. 6
- 1.4 Energy consumption in heavy-duty applications [14].... 7

- 2.1 Mechanical losses distribution in light-duty vehicle [15]. 20
- 2.2 Sliding and rolling friction..... 22
- 2.3 Schematic of a Stribeck curve. Source: [17] 23
- 2.4 Hertz Contact pressure vs. Elastohydrodynamic pressure 25
- 2.5 Schematic definition of viscosity 28
- 2.6 Variation of viscosity with pressure. Source: [46] 31
- 2.7 Variation of viscosity with shear rate. 32
- 2.8 ICE Mechanical losses distribution. 33
- 2.9 Piston rings scheme. Source: [57] 34
- 2.10 Piston rings friction forces. Oil temperature = 90°C. IMEP = 10.3 bar 36
- 2.11 Crankshaft bearings. 37
- 2.12 Typical valvetrain configuration for heavy-duty applica-
tion. 40
- 2.13 Typical valvetrain configuration for light-duty application.
Source: [53]..... 40
- 2.14 Schematic figure of the piston-ring friction forces. 42

2.15	Surface roughness orientation. Source: [79].....	45
2.16	Hydrodynamic and asperity pressure between a flat of OCR and cylinder. Source: [27].	46
2.17	Skirt coordinates system.	47
2.18	Fluid film geometry for a dynamical loaded journal bearing. Source: [96]	50
3.1	Scheme of pressure sensors installed in the engine	65
3.2	ROTOTEST Transient vehicle test cell	67
3.3	Force balance in piston ring assembly	68
3.4	Blow-by model scheme. Source: [1]	71
3.5	Groove pressure in different ring volumes	72
3.6	Piston nodes distribution	73
3.7	Temperature distribution on piston assembly. Left: Cylinder temperature at different axial position and full load. Right: Piston-rings assembly at different engine loads	74
3.8	Variation of Patir and Cheng flow factors with Peklenik number	75
3.9	Piston ring profiles.....	76
3.10	SRV Reciprocating Tribometer.....	78
3.11	Averaged Coefficient of Friction for load equal to 10N ..	80
3.12	Averaged Coefficient of Friction for load equal to 100N .	80
3.13	Averaged Cycle Coefficient of Friction for both load	81
3.14	Force and moment balance in piston	81
3.15	Skirt pad angles	82
3.16	Journal Bearing nodes with symmetric half bearing assumption	84
3.17	Hertz contact area	86
4.1	Engine measured points	98
4.2	Dynamic viscosity of 5W-30 used for model validation ..	99

4.3	Steady state model validation	100
4.4	Friction engine maps for each tribological pair	101
4.5	Mechanical losses distribution	102
4.6	Friction losses in piston rings - Low load	104
4.7	MOFT on piston-ring assembly	104
4.8	Friction power on piston rings	106
4.9	Instantaneous Stribeck curve for piston-rings.	107
4.10	Average Stribeck curve por piston-rings.	108
4.11	Inst. Stribeck curve for piston skirt.	108
4.12	Piston skirt friction force curves at two different engine operating points.	109
4.13	Inst. Stribeck curve con-rod bearing.	110
4.14	MOFT con-rod bearing.	111
4.15	Asperity pressure con-rod bearing.	111
4.16	Load supported by main bearings.	112
4.17	Instantaneous Stribeck curve and CoF for MB 3.	113
4.18	MOFT for MB 3.	114
4.19	Friction losses in camshaft	114
4.20	Hertz Stress in lobe and roller.	115
4.21	Average Stribeck curve for cam-roller contact.	116
4.22	MOFT in cam-roller contact.	116
4.23	Speed profiles real driving cycle	118
4.24	Accumulated energy in the vehicle wheel.	120
4.25	Comparison between experimental engine speed and theoretical engine speed.	121
4.26	Comparison between experimental fuel consumption and theoretical fuel consumption.	122
4.27	Time distribution in each cycle measured.	123
4.28	Engine fuel consumption maps.	125

4.29	Variation of mechanical losses distribution with temperature	127
4.30	Friction engine maps in %	128
4.31	Energy dissipated by friction in the driving cycle.	129
4.32	Engine mechanical maps.	131
5.1	Engine oils shear thinning curves.	138
5.2	Engine oil temperature	139
5.3	Engine friction maps	140
5.4	Engine friction savings (%)	141
5.5	Engine friction in piston-rings and skirt.	142
5.6	Engine friction in piston-rings and skirt.	142
5.7	Top compression ring MOFT	143
5.8	Stribeck Curve for TCR.	144
5.9	Friction forces in piston skirt.	144
5.10	Friction savings (%) in engine bearings.	145
5.11	Asperity friction force and MOFT in main bearings.	145
5.12	Maximum asperity pressure in main bearings.	147
5.13	Friction savings (%) in the entire camshaft	148
5.14	Friction in the entire camshaft.	148
5.15	Engine oil temperature evolution during the WLTC cycle	150
5.16	Friction correction coefficient.	150
5.17	Engine oils viscosity tested.	151
5.18	WLTC cycle speed profile.	152
5.19	Fuel consumption for the cycle depending on the lubricant used.	153
5.20	Lubricant fuel savings (%) divided in WLTC cycle stages.	154
5.21	Vehicle consumed energy during the WLTC cycle.	157
5.22	Friction losses in piston-ring assembly.	161
5.23	Total friction losses in piston-ring assembly.	162

5.24	Total friction losses in piston-skirt.	163
5.25	Engine bearings FMEP.	164
5.26	Total friction losses in camshaft.	165
5.27	Fuel saving obtained from the cylinder surfaces.	166
5.28	Fuel saving obtained from the cylinder surfaces.	167

Index of Tables

- 1.1 Comparison of energy and costs due to friction and wear for the most four important economic sectors. Adapted from [7] 4

- 3.1 Engine tested characteristics 64
- 3.2 Test cell instrumentation 65
- 3.3 Tested vehicle specifications 66
- 3.4 Rings installed tension 73
- 3.5 Parameters used in Greenwood-Tripp model 77
- 3.6 SRV experimental assembly characteristics 78
- 3.7 SRV experimental test characteristics 79
- 3.8 Bearings geometry 85
- 3.9 Parameters used in Greenwood-Tripp model 85
- 3.10 Auxiliaries coefficients 90

- 4.1 Experimental engine operating points 98
- 4.2 Experimental vs. simulation results 124
- 4.3 Mechanical losses distribution during driving cycles 130

- 5.1 Lubricants used in the analysis and their properties. 138
- 5.2 WLTC cycle characteristics 152
- 5.3 Total fuel consumption and fuel savings for the different lubricants used. 153

5.4	Lubricants fuel consumption by cycle stages	155
5.5	Lubricants energy consumption	156
5.6	Engine condition	159
5.7	Surface finishing characteristics. Source: [7]	160

Nomenclature

Latin

a	Fitting coefficient
A	Area
b	Fitting coefficient
c	Fitting coefficient
C	Bearing clearance
cm	Centimeters
CO	Carbon monoxide
CO_2	Carbon dioxide
d	Fitting coefficient
D	Bearing diameter
E	Young's modulus
F	Force
f	Gaussian distribution
h	Film thickness
\bar{h}	Average film thickness
HC	Hydrocarbon
I	Inertial moment
k	Fitting coefficient
m	Mass
M	Ring mass
\dot{m}	Mass flow

n	Pump speeds
N	Power
NO_x	Nitrogen oxides
p	Pressure
PM	Particulate Matter emissions
R	Universal gas constant
S_a	Surface Arithmetic mean deviation
$S_{mr1,2}$	Surface material portion
S_k	Surface core roughness depth
S_{pk}	Surface peak height
S_{vk}	Surface valley height
t	Time
T	Temperature
u	sliding velocity
U	Relative velocity between two bodies
V	Volume
VGT	Variable geometry turbine
\dot{V}	Volume flow
x	axial direction
y	Vertical direction

Greek

μ	Dynamic viscosity
α	Viscosity-pressure coefficient
β	Asperity radius
$\dot{\beta}$	Viscosity-temperature coefficient
γ	Isentropic exponent
γ_p	Peklenik number
$\dot{\gamma}$	Shear rate
Δ	Increment
ϵ	Eccentricity
η	Efficiency
$\lambda_{0.5}$	Auto-correlation function
ν	Kinematic viscosity

ρ	Density
σ	Surface roughness
τ	Shear stress
ν	Poisson ratio
ϕ	Flow factors
ω	Rotational bearing speed

Acronyms

ALT	Alternative
AW	Anti-Wear
BMEP	Brake Mean Effective Pressure
BSFC	Brake Specific Fuel Consumption
CAD	Crank Angle Degree
CAN	Controller Area Network
CGS	Centimetre-gram-second
CI	Compression Ignition
CoF	Coefficient of Friction
CPU	Central Processing Unit
DOC	Diesel Oxidation Catalyst
DI	Direct Injection
DPF	Diesel Particulate Filter
ECU	Electronic Control Unit
EGR	Exhaust Gas Recirculation
EHD	Elastohydrodynamic
EHL	Elastohydrodynamic lubrication
EP	Extreme-pressure
FMEP	Friction Mean Effective Pressure
FWD	Front Wheel Drive
GCI	Gray Cast Iron
GDI	Gasoline Direct Injection
GHG	Greenhouses Gases
GNP	Gross National Product

HPEGR	High Pressure EGR
HSDI	High Speed Direct Injection
HTHS	High Temperature High Shear rate
ICE	Internal Combustion Engine
IMEP	Indicated Mean Effective Pressure
KV	Kinematic Viscosity
LNT	Lean NO _x Trap
LPEGR	Low Pressure EGR
LVEO	Low Viscosity Engine Oil
MOFT	Minimum Oil Film Thickness
MTM	Mini-Traction Machine
OCR	Oil Control Ring
OEM	Original Equipment Manufacturer
PAO	Poly Alpha Olefins
PMA	Piezo resistive transducers
SCR	Second Compression Ring
SUV	Sport Utility Vehicle
TCR	Top Compression Ring
TEHD	Thermo elasto hydrodynamic
THD	Thermo hydrodynamic
TWAS	Twin Wire Arc Spray
UK	United Kingdom
USA	United States of America
VGT	Variable Geometry Turbine
VI	Viscosity Index
VM	Viscosity Modifier
VVT	Variable Valve Timing
WCAC	Water Cooled Air Cooler
WLTC	Worldwide Harmonized Light Vehicles Test Cycle
ZDDP	zinc dialkyl dithiophosphates

Chapter 1

Introduction

Contents

1.1	Overview: background and context	3
1.1.1	Energy Consumption in Transportation	4
1.1.2	Energy consumption in passenger cars	7
1.1.3	Mechanical losses in ICE	8
1.1.4	Modeling friction losses in ICE	9
1.2	Objectives of the thesis	10
1.2.1	Validate a steady-state friction model	10
1.2.2	Validate a transients friction model	11
1.2.3	Assessment of performance of different Low Viscosity Engine Oils in model validated	11
1.2.4	Evaluation of different cylinder surfaces in the model validated	11
1.3	Thesis document structure	12
1.4	Thesis publications	13
	Bibliography	14

1.1 Overview: background and context

In 1966 a report presented by P. Jost [1] defined by first time the tribology as *"The science and technology for understanding and controlling friction, wear, and lubrication of such interacting surfaces in relative motion."* In this report, Jost estimated that UK could saved around 515 millions pounds per year (at 1965 values) through tribology and this correspond to 1.3% and 1.6 % of GNP (Gross National Product) in this time. Moreover, Jost estimates that the first 20 % of such savings can be achieved without any extra investment effort [2, 3]. Latest reports followed by different states showed that in USA a total of 0.7% of GNP could be saved (at 1980 values) [4], 0.4% of GNP from Canadá (at 1986 values) [5] and 2%-7% in China [6]. This savings could be achieved in a 1/50 ratio investment/benefit, i.e. one dollar invest it returns 50 dollar of benefit. From there, tribology was recognized as a source of large potential economic savings.

Since then the efforts to better understand the tribological phenomena in the different industrial field has exponentially grown. From Jost report, it has been developed different solutions to improve the friction, lubrication and wear of the mechanisms, for example: the use of low viscosity oils rheologically enhanced with viscosity index improvers, the different surface finishings, new materials and improved mechanical designs [7]. This strategies lead to increase the primary energy saved in the key industrial sectors: Advanced Manufacturing, Power Generation and Transportation.

Holmberg et al. [8] estimated that the losses produced by tribology in Industrial sector (paper machines) could be reduced until 11% in short term and 23% at mid-long term. The authors propose solution such as the usage of low-friction and highly durable coatings, low-viscosity and low-shear lubricants between others. This savings could save 2000 M euro and 4000 M euro and until 22.7 million tonnes of CO_2 . Moreover, another important industrial activity which friction and wear are present is mining. In this industry, the tribological mechanisms are harder due to very high loading conditions, high levels of dust and often wet environments. A study carried out in [9] shows the energy losses produced by friction and, especially, wear in mining activities. The study concluded that the mining activities consume about 6.2% of

the total global energy, which 38% (4.6 EJ) of this energy is assigned to overcome friction. Moreover, 2 EJ are extra energy consumed due to wear of the mechanical parts related with the activity. In total, the CO_2 emitted can be estimated in 970 million tonnes, i.e., 2.7% of world CO_2 emissions. Consequently, the authors affirm that applying new technology for friction reduction and wear protection can reduce by 15% in short term and 30% in long term the energy consumption due to overcome friction.

As a brief summary, table 1.1 illustrate the percentage of energy to overcome friction in different sectors where energy is used.

Sector	Energy to overcome friction as part of total energy use (%)	Energy due to wear compared to energy loss due to friction (%)	Cost due to wear compared to cost due to friction (%)
Transportation	30	10	22
Industry	20	14	35
Energy industry	20	22	53
Residential	10	14	35
Average	20	15	37

Table 1.1: Comparison of energy and costs due to friction and wear for the most four important economic sectors. Adapted from [7]

1.1.1 Energy Consumption in Transportation

Figure 1.1, shows the percentage of the total final energy consumed by sector. In last 50 years, the total energy consumption was multiplied by 2.3 being the share of this energy more or less constant.

The transport is the second sector which consumes a major quantity of global energy. This fact is given because in the world there are around 1,600 million of vehicles. Within of this global numbers and it can be

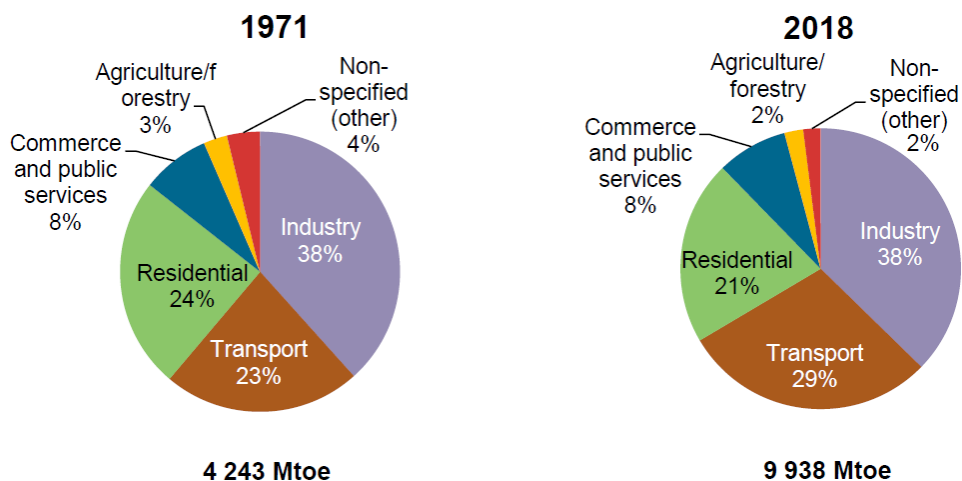


Figure 1.1: World total final consumption by sector [10]

observed on Figure 1.2, road traffic encompasses the major energy used (73%), followed by marine (10%), aviation (10%) and rail (3%) traffic [11, 12].

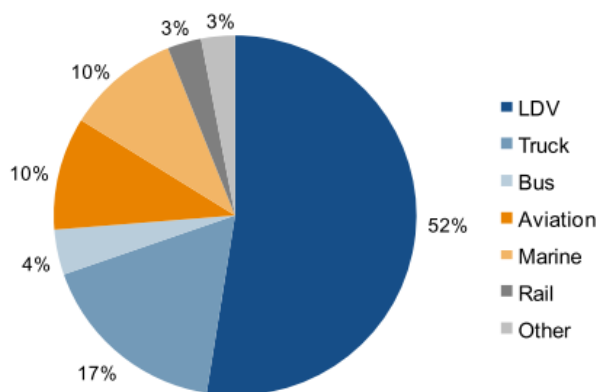


Figure 1.2: Energy used in transport scenarios [12]

In a first approximation a total of 20% of the energy usage in the aforementioned sectors go to overcome the friction. This statement lead

to the energy lost by friction has an important weight in the CO_2 emitted to the atmosphere.

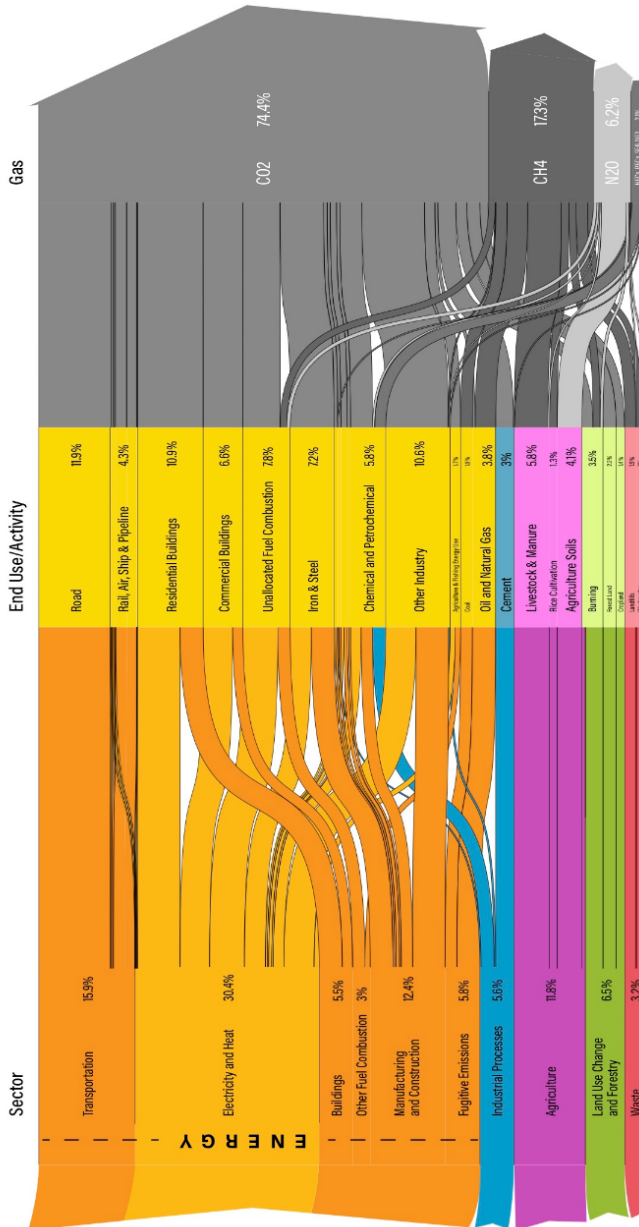


Figure 1.3: World Greenhouse Gas Emissions in 2016 [13].

Attending to figure 1.3, the contribution to the CO_2 emissions from transport sector account 15%. In other words, the energy destined to

overcome the friction in the transport road sector contribute to 1% of the total CO_2 emitted to the atmosphere. This data lead to introduce different strategies to find new tribological solutions to reduce friction and wear.

Focusing on road traffic, in heavy-duty applications, which it takes 21% of the energy consumption of the transport sector, the energy converted into mechanical power is estimated in 50%. The rest of energy is lost by cooling (20%) and exhaust energy (30%) [14] (see figure 1.4). However, some of the mechanical power produced is lost due to frictional power losses in the transmission, gearbox, final drive and running the resistances of the vehicle. In total, approximately 33% of the mechanical power is lost due to frictional power losses in the transmission, gearbox, final drive and running the resistances of the vehicle. In total, approximately 33% of the mechanical power is lost due to frictional power losses in the transmission, gearbox, final drive and running the resistances of the vehicle. Finally, the useful energy used to move the heavy-duty vehicle is approximately 34%.

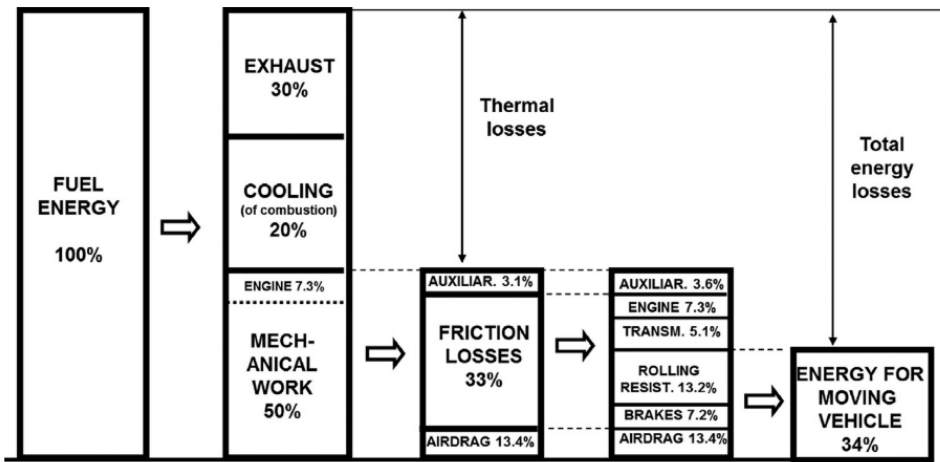


Figure 1.4: Energy consumption in heavy-duty applications [14].

1.1.2 Energy consumption in passenger cars

In past decades, the effort to reduce the energy consumption of transportation, and, especially, in passenger cars have grown. Different solutions to this problematic situation have been considered. From improving the ICE (Internal Combustion Engine) efficiency until

solutions based on a different degree of vehicle electrification. Focusing in ICE, the nature of combustion process lead to produce pollutants emissions to the ambient in exhaust gases. In Diesel engines the main contaminants are NO_x and Particulate Matter (PM), whilst, gasoline engines produce, mainly, unburned hydrocarbons (HC) and CO emissions. Apart of this pollutant emissions, as a consequence of combustion process, the ICE also emit CO_2 , which it is a indicative of a complete combustion. However, this gas contributes to climate change rising the Earth temperature.

This problem, lead to European Parliament and the Council adopt new normative to control the CO_2 emitted to the atmosphere [15]. On it, new targets were implemented to commit with the Paris Agreement. Initially a total emission of 95 g/km of CO_2 was stipulated for 2020. From there, the reduction of CO_2 emitted by cars will gradually reduce. 15% reduction from 2025 and 37.5% from 2030. To comply this specifications, in 2030 a passenger car must emit approximately 60 g/km of CO_2 .

In typical passenger cars, approximately 17% (12% within the engine and 5% in transmission) of the fuel energy introduced go to overcome ICE friction [16]. In this scenario, the tribologist plays a key role in developing new tribological solutions to reduce friction and wear. In the actual framework, two solutions can be tackled in order to reduce the friction in passenger cars:

- Introducing new lubricants rheologically improved which reduces the friction losses in the ICE and cylinder coatings
- Implementing new designs in the future vehicles considering: decreasing the drag coefficient and improving the tyres designs.

1.1.3 Mechanical losses in ICE

Because this thesis purpose is optimize the mechanical and friction losses in an light-duty ICE, will make reference to the mechanical friction forces in the powertrain system that it is defined as the difference between the net indicated mean effective pressure (IMEP) and the brake mean effective pressure (BMEP). As introduced before, due to friction losses

in ICE, around 12% of the energy introduced in the vehicle is lost. This mechanical losses is expended as follows [17]:

- Pumping losses: Power required to introduce fresh mixture through the intake system and to eject the burned gases from combustion process through exhaust.
- Friction losses: To overcome the resistance that two mechanical parts offer in relative motion between them. Normally a lubricant fluid is used to diminish the force. We can find this phenomena in engine bearings, piston-ring assembly and camshaft, mainly.
- Auxiliary losses: To drive the engine accessories necessary to its performance, i.e.: water pump, oil pump, fuel pump.

Attending that the biggest portions in the mechanical losses are related with friction losses, this thesis tackle this problematic from a simulation point of view, that is, validating an engine model from the experimental data obtained from engine test bench. This thesis addresses the friction losses from a global point of view, that is, studying how the different tribology technology affect to piston-ring assembly, engine bearings and camshaft. It also studies and quantifies the amount of fuel that can be saved by implementing rheologically optimized oils and new cylinder surface finishes.

1.1.4 Modeling friction losses in ICE

The friction losses are studied through a validated model. The study of friction phenomena in any scope, and especially in ICE through validated and well-demonstrated model, can improve the final result obtained and helps to better understand the physical phenomena that occurs in ICE. Simulation tools provide extra information that it can not be found in the experimental test. In the field of tribology applied to ICE are: the minimum oil film thickness (MOFT) between two mechanical parts, the quantity of friction caused by viscosity forces (hydrodynamic) and direct contact between surface asperities (boundary), the lubrication regime of each different mechanical elements, that is especially useful to decided what strategy would improve the friction losses, etc.

Not only numerical approach is useful to understand in a best way the phenomenon that occur in experimental tests [18] but also optimum parameters could be pre-determined for specific applications and working conditions, thus, the time and economy costs associated to the experimental test decrease. This reason lead to make a assessment of the friction losses in ICE in this doctoral thesis.

1.2 Objectives of the thesis

This doctoral thesis pursues the main objective of studying and optimizing the friction losses in ICE to make it more efficient and, with it, contribute to diminish the quantity of CO_2 emitted to the atmosphere. To meet this goal, the next steps have been followed:

1.2.1 Validate a steady-state friction model

As described in section 1.1.4, first step to assess the friction in ICE is create and validate a model which represent the experimental results obtained in the test bench. For this purpose, a 4 stroke CI-Diesel engine has been tested. By means of IMEP method, that is, considering that FMEP is the difference between IMEP and BMEP obtained in the test, the model has been checked. From the test bench, some thermodynamic variable has been taken, that is, in-cylinder pressure, oil pressure, oil temperature, in-cylinder temperature, blow-by.

Also, the detailed geometrical characteristics of the engine has been included in the model, from macro-geometrical data such as: cylinder bore, rod length, bearing width... until micro-geometrical data such as: piston-ring shape, mechanical roughness of material and so on. Finally, attending that some engine data were not available, some parameters needed for simulation have been considered from bibliography, that is: boundary friction coefficient, and mechanical properties of the material to solve the asperity model.

1.2.2 Validate a transients friction model

Next step in doctoral thesis has been making a transient model in order to have a first approximation of how much friction energy is dissipated in a vehicle during a real driving cycle. This approximation has been also validated from a vehicle test bench, on which, from parameters measured on the vehicle the model has been proved. This model is able to estimate the friction and fuel consumption of the engine under study in a real driving cycle and the mechanical losses distribution. This is useful to understand how much energy is dissipated by different mechanical parts of the engine where friction is present, that is, piston-assembly, engine bearings, camshaft and auxiliaries. From that, is possible to assess different strategies to diminish the friction losses in an ICE and optimize the fuel consumption.

1.2.3 Assessment of performance of different Low Viscosity Engine Oils in model validated

Focusing in the aim of the thesis, different low viscosity engine oils have been evaluated. Mainly, through its rheological properties which define its performance. This physical properties have been obtained in the laboratory with different equipment, that is, viscosity in function of temperature and shear rate, density, coefficient of friction. Along this chapter, it will be emphasized the importance of considering the variation of viscosity with shear rate, since in the majority of the cases the working conditions in the mechanical parts lead to the oil to work under high shear rate and, hence, there are differences between considering Newtonian or Non-Newtonian behavior.

1.2.4 Evaluation of different cylinder surfaces in the model validated

To conclude the study of friction optimization in reciprocating internal combustion engines, a study of the potential friction savings of combining low viscosity oils and surface finishes of the piston-liner assembly is carried out. For this purpose, the different surface parameters

that characterize the cylinder are introduced into the model and analyzed against different oils. During this chapter, the main advantages and disadvantages of using surface finishes will be analyzed, as well as the lubrication regimes used depending on the engine speed, trying to make a comparison with the homologation cycle in hybrid vehicles and their potential fuel saving.

1.3 Thesis document structure

In this brief subsection, the structure of the whole document is described. The purpose of this section is guiding to the reader to better understand the content of the doctoral thesis.

- Chapter 1: This chapter is a brief introduction about this thesis topic. This chapter tries to explain the importance of optimizing the friction losses in an ICE due to its impact on the environment in terms of CO_2 emissions emitted.
- Chapter 2: In this chapter a literature review is performed, analyzing lubrication in ICE, the main tribological engine pairs and the models currently used to study the tribology phenomenon.
- Chapter 3: This chapter describes the engine used, the experimental test cells and the main equations and assumptions carried out in the model developed.
- Chapter 4: Following the thesis objectives, this chapter shows both the steady-state model and transient model validated and the main results that it can be obtained from it. Also, the main tribological parameters are shown.
- Chapter 5: Finally, in this chapter the main strategies in order to optimize the friction losses in ICE are assessed. From the advantages of using low viscosity engine oil until the friction saving coming from the usage of different cylinder surfaces.
- Chapter 6: In this chapter the main conclusions of the doctoral thesis and the future work to be carried out are exposed.

1.4 Thesis publications

Finally, the development of a doctoral thesis involves research publications, both in indexed journals and international conferences. The publications resulting from the study of this doctoral thesis are detailed below.

JCR Publications

1. B. Tormos, J. Martín, D. Blanco-Cavero and A. J. Jiménez-Reyes, "One-Dimensional Modeling of Mechanical and Friction Losses Distribution in a Four-Stroke Internal Combustion Engines," *Journal of Tribology*, vol. 142, no. 1, Jan. 2020.
2. B. Tormos, J. Martín, B. Pla and A. J. Jiménez-Reyes, "A methodology to estimate mechanical losses and its distribution during a real driving cycle," *Tribology International*, vol. 145, Dec 2020.

Conferences papers

1. E. Tomanik, F. Profito, B. Tormos, A. Jiménez et al., "Powertrain Friction Reduction by Synergistic Optimization of the Cylinder Bore Surface and Lubricant Part 1: Basic Modelling," SAE Technical Paper 2021-01-1214, 2021
2. B. Zhmud, E. Tomanik, A. Jiménez, F. Profito et al., "Powertrain Friction Reduction by Synergistic Optimization of Cylinder Bore Surface and Lubricant - Part 2: Engine Tribology Simulations and Tests," SAE Technical Paper 2021-01-1217, 2021
3. B. Tormos, A. Jiménez, T. Fang, R. Mainwaring et al., "Numerical Assessment of Tribological Performance of Different Low Viscosity Engine Oils in a 4-Stroke CI Light-Duty ICE," SAE Technical Paper 2022-01-0321, 2022.

Bibliography

- [1] Jost H. P. *Lubrication (tribology) education and research. A report on the present position and the industry's needs.* London, UK: Department of Education and Science. 1966.
- [2] Jost H. P. and Schofield J. “Energy saving through tribology: A techno-economic study.”. *Proceedings - Institution of Mechanical Engineers*, Vol. 195, pp. 151–173, 1981.
- [3] Jost H. P. “Tribology - Origin and future”. *Wear*, Vol. 136, pp. 1–17, 1990.
- [4] Pinkus O. and Wilcock D.F. *Strategy for energy conservation through tribology.* 1977.
- [5] National Research Council of Canada: Associate Committee on Tribology. *A strategy for tribology in Canada: enhancing reliability and efficiency through the reduction of wear and friction.* 1986.
- [6] Tribology Institution of the Chinese Mechanical Engineering Society. *An investigation on the application of tribology in China.* 1986.
- [7] Holmberg K. and Erdemir A. “Influence of tribology on global energy consumption, costs and emissions”. *Friction*, Vol. 5, pp. 263–284, 2017.
- [8] Holmberg K., Siilasto R., Laitinen T., Andersson P. and Jäsberg A. “Global energy consumption due to friction in paper machines”. *Tribology International*, Vol. 62, pp. 58–77, 2013.
- [9] Holmberg K., Kivikytö-Reponen P., Härkisaari P., Valtonen K. and Erdemir A. “Global energy consumption due to friction and wear in the mining industry”. *Tribology International*, Vol. 115, pp. 116–139, 2017.
- [10] International Energy Agency. *Statistics report World Energy Balances.* 2020.
- [11] Erdemir A. and Holmberg K. “Energy consumption due to friction in motored vehicles and low-friction coatings to reduce it”. *Coating Technology for Vehicle Applications*, Vol. 47, pp. 1–24, jan 2015.
- [12] World Energy Council. *Global Transport Scenarios 2050.* 2011.
- [13] International Energy Agency. *Energy consumption in transport in IEA countries.* 2018.
- [14] Holmberg K., Andersson P., Nylund N., Mäkelä K. and Erdemir A. “Global energy consumption due to friction in trucks and buses”. *Tribology International*, Vol. 78, pp. 94–114, 2014.
- [15] European Union. *REGULATION (EU) 2019/ 631 OF THE EUROPEAN PARLIAMENT AND OF THE COUNCIL - of 17 April 2019 - setting CO2 emission performance standards for new passenger cars and for new light commercial vehicles, and repealing Regulations (EC) No 443 / 2009 and (EU) No 510 / 2011.* 2019.

-
- [16] Holmberg K., Andersson P. and Erdemir A. “Global energy consumption due to friction in passenger cars”. *Tribology International*, Vol. 47, pp. 221–234, mar 2012.
 - [17] Heywood J.B. *Internal combustion engine fundamentals*. Mc Graw-Hill series in mechanical engineering. McGraw-Hill, New York/etc, 1988.
 - [18] Grützmacher P., Profito F. and Rosenkranz A. “Multi-scale surface texturing in tribology-current knowledge and future perspectives”. *Lubricants*, Vol. 7 n° 11, 2019.

Chapter 2

Literature Review: Friction losses in ICE

Contents

2.1	Introduction	19
2.2	Lubrication in ICE	21
2.2.1	General lubrication theory	21
2.2.2	Hydrodynamic lubrication	22
2.2.3	Elastohydrodynamic lubrication	24
2.2.4	Mixed lubrication	24
2.2.5	Boundary lubrication	25
2.2.6	Engine oil properties	26
2.2.6.1	Introduction	26
2.2.6.2	Viscosity	28
2.2.6.3	Effect of temperature on viscosity ..	29
2.2.6.4	Effect of pressure on viscosity	30
2.2.6.5	Effect of shear rate on viscosity	31
2.2.6.6	Viscosity index	32
2.3	Mechanical losses in ICE	33
2.3.1	Piston assembly	33

2.3.1.1	Piston rings	34
2.3.1.2	Piston skirt	36
2.3.2	Crankshaft	37
2.3.2.1	Journal bearings	37
2.3.2.2	Con-rod bearings	38
2.3.3	Valvetrain	39
2.4	Numerical models applied to assess the friction in ICE	41
2.4.1	Piston-ring assembly	41
2.4.1.1	Classical Reynolds Equation and Stochastic Asperity Contact Models	42
2.4.1.2	Average Reynolds Equation (Patir and Cheng's average flow model)	43
2.4.1.3	Deterministic method - Quasistatic approximation	44
2.4.1.4	Deterministic method - Full approximation	45
2.4.1.5	Other piston ring model considerations	45
2.4.2	Piston-skirt	47
2.4.3	Bearings	48
2.4.3.1	Impedance Approach	48
2.4.3.2	Mobility Approach	49
2.4.3.3	Reynolds equation	49
2.4.4	Valvetrain	50
	Bibliography	52

2.1 Introduction

Along last decades, the efforts in transport sector to reduce fuel consumption, and consequently, Greenhouse gases (GHG) emissions to the atmosphere, have increased exponentially in order to fulfill with Kyoto and Paris Agreements on climate change [1]. Focusing on the road traffic, and according to this doctoral thesis framework, the passenger cars with light-duty engines, are one of the biggest GHG contributors to the atmosphere.

Different alternatives are presented by light-duty vehicle manufacturers in order to increase its global efficiency. From external factors independent of ICE, such as: aerodynamics, tyre rolling friction, weight reduction, until processes related with ICE. As cited by several authors, there are several solutions to improve vehicle efficiency:

- *Solutions inside ICE:* In this context, there are presented the solutions related with the thermodynamic process and design considerations that occur inside ICE, i.e., low friction lubricants [2, 3], cylinder deactivation [4, 5], variable valve timing (VVT) [5, 6], turbocharging and downsizing [7, 8], gasoline direct injection (GDI) [9, 10]...
- *Solution outside ICE:* In this part, several different solutions are found, i.e., Continuously Variable Transmission [11, 12], vehicle mass reduction, low rolling resistance tires, low drag brakes, aero drag reduction...
- *Driving parameters:* Not only the fuel consumption depends on vehicle engineering design but also human factors and its driving style are key parameters to contribute to fuel efficiency [13]. In this field, some driving parameters are mentioned: follow speed limit, cruising speed, smooth acceleration and deceleration, safe headway, highest gear possible, increasing tyre pressure, these parameters are consistent with earlier research conducted by Hooker [14], that suggests that human behavior has an important effect on reducing fuel consumption.

In this context, the potential solutions are varied and some of them can be set up in short-term due to its well demonstrated potential to

reduce fuel consumption. However, further development is necessary to determine the degree of improvement. Some of them are: homogeneous-charge compression ignition, plug-in hybrids, diesel hybrids and advanced materials and body designs. Even some of this technologies have been demonstrated that it contributes to increase the vehicle efficiency, it will not be possible for some of them to become real solutions for significant technical and economic challenges. Among these above-mentioned solutions, the reduction of mechanical losses in ICE by means of tribological solutions play a key role in the goal of diminishing the CO_2 emitted to the atmosphere, due to their advantageous cost-benefit ratio.

As previously introduced, the mechanical losses in ICE can be defined as the difference between the work carried out in the combustion chamber (indicated work) and the work available in the drive shaft (brake work). Approximately, in a conventional passenger car, 12% of the energy introduced in the vehicle is lost by mechanical losses in ICE. This is only a small proportion of the total losses, but they represent a significant fraction of the output power. Figure 2.1 represents an estimation about the losses distribution in a passenger car.

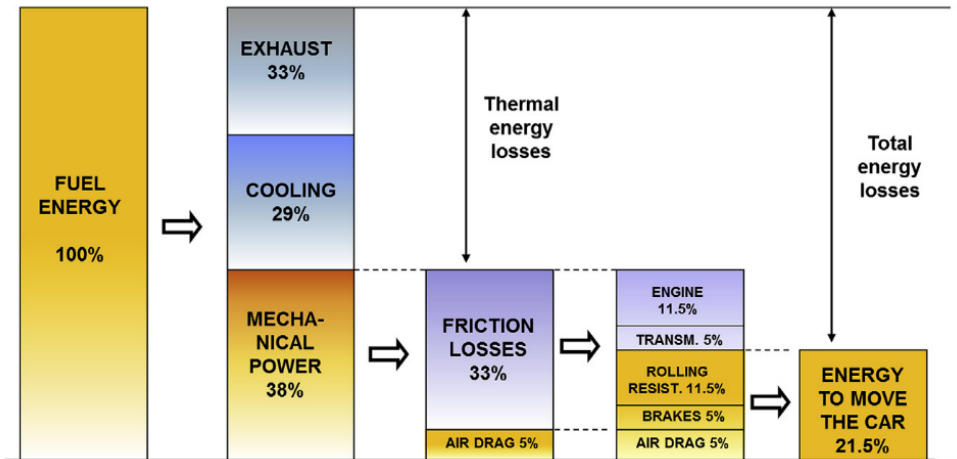


Figure 2.1: Mechanical losses distribution in light-duty vehicle [15]

According to [16] the total fuel that can be saved through reducing vehicle friction can be arrive until 61% in long term, that is, in 15-20

years. This potential savings can be accomplished with the applications of new tribology technologies. In total, the authors of this paper work, estimate that the quantity of CO_2 saved to the atmosphere could be 960 millions of tonnes. Not only CO_2 is reduced applying new tribology, but also in monetary terms it would equal to 576,000 millions euros.

2.2 Lubrication in ICE

According to [17], lubrication is the technology utilized to reduce friction between two surfaces when one is moving relative to the other and to protect surfaces from wear by providing a lubricant that can support a dynamic or static load.

2.2.1 General lubrication theory

The friction force can be defines as the resistance presented in a body when moving against another. In general terms, two kind of relative motion can arise: sliding and rolling [18]. Figure 2.2 shows both kind of pure movement between two bodies. In both relative motion, a tangential force F is necessary to start the movement in one of the bodies. As said, the sliding or rolling movement will oppose resistance to the movement, that is, the friction force acting. The ratio between the friction force and the normal force F_n is known as *coefficient of friction*, normally, expressed with the nomenclature CoF

$$CoF = \frac{F_{friction}}{F_n} \quad (2.1)$$

The coefficient of friction between two metals in direct contact (dry sliding) is rarely lower than 0.5. In this part, lubricants play a key role, since its principal duty is reducing the frictional force between two surfaces [19]. The fluid introduced between two surfaces, lubricant, has a lower shear strength than either of the surfaces themselves, this helps to reduce the coefficient of friction. Depending on application where the lubricant is used, it can be found that the lubricant can not completely prevent asperity contact, but, it can reduce it and even eliminate the

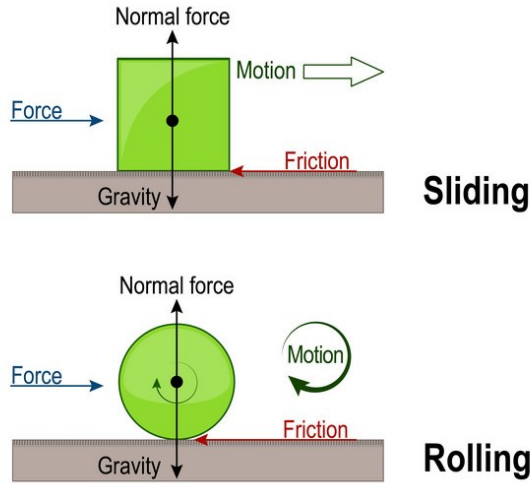


Figure 2.2: Sliding and rolling friction.

adhesive forces between the surfaces. This situation can be found in the camshaft mechanism of an ICE where the oil film thickness is lower than the surface roughness. But, in function of load, speed and temperature of the lubricant, different lubrication regimes can be identified such as, hydrodynamic lubrication, mixed lubrication and boundary lubrication, explained in more detail below. In 1902, Richard Stribeck made the first experiments detailing a clear view of the value of coefficient of friction against speed [20]. Figure 2.3 presents an example of the Stribeck curve and the different lubrication regimes that can be found between two surfaces in function of relative speed (ω), dynamic viscosity of the fluid (μ) and the load carried out (F_n). The number presents in x axis is commonly known as Hersey number.

2.2.2 Hydrodynamic lubrication

Hydrodynamic lubrication defines the situation in which two surfaces are separated by certain quantity of lubricant fluid film such that there is not possibility that these surfaces come into contact between them, so, the wear is eliminated. Hydrodynamic lubrication takes place in conformal contacts and between two separated surfaces, when

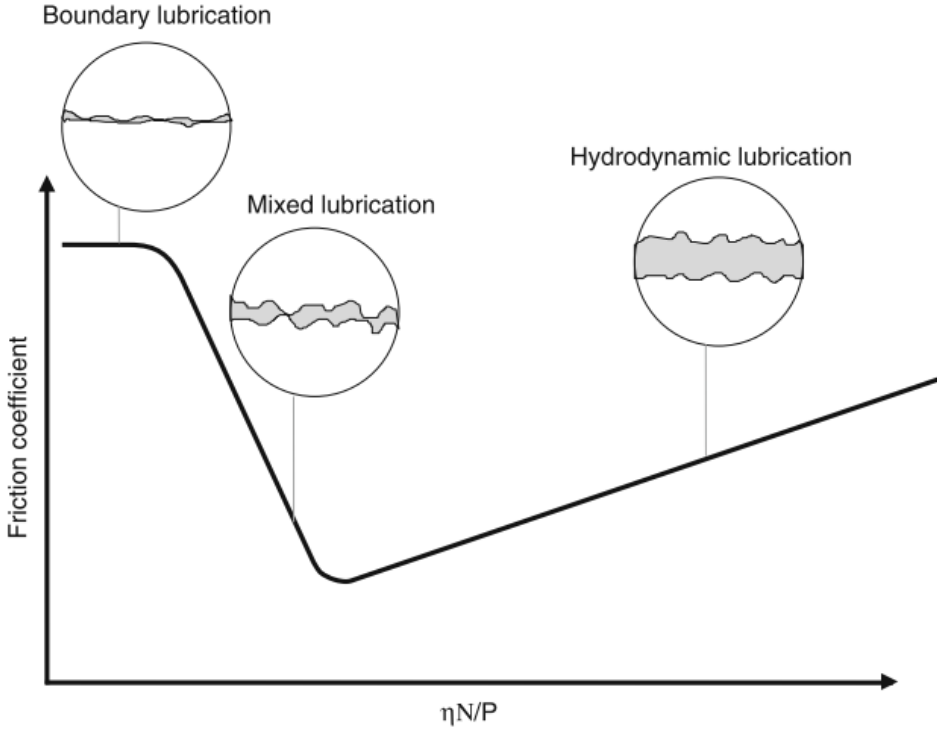


Figure 2.3: Schematic of a Stribeck curve. Source: [17]

it exists low pressure between them [21]. Also, other conditions for the appearance of this lubrication regime is a high relative velocity between both surfaces and a high dynamic viscosity of the lubricant fluid that is present in the interface. But the essence of hydrodynamic lubrication was first clarified experimentally by British railroad engineer Beauchamp Tower in 1883 [22, 23]. From this Tower's Experiment, Osborn Reynolds formulated a theory of lubrication in 1886 [24]. Since then, Reynold's theory has been the foundation of the theory of hydrodynamic lubrication.

After considerations and hypothesis, the Reynolds equation, in x-direction, can be expressed as follow:

$$\frac{\partial}{\partial x} \left(\frac{\rho h^3}{12\mu} \frac{\partial p}{\partial x} \right) = \frac{U}{2} \frac{\partial(\rho h)}{\partial x} + \frac{\partial(\rho h)}{\partial t} \quad (2.2)$$

In this equation x is the space coordinate, t represents the time, ρ the fluid density, μ is the fluid dynamic viscosity, p is the fluid pressure, U the surface speed and h the separation of the two surfaces. The left hand side of the equation describes the Poiseuille terms which represents the pressure driven flow. The first term on the right hand side is the Couette term, that represents the shear driven flow. Finally, the last term is called the squeeze term and it balances the mass-flow continuity for a time dependent flow situation.

2.2.3 Elastohydrodynamic lubrication

When the contacting surfaces are counterformal, i.e., non-conforming, then the local pressure in the contact part, that is, line or point, will generally be much higher than those found in hydrodynamic lubrication. An example of this phenomena can be found in the contact between cam and follower in engine camshaft, between gear teeth, etc. In those cases mentioned, it would be wrong applied the classical hydrodynamic theory. That is because in extreme EHD (elastohydrodynamic) cases the film thickness can achieve values around tenths of micron. According to classical hydrodynamic theory this phenomena would be dominated by asperity contact. However, the very high pressure in the film increases the viscosity of the lubricant, and this results in a film thickness greater than that predicted by the classical theory. This lubrication phenomena have almost Hertzian contact pressure profile within the Hertzian contact area as shown in figure 2.4

2.2.4 Mixed lubrication

The mixed lubrication regime is characterized by the interaction of a lubricated contact whose surface roughness affect the performance of the contact. Also, because the hydrodynamic and boundary lubrication regimes are acting in the contact, the term *mixed* is commonly used. In this regime the oscillations on local pressures can lead to important stress peaks, which can have adverse effects on both solids and lubricant [25]. So, the asperity contact begin to be present and become increasingly severe. The mixed lubrication is typically found in the surround of dead center of the piston assembly and in the cam contact in an internal

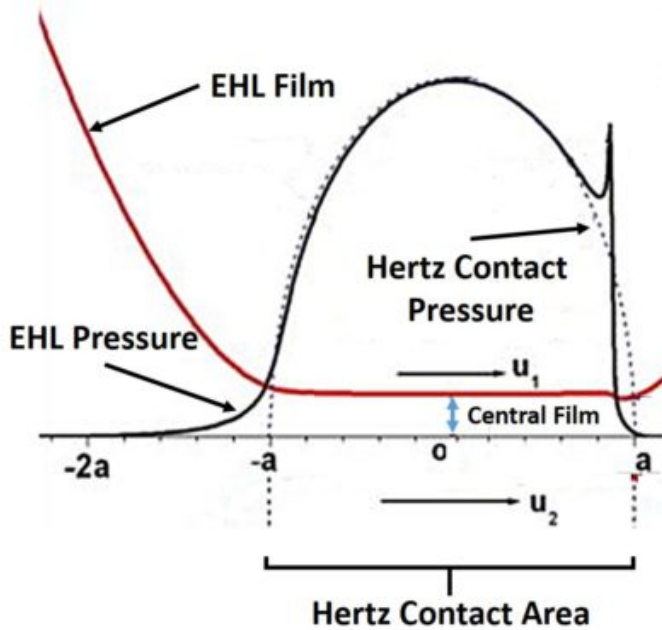


Figure 2.4: Hertz Contact pressure vs. Elastohydrodynamic pressure

combustion engine [26]. To determine numerically the mixed lubrication regime, two main categories are present:

- *Deterministic approximation*: That is, considering the micro-irregularities on the asperity as the main source of hydrodynamic support. [27–31]
- *Stochastic modeling*: The simplest approach that it is commonly used in the numerical approach of friction modeling. The most used stochastic thin film lubrication model is the one proposed by Patir and Cheng [32, 33].

2.2.5 Boundary lubrication

The term *boundary lubrication* was developed by Hardy and Doubleday in 1922 [34]. In this work, the authors studied the friction of surfactant molecules. This regime describes the situation which the

load applied is mainly supported by asperity, with partial or totally absence of lubricant. This situation is predominant when components have rough surfaces and they operate at high pressure and low relative velocity. In last decade, the lubricants manufactures have been focused on diminishing the oil viscosity in order to reduce the hydrodynamic friction losses, but, in contrast the lubrication regime tends to be boundary. Mainly, there are two main strategies to decrease the effects of boundary regime:

- Including in the oil different additives to control boundary friction and wear, such as, friction modifiers, antiwear and extreme pressure additives [35–37].
- Including in the engine new types of surface coatings which provides very low coefficient of friction and wear [38–40].

2.2.6 Engine oil properties

2.2.6.1 Introduction

In an ICE, the engine oil have the function of reducing the friction between two tribological mechanical parts and providing a longer life of the mechanism, that is, reducing the wear. The typical composition is around 60-85% base stock and 15-40% additives [41]. In this composition, the base stock can have three different sources: biological, mineral and synthetic, but for automotive industry the typical are mineral and synthetic. Each of them presents different characteristics and properties and it will be used depending on its application.

- *Mineral base:* This bases are extracted from the refining of crude petroleum. In the process, the unwanted hydrocarbons and the natural contaminants are removed.
- *Synthetic base:* This bases are a product of complex chemical transformations that are performed either directly on drilled crude petroleum of using preselected molecules. This bases present a better performance than the mineral ones in terms of durability, flow at low temperatures and stability.

This bases are classified by the American Petroleum Institute into five group based on how the oils are processed [42].

- **Group I:** Solvent-refined mineral oil. Base contain less than 90% saturates and/or greater than 0.03% sulfur and have a viscosity index greater than or equal to 80 and less than 120.
- **Group II:** Hydroprocessed. Base contain greater or equal to 90% saturates and less than or equal to 0.03% sulfur and have a viscosity index greater than or equal to 80 and less than 120.
- **Group III:** Hydrocracked. Base contain greater than or equal to 90% saturates and less than or equal to 0.03% sulfur and have a viscosity index greater than or equal to 120.
- **Group IV:** The bases are polyalphaolefins (PAO) totally synthetic. These synthetic lubricant basestocks are manufactured through a process called synthesis. They have a much wider temperature range and are excellent for use in extreme cold conditions and high temperature applications..
- **Group V:** Base include all other base stocks not included in Group I, II, III or IV.

But not only the base group composes an engine oil but also lubricant additives are added to improve the performance of the engine oil. Some of them are:

- *Anti-oxidants additives:* which are used to extend the operating life of the oil and avoid the lubricant oxidation.
- *Corrosion inhibitors:* that reduces or eliminates internal rust and corrosion forming a chemical protective barrier.
- *Viscosity Index Improvers:* That partially prevent the oil thinning out as the temperature increases. And they are also responsible for better oil flow at low temperatures, improving fuel economy.
- *Anti-wear (AW) Agents:* These additive are typically used to protect machine parts from wear and loss of metal during boundary lubrication conditions. The most common is Zinc Dialkyl DithioPhosphates (ZDDP).

- *Extreme Pressure (EP) Additives*: They react chemically with metal surfaces to form a sacrificial surface film that prevents the welding and seizure of opposing asperities caused by metal-to-metal contact.
- *Friction Modifiers*: They alter the friction between engine components. The emphasis is on lowering friction to improve fuel economy.

2.2.6.2 Viscosity

After a brief discussion about different lubrication regimes, the lubricant properties themselves must be analyzed. In engine oils, the most important property is its viscosity. Viscosity provides a measure of the resistance of a fluid to shearing flow, and may be defined as the shear stress on a plane within the fluid, per unit velocity gradient normal to that plane [43] as shown in figure 2.5.

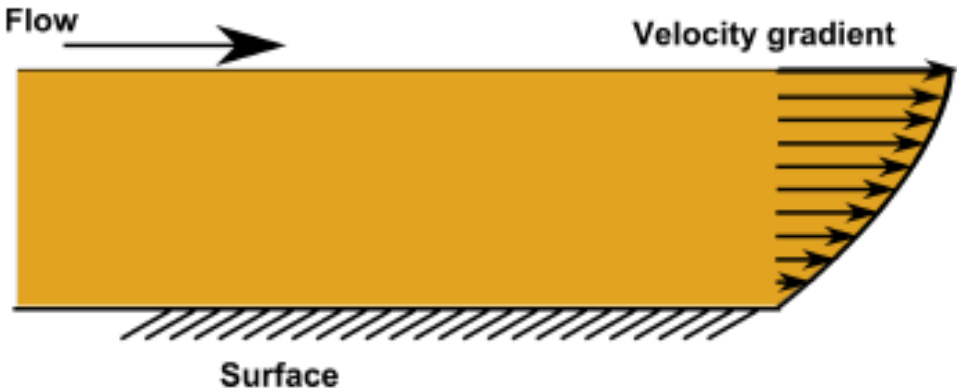


Figure 2.5: Schematic definition of viscosity

In mathematical form, it can be defined as follows:

$$\tau = \mu \frac{du}{dy} \quad (2.3)$$

Where du is the velocity variation of the fluid, and dy the height variation of the fluid caused by shear stress. Also, a new term can be defined:

$$\dot{\gamma} = \frac{du}{dy} \quad (2.4)$$

Where $\dot{\gamma}(s^{-1})$ is known as shear rate.

Although the international measurement system for dynamic viscosity is *Pas*, the commonly system used is the CGS system where the unit is the Poise (P), that is defined as the force in dynes required to move 1 cm^2 layer of fluid parallel to another static layer of 1 cm^2 at a distance of 1 cm within the fluid at a speed of 1 cm/s [41]. In ASTM standars, the dynamic viscosity is quoted as centipoise (cP).

2.2.6.3 Effect of temperature on viscosity

The viscosity of an engine oil has a strong exponential dependence with the temperature. In some cases, the fall could be around 80% with a temperature increase of 25% [41]. During last century, a lot of viscosity-temperature equations have been developed. The simplest fit, called Reynolds viscosity equation is:

$$\mu = \mu_0 \cdot e^{-\dot{\beta} \cdot \Delta\theta} \quad (2.5)$$

Where μ_0 is the viscosity at temperature of reference. $\Delta\theta$ is the difference between reference temperature and the temperature desired and $\dot{\beta}$ is the viscosity-temperature coefficient of the fluid. This fitting equation is not very accurate at very low temperature. Another fit is the equation proposed by Vogel (1921).

$$\mu = a \cdot e^{\frac{b}{\theta-c}} \quad (2.6)$$

The fitting coefficients a , b and c , must be adjusted from data supplied by the lubricant manufacturer, and θ is the temperature at which the dynamic viscosity is evaluated.

Finally, another method of calculating viscosity is used by American Society for Testing Materials (ASTM) [44]. It is based on the expression:

$$\log\log(\nu + 0.6) = d - e \cdot \log\theta \quad (2.7)$$

The solution calculates the kinematic viscosity ν at supplied temperature θ in K. To fit the parameters d and e , at least two viscosity data must to be known.

2.2.6.4 Effect of pressure on viscosity

The viscosity of a lubricant increases exponentially with the pressure increasing. This effect is important when concentrated contacts are given, i.e. in EHL conditions. Barus [45] showed the variation of the viscosity with pressure at constant temperature:

$$\mu_s = \mu_0 \cdot e^{\alpha p} \quad (2.8)$$

Where μ_s is the dynamic viscosity at pressure, p . μ_0 is the viscosity at reference pressure and α is the pressure viscosity coefficient of the engine oil. Figure 2.6 represents the variation of the viscosity with pressure and fitted with Barus equation.

However, Barus equation is not accurate when high pressure is achieved by the oil. As a consequence, Roeland [47] and later Houpert [48], developed an equation for the dependence of viscosity on pressure:

$$\mu_s = \mu_0 \cdot e^{\alpha^* p} \quad (2.9)$$

and

$$\alpha^* = [\ln(\mu_0) + 9.67] \left(-1 + \left(\frac{\Theta - 138}{\Theta_0 - 138} \right)^{-s_0} (1 + 5.1 \cdot 10^{-9} p)^z \right) \quad (2.10)$$

p is evaluated in Pa and Θ in K. Moreover z and s_0 are constants, that are calculated as follow:

$$z = \frac{\alpha_0}{5.1 \cdot 10^{-9} \cdot [\ln(\mu_0) + 9.67]}, s_0 = \frac{\beta_0 (\Theta_0 - 138)}{\ln(\mu_0) + 9.67} \quad (2.11)$$

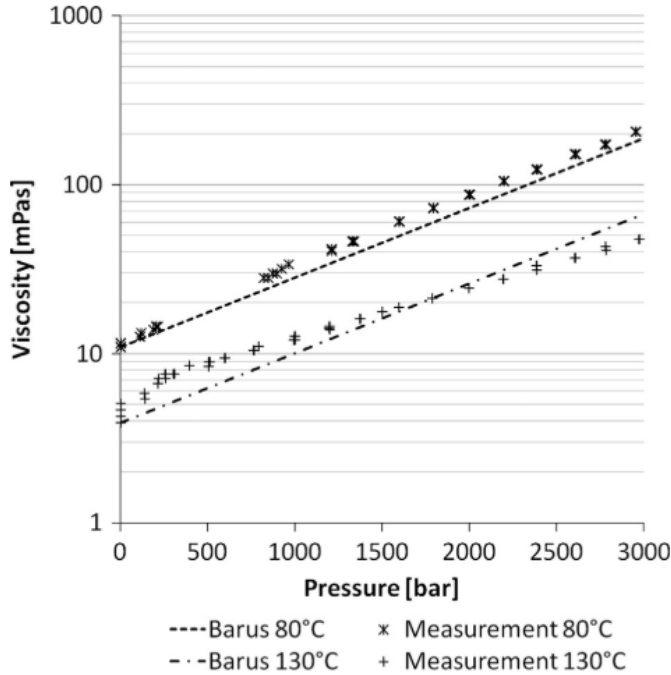


Figure 2.6: Variation of viscosity with pressure. Source: [46]

2.2.6.5 Effect of shear rate on viscosity

Shear rate is the rate at which a fluid is sheared during flow. In more technical terms, it is the rate at which fluid layers move to each other. Figure 2.7 shows the typical engine oil performance against shear rate.

In engine oils, the Non-Newtonian behavior is pseudo-plastic. Depending on the tribological pair of the engine, the shear rate values found can be very different. In journal bearings and piston skirt, where hydrodynamic regime is present, and, therefore, the oil film is thicker, the shear rate found is within the range of $10^5 s^{-1} - 10^6 s^{-1}$. In piston rings, the predominant regime is mixed, so higher shear rate range is found, normally between $10^6 s^{-1}$ and $10^7 s^{-1}$. Finally, in camshafts the higher shear rate values that can arise are of the order of $10^8 s^{-1}$ [49].

Although many authors have proposed different equations that adjust the viscosity variation with the shear rate, the more commonly used and followed in this doctoral thesis is the Cross equation [50]:

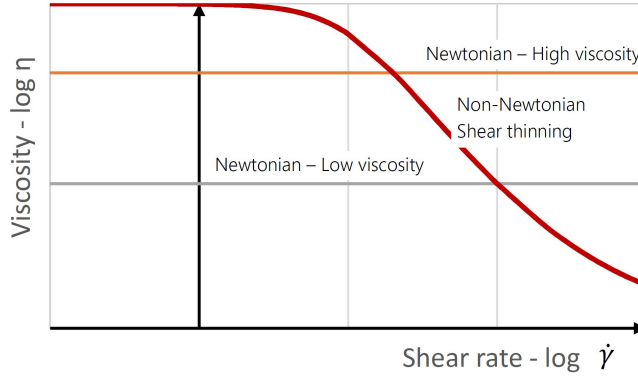


Figure 2.7: Variation of viscosity with shear rate.

$$\mu(\dot{\gamma}, T) = \mu_0(T) \cdot \left(\frac{\mu_\infty}{\mu_0} + \frac{1 - \frac{\mu_\infty}{\mu_0}}{1 + \left(\frac{\dot{\gamma}}{\dot{\gamma}_c}\right)^m} \right) \quad (2.12)$$

In this equation $\mu(\dot{\gamma}, T)$ corresponds with the viscosity of the oil at shear rate $\dot{\gamma}(s^{-1})$ and temperature $T(C)$. $\mu_0(T)$ is the Newtonian viscosity of the oil at temperature $T(C)$. μ_∞ is the viscosity of lubricant at infinity shear rate, that should lie slightly above the viscosity of the polymer-free formulation [51]. $\dot{\gamma}_c$ is the inception of shear thinning and, normally, depends on the temperature. Finally m is a fitted coefficient that takes a value between 0.5 and 1.

2.2.6.6 Viscosity index

The viscosity index is an arbitrary, unit-less measure of a fluid's change in viscosity relative to temperature change. It shows how the temperature change can affect viscosity of an oil. The higher the VI, the smaller the change in fluid viscosity for a given change in temperature and vice versa. Next equation shows how it is calculated:

$$VI = \frac{\nu_0 - \nu}{\nu_0 - \nu_{100}} \cdot 100 \quad (2.13)$$

Being ν_0 the kinematic viscosity of the oil with viscosity index equal to 0 at 40°C and ν_{100} the kinematic viscosity of the oil with viscosity index equal to 100 at 40°C. Finally ν represent the viscosity of the candidate oil at 40°C. Typical values of modern multigrade oils are around 160. This measurement system is defined in standard ASTM D2270.

2.3 Mechanical losses in ICE

Mechanical frictional losses in an ICE are intrinsically related to mechanical parts moving relative to each other. In the engine, the main contribution to mechanical losses can be explained according figure 2.8 [52]. In this figure, the pumping losses are not included.

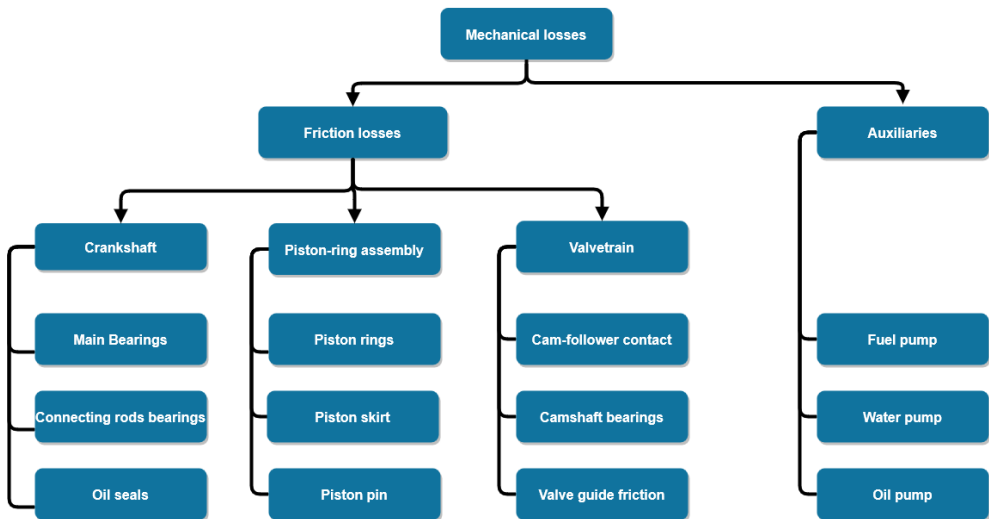


Figure 2.8: ICE Mechanical losses distribution.

2.3.1 Piston assembly

The main purpose of the piston assembly is to convert the energy coming from the fuel into mechanical energy in the crankshaft. During this energy conversion, it is encountered undesirable factors that make the energy conversion less efficient. These are, friction, oil consumption

and noise [53]. According to Tomanik et al. [54] reducing 40% the piston ring friction lead to a 10% of fuel savings. Hence, reducing friction in the piston assembly plays a key role in reducing engine fuel consumption.

2.3.1.1 Piston rings

The piston ring were designed to seal the combustion chamber gases in order to prevent the passage of gases into the crankcase through the piston/ cylinder wall clearance. The current configuration is those adopted by Priest and Taylor, consisting of allowing the combustion chamber gases to pass behind the ring (groove side) to provide a better seal [55]. The main function of the rings is not only to seal the combustion chamber, but also to transfer the heat generated by combustion to the cylinder walls and prevent excessive oil consumption in the combustion chamber, which would increase the pollutant emissions emitted into the atmosphere. The slap noise is the impact between the piston skirt and cylinder liner specially at cold starts [56], also the piston rings sustain the piston in the radial plane, reducing the lateral motion.

In a light duty engine, three different rings are found in the piston. They are located in the piston grooves (Fig. 2.9) normally named as:

- Top compression ring
- Second compression ring
- Oil control ring

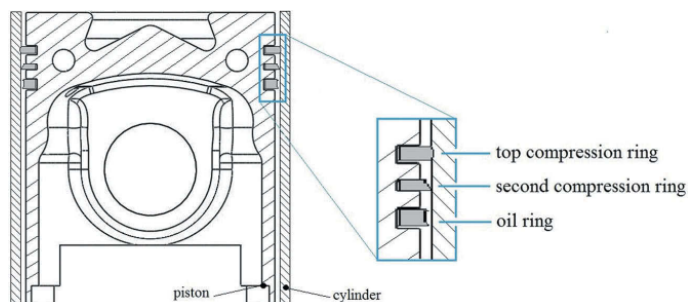


Figure 2.9: Piston rings scheme. Source: [57]

The role of the rings is different in the engine operating conditions. The top compression ring is the main seal between the combustion chamber and the crankcase. The second compression ring has the function of improving the sealing of the combustion chamber, increasing the efficiency of the first ring. Finally, the main task of the oil control ring is regulating the oil supply to the top compression ring [57].

In figure 2.10 an example of the friction mean effective pressure (FMEP) of each different ring installed in the piston is shown. This results come from the model developed in this thesis. The engine operating condition in the presented plot is IMEP = 10.3 bar and hot condition, that is, oil crankcase temperature equal to 90 °C. At low engine speed, the predominant lubrication regime found in the rings is boundary. The operating conditions are the most favorable for the emergence of this regime. However, following the basic theory of lubrication, the higher the engine speed, the higher the contribution of hydrodynamic friction losses. According to the authors in [28, 29], the major contributor to the FMEP in piston rings is the oil control rings, as observed in the figure. Depending on piston-ring configuration, oil temperature and engine working condition, the piston-ring assembly show a more hydrodynamic or more mixed/boundary lubrication regime.

Mufti et al. [58] also shows the oil control ring as the maximum contributor to the friction losses in piston rings because the assumption that boundary lubrication occurs throughout the stroke, but at hot condition the top compression rings friction losses becomes equal to the oil control rings because its lubrication regimen. However, other authors show a more hydrodynamic regime in the piston-ring assembly. Carden et al. [59] calculated by modelling the mechanical friction losses in the piston ring assembly for a heavy duty engine. Their investigation led to the conclusion that in the mid-stroke the predominant regime was hydrodynamic for the rings and the major contributor to the mechanical losses was the top compression ring. Taylor et al. [60] measured in motored condition the friction produced by the piston-ring assembly with different lubricating oils. The tests showed a tendency towards a hydrodynamic regime of the assembly.

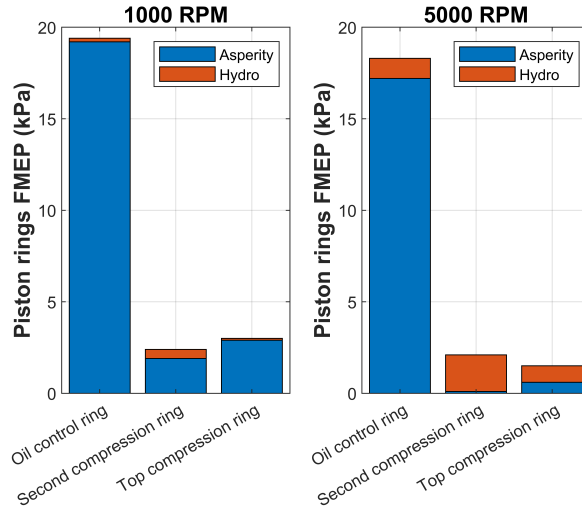


Figure 2.10: Piston rings friction forces. Oil temperature = 90°C . IMEP = 10.3 bar

2.3.1.2 Piston skirt

The piston skirt is the frictional part of the piston that it is not in contact with the combustion gases. That main purpose of the skirt is guiding the piston along the cylinder and provide stability along the up-stroke and down-stroke. The piston skirt must comply with a few requirements related to its strength. First, it must support the lateral forces without a great deformation and it should elastically adapt to the deformations of the cylinder. The combustion temperature and pressure deforms the piston skirt to an oval in the thrust and anti-thrust direction. This increase the skirt diameter in the pin direction. The skirt could collapse due to plastic deformation [61]. The skirt also accommodates the piston during the piston tilt or piston slap conditions, occurring during the surround of dead centers [62]. In order to ensure correct guidance of the skirt to the piston and an oil film, the skirt is always designed with a low clearance. In general terms, the requirements of the piston skirt are:

- Must support lateral load without too much deformation

- Must be adapted to the cylinder deformation
- The piston skirt must be designed to operate under extreme thermal stress.

2.3.2 Crankshaft

In the crankshaft the friction losses come from the bearings. There are two different types of bearings in crankshaft, that is, connecting-rod and journal bearings, as shown in figure 2.11.

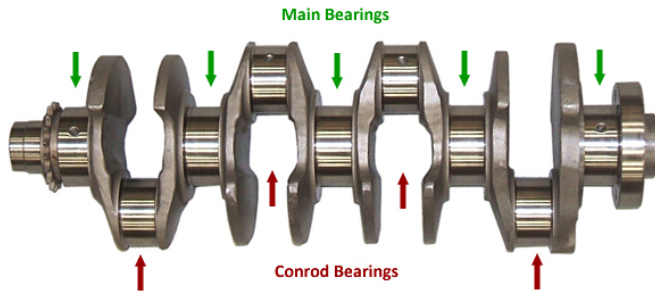


Figure 2.11: Crankshaft bearings.

2.3.2.1 Journal bearings

Journal bearings are the most common types of hydrodynamic bearings. The main aim of the journal bearing is to support the crankshaft. It is commonly used both in crankshaft and camshaft. Engine journal bearings operate under hydrodynamic lubrication, apart from during start/stop condition or under very high loads where elastohydrodynamic lubrication and mix lubrication can become important in lubricating surfaces [63]. The load coming from the in-cylinder pressure is supported by the oil film generated in the bearing. This phenomenon is called bearing load-carrying capacity.

Rao [64] describes a series of advantages of using journal bearings:

- They are often constructed in divided parts or as a whole body and their assembly is simple
- The small clearance renders them usable in high-accuracy constructions
- A hydrodynamic lubricating film is formed between the working surfaces, therefore minimizing the wear of the working parts and maximizing the lifespan of the journal bearing.
- They can withstand large applied loads.

However, the author also describes disadvantages of using them:

- High friction coefficient during the start/stop process
- It is necessary a significant amount of lubricant

2.3.2.2 Con-rod bearings

The role of the con-rod bearings is to sustain the transmitted forces through the connecting rod, which are due to combustion pressure and inertial imbalance, as well as transmitting the torque to drive the crankshaft [53]. Comparing the different parts of the engine, the con-rod bearings support high tensile, compressive and bending stress. If abnormal performance occurs during operation in the con-rod it would have catastrophic consequences on the engine. In the con-rod design, a different approach needs to be considered. At one extreme, the con-rod can have strong load forces, that is, when a Diesel engine operates at low speed and high load. In the other extreme, in gasoline engines, when they are working under high engine speed and low load, the inertia forces are dominating. This considerations are important in order to get a proper design of the con-rod bearing.

Broadly speaking, there are 4 types of connecting rod bearings that can be found in an internal combustion engine. Depending on the type of engine and its specifications, the configuration will differ [65]:

- Plain

- Angle split
- One piece
- Articulated

In light-duty engines the more typical configuration of the connecting-rod is plain. This solution permit the usage of different material types. An angled split connecting rod allows it to be removed from the top of the engine, which aids engine rebuilding while the cylinder block is still in the vehicle. This configuration is typical in truck and locomotive large engines. The main problem of this configuration is the asymmetrical loading supported by the con-rod bearing. The one piece connecting-rod provide a better bearing behavior in terms of friction being lighter and less expensive that a plain rod. Finally, the articulated rod is the more commonly used in radial engines. This solution reduces the axial length for multiple cylinders. Its main application is the radial aircraft engines.

2.3.3 Valvetrain

The main function of the valvetrain system is to synchronize the air inlet to the cylinder and the exhaust gas outlet to perform the combustion process. Therefore, incorrect operation can lead to combustion problems and failure of the entire engine. Air management in the engine is carried out by the intake and exhaust valves. The camshaft, via the cam, drives the mechanism and the intake valve opens continuously. At the moment of the exhaust, the exhaust cam actuates the mechanism to gradually open the exhaust valve and expel the gases coming from the combustion. This process is cyclical.

The valvetrain is a mechanism with a high load supported. As each component has a mass, stiffness and damping the cyclic motion can lead to induce high level of vibrations. Figure 2.12 shows a typical camshaft schematic for a heavy-duty application. This configuration cannot be adopted for a lighter engine due to its vibration level when rotating at high speed.

For light-duty applications, different configurations can be applied as shown in Figure 2.13. This system shows a lower mass of its components

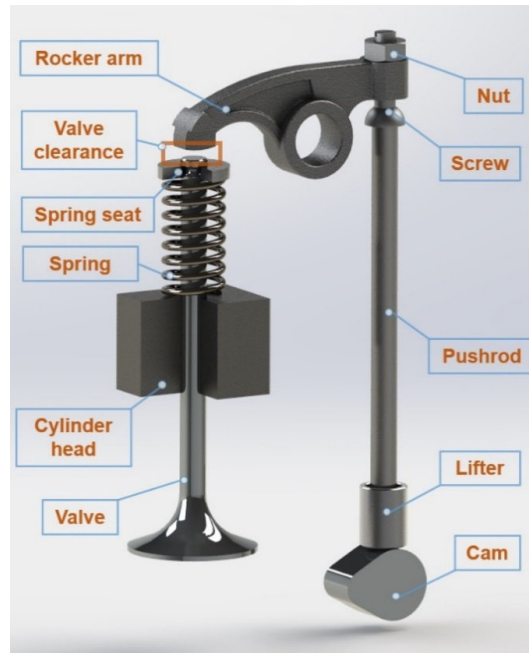


Figure 2.12: Typical valvetrain configuration for heavy-duty application.

and a faster actuation, so the reduction of the moment of inertia is an advantage for its use.



Figure 2.13: Typical valvetrain configuration for light-duty application. Source: [53].

A study carried out by Tong [66] showed that the best configuration in order to reduce valvetrain friction is roller follower. This is because the coefficient of friction of a rolling mechanism is lower than sliding friction.

This is the main problem of the direct acting system. The same author predict that at low engine speed the contribution of valvetrain friction can become up to 20%-25% of the total engine friction losses. Due to its lubrication regime is mainly boundary, the best strategy to reduce valvetrain friction is adding friction modifier additives to the engine oil [67, 68].

2.4 Numerical models applied to assess the friction in ICE

The mechanical friction losses in internal combustion engines are composed of the engine's own sub-components, namely, piston-ring assembly, crankshaft, valvetrain and auxiliary drive. The quantification of the losses of each of the components is a very difficult task to tackle from an experimental point of view. Knauder, Allmaier et al. [69, 70], combined experimental measurement with journal bearing simulation results in order to characterize the engine friction losses. Other authors [71–73] have used the floating liner test rig to measure the friction losses in piston-ring assembly. In general terms, different experimental facilities can be built to characterize the mechanical friction losses in an internal combustion engine, however, the main handicap of this methodology is the cost associated with the experimental realization and the need to have several facilities. Therefore, it is necessary to obtain numerical models that characterize the mechanical friction losses in each subcomponent of the reciprocating internal combustion engine.

2.4.1 Piston-ring assembly

The piston-ring assembly is the major contributor to the friction losses in an engine. Its contribution is between 40% - 50% of the total mechanical losses, in others terms, it represents around 6% of the energy introduced in the vehicle [15]. On piston-ring assembly, the entire lubrication spectrum can be found during its operation, hydrodynamic (mid-stroke), mixed and boundary (around dead centers). This lubrication condition lead to include different models to take into

account the different boundary condition in each crankangle. Different authors have developed complete ring-pack models in order to study the friction losses on it [31, 74–77].

A schematic of the frictional forces acting on the ring is shown in Figure 2.14.

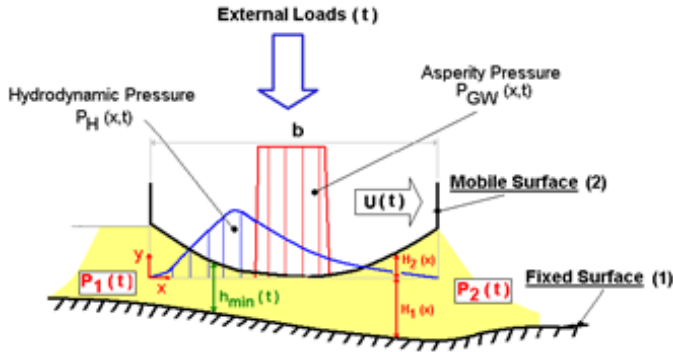


Figure 2.14: Schematic figure of the piston-ring friction forces.

2.4.1.1 Classical Reynolds Equation and Stochastic Asperity Contact Models

The hydrodynamic friction force is governed by the viscous forces of the lubricant. To obtain the viscous forces, firstly it is necessary to obtain the pressure distribution along the ring face, the pressure distribution of thin viscous fluid films in lubrication theory is calculated through classical Reynolds equation, derived from the general Navier-Stokes equations:

$$\frac{\partial}{\partial x} \left(\frac{\rho h^3}{12\mu} \frac{\partial p}{\partial x} \right) = \frac{U}{2} \frac{\partial(\rho h)}{\partial x} + \frac{\partial(\rho h)}{\partial t} \quad (2.14)$$

where p is the hydrodynamic film pressure of the lubricant. μ and ρ are the dynamic viscosity and density of the oil, explained in more detail in the section 2.2.6. U is the slide velocity of the mobile surface, considering that cylinder surface is fixed, and h is the geometry of the lubricant film.

But not only in the ring there is the pressure generated by the oil film, but also the pressure generated by the asperities of the two surfaces are present. The stochastic asperity model, developed by Greenwood-Tripp [78], is used for this purpose. In the Greenwood-Tripp model spherical shape of the asperity is assumed with constant radius β . Moreover the peaks are uniformly distributed with density η of peaks per area unit. Taking into account the assumptions proposed by G-T, the pressure contact is calculated as:

$$p_{asp} = \frac{16\sqrt{2}}{15}\pi(\sigma\beta_0\eta)^2 E\sqrt{\frac{\sigma}{\beta_0}}f_{\frac{5}{2}}\left(\frac{h}{\sigma}\right) \quad (2.15)$$

and

$$f_{\frac{5}{2}} = \frac{1}{\sqrt{2\pi}} \int_x^\infty (s-x)^{5/2} e^{\left(\frac{-s^2}{2}\right)} ds \quad (2.16)$$

Where h is the local film thickness between both surfaces. σ is the composite roughness height deviation $\sigma = \sqrt{\sigma_1^2 + \sigma_2^2}$; $\eta = \frac{\eta_1 + \eta_2}{2}$; $\beta_0 = \left(\frac{1}{\beta_1} + \frac{1}{\beta_2}\right)^{-1}$ and E is the elasticity modulus combined with the Poisson ratio of the material ν such as: $\frac{1}{E} = \left(\frac{1-\nu_1^2}{E_1} + \frac{1-\nu_2^2}{E_2}\right)$. It is assumed that the height of the asperities is fitted by a Gaussian distribution.

The formulation described is the first classical approximation to calculate the friction force generated by the ring-pack. However, as it will be mentioned in next subsections, different authors have developed others methods to better fit and calculated the friction force of the piston-ring assembly.

2.4.1.2 Average Reynolds Equation (Patir and Cheng's average flow model)

Patir and Cheng flow model [32, 33] developed the average Reynolds equation to take into account the influence of the surface roughness in the Poiseuille and Couette flow.

$$\frac{\partial}{\partial x} \left(\phi_p h^3 \frac{\partial p}{\partial x} \right) = 6U\mu \left(\frac{\partial \bar{h}_t}{\partial x} + \sigma \frac{\partial \phi_s}{\partial x} \right) + 12\mu \frac{\partial \bar{h}_t}{\partial t} \quad (2.17)$$

And also, the flow factors affect to the calculation of the oil shear stress:

$$\bar{\tau} = \frac{\mu(U_2 - U_1)}{h} (\phi_f \pm \phi_{fs}) \pm \phi_{fp} \frac{h}{2} \frac{\partial \bar{p}}{\partial x} \quad (2.18)$$

In equation 2.17, \bar{h}_t is the average separation between the surfaces, considering that the surfaces have a Gaussian separation. ϕ_p is the pressure flow factor that represents the surface impedance to flow in the direction of entraining motion. ϕ_s is the shear flow factor that it accounts the extra lubricant transport as a consequence of the shearing effects, induced by surface roughness. According to equation 2.18, ϕ_f and ϕ_{fs} directly affect the mean shear stress (Couette flow) and ϕ_{fp} is related with the horizontal forces induced by local hydrodynamic pressure in rough contacts (Poiseuille flow).

In general terms, flow and shear factors depends of the surface separation (σ/h) and the roughness orientation. The parameter that define the surface roughness was defined by Kubo and Peklenik and adopted the name of Peklenik number:

$$\gamma_p = \frac{\lambda_{0.5x}}{\lambda_{0.5y}} \quad (2.19)$$

Where $\lambda_{0.5}$ represents the length at which the auto-correlation function of a profile reduces to 50 percent of its initial value. And x and y represent the orientation which the autocorrelation function is applied. In purely terms, it will be defined totally transverse these surface whose Peklenik number would be equal to 0. Totally longitudinal would correspond to Peklenik number equal to ∞ and isotropic a Peklenik number equal to 1. This representation has been made in Figure 2.15.

2.4.1.3 Deterministic method - Quasistatic approximation

The classical Reynolds or average Reynolds equation is relatively good in barrel-shaped rings profiles but have the limitations of not predicting oil film pressure when flat parallel surfaces are considered. This case happens in Oil Control Rings (OCRs) in the piston-assembly. In this occasion, Li and Chen proposed a deterministic mixed-lubrication model

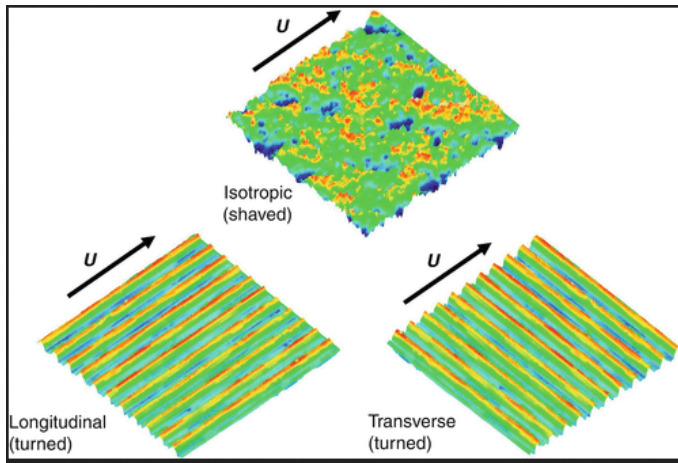


Figure 2.15: Surface roughness orientation. Source: [79].

applied to obtain the hydrodynamic pressure coming from the asperity of the surfaces roughness between a smooth flat surface and a rough cylinder [29, 30]. Similar studies were carried out by Profito and Tomanik [27] that applied the deterministic model to an actual cylinder bore of a Heavy-duty engine before and after 100 h of testing. All of them consider that oil viscosity and surface relative velocity are constants. They concluded that the smoothing of the highest peaks cause significant increase of the hydrodynamic pressures load. In Figure 2.16 the results from the deterministic simulation are depicted. As mentioned at the beginning of the subsection, there is hydrodynamic pressure generated at the microlevel of the surface roughness [80].

2.4.1.4 Deterministic method - Full approximation

The fully deterministic simulations calculate the instantaneous load equilibrium in each crankangle of the cycle. The surface separation and velocity are calculated, not imposed. It accounts for actual ring profile and working conditions but, the main handicap is the CPU time consumption [81].

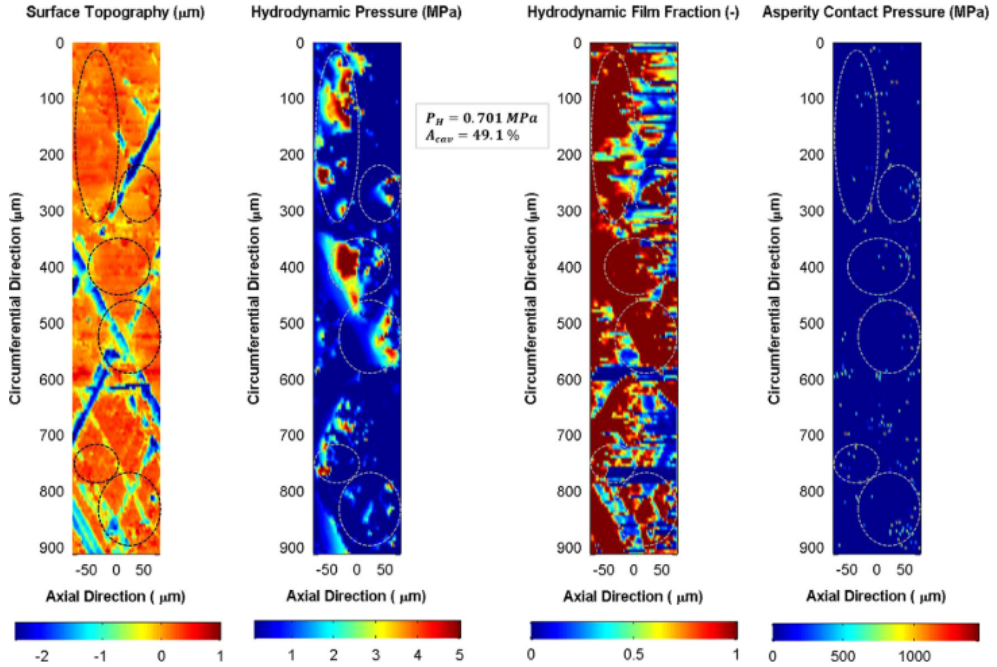


Figure 2.16: Hydrodynamic and asperity pressure between a flat of OCR and cylinder. Source: [27].

2.4.1.5 Other piston ring model considerations

Although the models presented in the previous sections give a good correlation of the frictional losses in the piston ring assembly, other authors have further developed the models by considering the elastohydrodynamic part of the piston rings. Tian [82] evaluated numerical and experimentally the torsion and wear of the ring liner. Moreover, he analyzed the changes that occur in the lubrication oil film. Chen et al. [83] studied the formability of the ring and the thermal effect through a 3D simulation model. Kirner et al. [84] analyzed the secondary movement of the piston and the variation of the oil film thickness. Different authors have studied different tribological performance of the piston rings. Focusing on the properly simulation investigation Gopi et al. [85] carried out a simulation investigation to determine the thermal and structural stress of the piston rings. Turnbull et al. [86] compared

different mathematical models that assess the dynamics of the flexible ring and the dynamic of the rigid ring body.

2.4.2 Piston-skirt

The most important consideration in order to model the piston skirt is the secondary piston motion. In Chapter 3 of this thesis an extensive analysis will be carried out of the dynamic of the piston skirt. A first approximation can be made considering the secondary piston motion and the hydrodynamic and asperity friction forces in the skirt. The Reynolds equation is solved by a finite difference grid of the pad surface.

$$\frac{\partial}{\partial y} \left(\phi_p h^3 \frac{\partial p}{\partial y} \right) + \frac{\partial}{\partial \theta} \left(\phi_p h^3 \frac{\partial p}{\partial \theta} \right) = 6U\mu \left(\frac{\partial \bar{h}_t}{\partial y} + \sigma \frac{\partial \phi_s}{\partial y} \right) + 12\mu \frac{\partial \bar{h}_t}{\partial t} \quad (2.20)$$

Where θ and y are the coordinate system according to Figure 2.17:

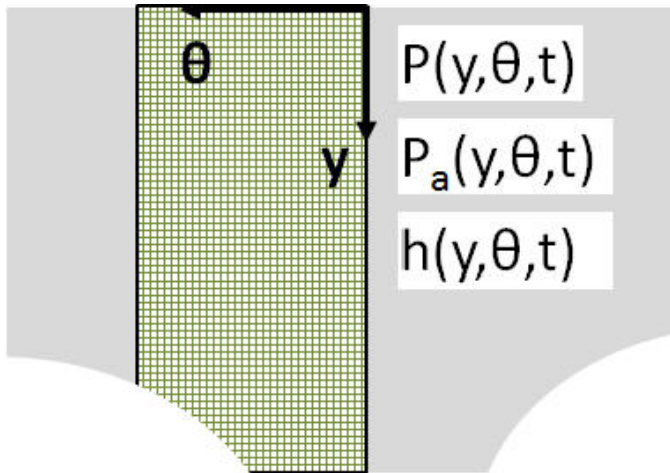


Figure 2.17: Skirt coordinates system.

p is the hydrodynamic pressure of the oil, p_a is the asperity pressure that occurs in the skirt and it is calculated according equation 2.15.

The presented equation is the basic modeling of piston skirt. However, other authors consider other aspects that can influence in piston skirt

model. For example, Tan and Ripin [87] analyzed the contact produced between cylinder liner and piston skirt due to the secondary motion of the piston. Meng et al. [88] studied the vibration on tribological performance and its effect in lateral piston movement. Other authors [89] took into account the inertia of connecting rod to analyze the dynamic movement of the piston, friction losses and lubrication film.

But, one key factor to study is the deformation of the piston produced by temperature. Pelosi and Ivantysynova [90] studied the contact of the cylinder and the piston skirt thermal deformation and the influence of heat flow. Ning et al. [91] developed, considering the deformations of the piston, a lubrication model in the piston skirt. However, in general terms, the deformations experienced by the piston are ignored for the development of the dynamic model [92].

2.4.3 Bearings

Different approach can be done in order to solve the tribology in engine bearings. From numerical solution coming from of the Reynolds equation, that normally consumes few CPU resources until the solution of Reynolds equation considering deformation and the energy equation of Navier-Stokes. As the framework of this thesis consists of solving a 1D model, the more typical solution will be described.

2.4.3.1 Impedance Approach

This approach predicts the forces and torque transferred at a journal bearing between two parts as a function of the states of the parts. Both forces and torque transmitted in a journal bearing depends on the oil pressure and shear stress distribution in the bearing oil film. The oil film pressure is dominated by Reynolds equation and time and axial and tangential coordinates in the film are the independent variables. The solution domain is the entire film. The pressure of the lubricant outside the bearing constitutes the boundary condition for the solution of the equation. The force and torque transmitted to the bearing can be calculated by integrating the oil film pressure and shear stress over the domain. To avoid high computational cost, the solution of the

running maps is calculated based on non-dimensional groups including the variables oil viscosity, bearing radius, eccentricity and speed.

2.4.3.2 Mobility Approach

This approach is the most common method to solve the engine bearings tribology phenomena. This method seek the solution as a function of the known load vector rather than load as a function of states [93]. This model uses non-linear functions fits obtained by numerical solutions of the Reynolds equation [94]. This fit is based on solutions varying not only eccentricity vector magnitude and angle, but also the length/diameter ratio. This methodology has been used in this thesis. In Chapter 3 a more detailed explanation will be made.

2.4.3.3 Reynolds equation

To solve with a more accurate resolution the fluid problem in journal bearing the partial differential Reynolds equation is used. In 1965, Booker [95] studied the 2D Reynolds equation which determine the pressure distribution along the bearing in function of its key parameters as angular velocity ω_J , bearing diameter D , bearing clearance C and lubricant viscosity μ according to next expression:

$$\frac{\partial}{\partial \theta} \left[(1 + e \cos \theta)^3 \frac{\partial p}{\partial \theta} \right] + \left(\frac{D}{2} \right)^2 \frac{\partial}{\partial y} \left[(1 + e \cos \theta)^3 \frac{\partial p}{\partial y} \right] = 12\mu \left(\frac{D}{2C} \right)^2 \left[\frac{de}{dt} \cos \theta + e \left(\frac{d\phi}{dt} - \omega_J \right) \sin \theta \right] \quad (2.21)$$

Variables θ , ϕ , $e = \epsilon/C$ and ω_J are shown in Figure 2.18.

However, hydrodynamic (HD) and elasto-hydrodynamic (EHD) approximation are based in the Reynolds equation (eq. 2.14). Different authors consider the solution of the Reynolds equation with and without shell deformation [97–99]. The load and deformation coming from the inertia were treated in the EHD lubrication theory by Van de Tempel [100] insisting that inertial load has a important role in the EHD lubrication theory. The body force is derived from engine dynamics and structural analysis. Normally, in engine bearings, oil film is considered

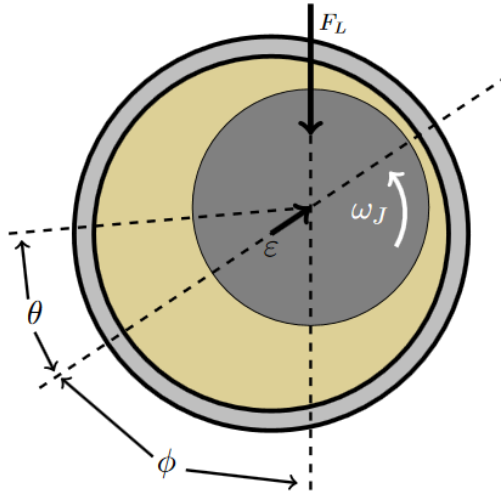


Figure 2.18: Fluid film geometry for a dynamical loaded journal bearing. Source: [96]

as isothermal. But, due to the load supported, the engine temperature in the bearings vary as a results of viscous heat dissipation. Therefore, authors propose the thermohydrodynamic (THD) analysis to improve the performance of the model. In general terms, the THD analysis is composed by Reynolds equation and energy equation in the oil film. Beaman [101] included heat conduction in the bushing and journal. Others authors consider the elastic and thermal deformation of the bearing [102]. In [103], the author compare the connecting rod bearing, validating a model with experimental results. On the other hand, Chamani [104] considers the TEHD analysis more accurately in the engines working under severe condition for a better prediction of the bearing performances in internal combustion engines.

2.4.4 Valvetrain

Modeling the engine valvetrain has been a challenge for engine developers since it is the third largest energy loss among the tribological system. Due to high contact pressure and relative oil film thin, the contact between cam and follower is modeled under elasto-hydrodynamic

lubrication theory, so the contact type is considered punctual or even lineal. The cam lubrication was approached for first time by Dyson and Naylor [105], they studied the tappet distresses which are scuffing and polishing. They thought that the appearance of these problems could be controlled by the temperature in the contact region. Lastly, Dyson [106] considered the Hertzian stress and lubricant film thickness over the cam cycle. At the contact zone, the load is a key parameter that controls the elasto-hydrodynamic lubrication being complicated to evaluate along the cam cycle.

The transient EHD analysis were carried out by Kushwaha [107] and Teodorescu et al. [108]. They found that at the flow reversal the constriction in the oil film moves quickly from one side of the contact patch to the other. Later, authors in [109] made a tribological analysis within a multi-physics approach in piston and valve train system. Wu et al. [110] studied in a TEHD model in cam tappet pair, the influence of considering the temperature in the model. They concluded that considering isothermal analysis give an overestimation of the film thickness at some angular position of the cam.

Other authors measured the oil film thickness in the cam contact and developed numerical models. Dowson and Higginson developed a simple formula to estimate the oil film thickness in the contact [111]. That formula was modified by different researchers in [112]. Shirzadegan et al. [113] developed a steady-state model of cam-roller follower system to predict the film thickness variation and contact pressure distribution in an engine cycle. This model is based on a previous work developed by Habchi et al. [114] and they concluded that the edge effects associated with the profile, smoothed the pressure distributions in the film and neglecting the profiled shape of the roller cause and overestimate of the minimum oil film thickness.

Bibliography

- [1] Kobayashi S., Plotkin S. and Ribeiro S. K. “Energy efficiency technologies for road vehicles”. *Energy Efficiency*, Vol. 2 n° 2, pp. 125–137, jan 2009.
- [2] Macián V., Tormos B., Ruíz S. and Ramírez L. “Potential of low viscosity oils to reduce CO2 emissions and fuel consumption of urban buses fleets”. *Transportation Research Part D: Transport and Environment*, Vol. 39, pp. 76–88, 2015.
- [3] Tormos B., Pla B., Bastidas S., Ramírez L. and Pérez T. “Fuel economy optimization from the interaction between engine oil and driving conditions”. *Tribology International*, Vol. 138, pp. 263–270, 2019.
- [4] Zammit J. P., McGhee M. J., Shayler P. and Pegg I. “Benefits of cylinder deactivation on a diesel engine and restrictions due to low boost”. *Internal Combustion Engines: Performance, Fuel Economy and Emissions*, pp. 95–108, 2013.
- [5] Zhao J., Xi Q., Wang S. and Wang S. “Improving the partial-load fuel economy of 4-cylinder SI engines by combining variable valve timing and cylinder-deactivation through double intake manifolds”. *Applied Thermal Engineering*, Vol. 141, pp. 245–256, 2018.
- [6] Shu J., Fu J., Zhao D., Liu J., Ma Y., Deng B., Zeng D., Liu J. and Zhang Y. “Numerical investigation on the effects of valve timing on in-cylinder flow, combustion and emission performance of a diesel ignition natural gas engine through computational fluid dynamics”. *Energy Conversion and Management*, Vol. 198, pp. 111786, 2019.
- [7] Dhingra R. and Das S. “Life cycle energy and environmental evaluation of downsized vs. lightweight material automotive engines”. *Journal of Cleaner Production*, Vol. 85, pp. 347–358, 2014.
- [8] Galindo J., Serrano J. R., Climent H. and Varnier O. “Impact of two-stage turbocharging architectures on pumping losses of automotive engines based on an analytical model”. *Energy Conversion and Management*, Vol. 51 n° 10, pp. 1958–1969, 2010.
- [9] Piqueras P., Sanchis E. J., Herreros J. M. and Tsolakis A. “Evaluating the oxidation kinetic parameters of gasoline direct injection soot from thermogravimetric analysis experiments”. *Chemical Engineering Science*, 2021.
- [10] Luján J. M., Climent H., Novella R. and Rivas-Perea M. “Influence of a low pressure EGR loop on a gasoline turbocharged direct injection engine”. *Applied Thermal Engineering*, Vol. 89, pp. 432–443, 2015.
- [11] Liu H., Han L. and Cao Y. “Improving transmission efficiency and reducing energy consumption with automotive continuously variable transmission: A model prediction comprehensive optimization approach”. *Applied Energy*, Vol. 274, 2020.

-
- [12] Mayet C., Welles J., Bouscayrol A., Hofman T. and Lemaire-Semail B. "Influence of a CVT on the fuel consumption of a parallel medium-duty electric hybrid truck". *Mathematics and Computers in Simulation*, Vol. 158, pp. 120–129, 2019.
- [13] Vaezipour A., Rakotonirainy A. and Haworth N. "Reviewing In-vehicle Systems to Improve Fuel Efficiency and Road Safety". *Procedia Manufacturing*, Vol. 3, pp. 3192–3199, 2015.
- [14] Hooker J. N. "Optimal driving for single-vehicle fuel economy". *Transportation Research Part A: General*, Vol. 22 n° 3, pp. 183–201, 1988.
- [15] Holmberg K., Andersson P. and Erdemir A. "Global energy consumption due to friction in passenger cars". *Tribology International*, Vol. 47, pp. 221–234, mar 2012.
- [16] Holmberg K. and Erdemir A. "The impact of tribology on energy use and CO₂ emission globally and in combustion engine and electric cars". *Tribology International*, Vol. 135, pp. 389–396, jul 2019.
- [17] Wang Y. and Wang Q. J. *Lubrication Regimes*. 2013.
- [18] Hutchings I. and Shipway P. *Friction and Wear of Engineering Materials*. 2017.
- [19] Payri F. and Desantes J. M. *Motores de Combustión Interna Alternativos*, volume 66. Reverté S.A., 2011.
- [20] Stribeck R. *Die wesentlichen Eigenschaften der Gleit- und Rollenlager*. 1902.
- [21] Vakis A., Yastrebov V., Scheibert J., Nicola L., Dini D., Minfray C., Almqvist A., Paggi M., Lee S., Limbert G., Molinari J., Anciaux C., Aghababaei R., Echeverri Restrepo S., Papangelo A., Cammarata A., Nicolini P., Putignano C., Carbone G., Stupkiewicz S., Lengiewicz J., Costagliola G., Bosia F., Guarino R., Pugno N., Müser M. and Ciavarella M. "Modeling and simulation in tribology across scales: An overview". *Tribology International*, Vol. 125, pp. 169–199, 2018.
- [22] Tower B. "First Report on Friction Experiments". *Proceedings of the Institution of Mechanical Engineers*, Vol. 35 n° 1, pp. 29–35, 1884.
- [23] Tower B. "Second Report on Friction Experiments". *Proceedings of the Institution of Mechanical Engineers*, Vol. 36 n° 1, pp. 58–70, 1885.
- [24] Reynolds O. "IV. On the Theory of Lubrication and its Application to Mr. Beauchamps Tower's Experiments, including an Experimental Determination of the Viscosity of Olive Oil". *Philosophical Transactions*, pp. 157–234, 1886.
- [25] Dobrica M. and Fillon M. "Encyclopedia of Tribology". *Encyclopedia of Tribology*, n° 2001, pp. 2284–2291, 2013.
- [26] Rahnejat H., Offner G., Knaus O., Turnbull R., Bewsher S., Mohammadpour M. and Rahmani R. "Effect of cylinder de-activation on the tribological performance of compression ring conjunction". *Proceedings of the Institution of*

- Mechanical Engineers, Part J: Journal of Engineering Tribology*, Vol. 231 n° 8, pp. 997–1006, 2017.
- [27] Profito F., Tomanik E. and Zachariadis D. “Effect of cylinder liner wear on the mixed lubrication regime of TLOCs”. *Tribology International*, Vol. 93, pp. 723–732, 2016.
- [28] Chen H., Li Y. and Tian T. “A novel approach to model the lubrication and friction between the twin-land oil control ring and liner with consideration of micro structure of the liner surface finish in internal combustion engines”. *SAE Technical Papers*, n° 2008-01-1613, 2008.
- [29] Li Y., Chen H. and Tian T. “A deterministic model for lubricant transport within complex geometry under sliding contact and its application in the interaction between the oil control ring and rough liner in internal combustion engines”. *SAE Technical Papers*, n° 2008-01-1615, 2008.
- [30] H. Chen. *Modeling the Lubrication of the Piston Ring Pack in Internal Combustion Engines Using the Deterministic Method*. Massachusetts Institute of Technology, 2009.
- [31] Gu C. and Zhang D. “Modeling and prediction of the running-in behavior of the piston ring pack system based on the stochastic surface roughness”. *Proceedings of the Institution of Mechanical Engineers, Part J: Journal of Engineering Tribology*, Vol. 233 n° 12, pp. 1857–1877, dec 2019.
- [32] Patir N. and Cheng H. “An Average Flow Model for Determining Effects of Three-Dimensional Roughness on Partial Hydrodynamic Lubrication”. *Journal of Tribology*, Vol. 100, pp. 12–17, 1978.
- [33] Patir N. and Cheng H. “Application of Average Flow Model to Lubrication Between Rough Sliding Surfaces”. *Journal of Lubrication Technology*, Vol. 101 n° 2, pp. 220–229, 1979.
- [34] Hardy B. and Doubleday I. “Boundary lubrication. The paraffin series”. *Proceedings of the Royal Society of London. Series A, Containing Papers of a Mathematical and Physical Character*, Vol. 100 n° 707, pp. 550–574, 1922.
- [35] Sgroi M., Asti M., Gili F., Deorsola F., Bensaid S., Fino D., Kraft G., Garcia I. and Dassenoy F. “Engine bench and road testing of an engine oil containing MoS₂ particles as nano-additive for friction reduction”. *Tribology International*, Vol. 105, pp. 317–325, 2017.
- [36] Yamamoto K., Hiramatsu T., Hanamura R., Moriizumi Y. and Heiden S. “The Study of Friction Modifiers to Improve Fuel Economy for WLTP with Low and Ultra-Low Viscosity Engine Oil”. *SAE Technical Papers*, n° 2019-01-2205, 2019.
- [37] Sagawa T., Nakano S., Shouganji I., Okuda S. and Nakajo T. “MR20DD Motoring Fuel Economy Test for 0W-12 and 0W-8 Low Viscosity Engine Oil”. *SAE Technical Papers*, n° 2019-01-2295, 2019.

- [38] Kano M. “Diamond-Like Carbon Coating Applied to Automotive Engine Components”. *Tribology Online*, Vol. 9 n° 3, pp. 135–142, 2014.
- [39] Zhmud B., Tomanik E., Grabon W., Schorr D. and Brodmann B. “Optimizing the Piston/Bore Tribology: The Role of Surface Specifications, Ring Pack, and Lubricant”. *SAE Technical Papers*, n° 2020-01-2167, pp. 1–8, 2020.
- [40] Tomanik E., Fujita H., Sato S., Paes E., Galvao C. and Morais P. “Investigation of PVD piston ring coatings with different lubricant formulations”. *ASME 2017 Internal Combustion Engine Division Fall Technical Conference, ICEF 2017*, Vol. 2, pp. 1–10, 2017.
- [41] Ramírez L. *Contribution to the assessment of the potential of low viscosity engine oils to reduce ICE fuel consumption and CO2 emissions*. Universitat Politècnica de València, 2016.
- [42] American Petroleum Institute. *Annex E - API Base oil interchangeability guidelines for passenger car motor oils and Diesel engine oils*. 2019.
- [43] Hutchings I. and Shipway P. “Lubricants and Lubrication”. In *Tribology. Friction and Wear of Engineering Materials*, pp. 79–105. 2016.
- [44] American Society for Testing Material. *Designation D341-20: Standard Practice for Viscosity Temperature Equations and Charts for Liquid Petroleum or Hydrocarbon Products*. 2020.
- [45] Barus C. “Isothermals, isopiestic and isometrics relative to viscosity”. *American Journal of Science*, Vol. s3-45 n° 266, pp. 87–96, 1893.
- [46] Sander D., Allmaier H., Priebsch H., Reich F., Witt M., Füllenbach T., Skiadas A., Brouwer L. and Schwarze H. “Impact of high pressure and shear thinning on journal bearing friction”. *Tribology International*, Vol. 81, pp. 29–37, 2015.
- [47] Roelands C. *Correlational aspects of the viscosity-temperature-pressure relationship of lubricants oils*. 1966.
- [48] Houpert L. “New results of traction force calculations in elastohydrodynamic contacts”. *Journal of Tribology*, Vol. 107 n° 2, pp. 241–245, 1985.
- [49] Taylor R. I. and De Kraker B. R. “Shear rates in engines and implications for lubricant design”. *Proceedings of the Institution of Mechanical Engineers, Part J: Journal of Engineering Tribology*, Vol. 231, pp. 1106–1116, 2017.
- [50] Cross M. “Rheology of non-Newtonian fluids: A new flow equation for pseudoplastic systems”. *Journal of Colloid Science*, Vol. 20 n° 5, pp. 417–437, 1965.
- [51] Marx N., Fernández L., Barceló F. and Spikes H. “Shear Thinning and Hydrodynamic Friction of Viscosity Modifier-Containing Oils. Part I: Shear Thinning Behaviour”. *Tribology Letters*, Vol. 66, 2018.
- [52] Heywood J.B. *Internal combustion engine fundamentals*. Mc Graw-Hill series in mechanical engineering. McGraw-Hill, New York/etc, 1988.

- [53] Rahnejat H. *Tribology and Dynamics of Engine and Powertrain: Fundamentals, Applications and Future Trends*. 2010.
- [54] Tomanik E., Profito F., Sheets B. and Souza R. “Combined lubricant - surface system approach for potential passenger car CO₂ reduction on piston-ring-cylinder bore assembly”. *Tribology International*, Vol. 149 n^o July, pp. 1–12, 2020.
- [55] Priest M. and Taylor C. M. “Automobile engine tribology - approaching the surface”. *Wear*, Vol. 241 n^o 2, pp. 193–203, jul 2000.
- [56] Cho S. H., Ahn S. T. and Kim Y. H. “A simple model to estimate the impact force induced by piston slap”. *Journal of Sound and Vibration*, Vol. 255 n^o 2, pp. 229–242, aug 2003.
- [57] Ferreira R., Martins J., Carvalho O., Sobral L., Carvalho S. and Silva F. “Tribological solutions for engine piston ring surfaces: an overview on the materials and manufacturing”. *Materials and Manufacturing Processes*, Vol. 35 n^o 5, pp. 498–520, apr 2020.
- [58] Mufti R. A., Priest M. and Chittenden R. J. “Analysis of piston assembly friction using the indicated mean effective pressure experimental method to validate mathematical models”. *Proceedings of the Institution of Mechanical Engineers, Part D: Journal of Automobile Engineering*, Vol. 222, pp. 1441–1457, 2008.
- [59] Carden P., Pisani C., Laine E., Field I., Devine M., Schoeni A. and Beyer P. “Calculation of crank train friction in a heavy duty truck engine and comparison with measured data”. *Proceedings of the Institution of Mechanical Engineers, Part J: Journal of Engineering Tribology*, Vol. 227, pp. 168–184, 2013.
- [60] Taylor R. I., Morgan N., Mainwaring R. and Davenport T. “How much mixed/boundary friction is there in an engine and where is it?”. *Proceedings of the Institution of Mechanical Engineers, Part J: Journal of Engineering Tribology*, Vol. 234, pp. 1563–1579, 10 2020.
- [61] GmbH Mahle. *Pistons and engine testing*.
- [62] Krishnanl A. *Simulation of an engine friction strip test*. Chalmers University, 2014.
- [63] Mufti R. and Priest M. “Theoretical and experimental evaluation of engine bearing performance”. *Proceedings of the Institution of Mechanical Engineers, Part J: Journal of Engineering Tribology*, Vol. 223 n^o 4, pp. 629–644, 2009.
- [64] Rao T., Rani A., Nagarajan T. and Hashim F. “Analysis of slider and journal bearing using partially textured slip surface”. *Tribology International*, Vol. 56, pp. 121–128, dec 2012.
- [65] Hoag K. and Dondlinger B. *Cranktrain Crankshafts, Connecting Rods, and Flywheel*. 2016.

- [66] Tung S. and McMillan L. “Automotive tribology overview of current advances and challenges for the future”. *Tribology International*, Vol. 37 n° 7, pp. 517–536, jul 2004.
- [67] Wong V. W. and Tung S. “Overview of automotive engine friction and reduction trends - Effects of surface, material, and lubricant-additive technologies”. *Friction*, Vol. 4 n° 1, pp. 1–28, mar 2016.
- [68] Phillips C., McQueen J., Gao H., Stockwell R., Hardy B. and Graham M. “Design considerations in formulating gasoline engine lubricants for improving engine fuel economy and wear resistance part I: Base oils and additives”. *SAE Technical Papers*, n° 2007-01-4143, 2007.
- [69] Knauder C., Allmaier H., Sander D. and Sams T. “Investigations of the Friction Losses of Different Engine Concepts. Part 1: A Combined Approach for Applying Subassembly-Resolved Friction Loss Analysis on a Modern Passenger-Car Diesel Engine”. *Lubricants*, Vol. 7 n° 5, pp. 39, apr 2019.
- [70] Knauder C., Allmaier H., Sander D. and Sams T. “Investigations of the Friction Losses of Different Engine Concepts. Part 2: Sub-Assembly Resolved Friction Loss Comparison of Three Engines”. *Lubricants*, Vol. 7 n° 12, pp. 105, nov 2019.
- [71] Nagano Y., Ito A., Okamoto D. and Yamasaka K. “A study on the feature of several types of floating liner devices for piston friction measurement”. *SAE Technical Papers*, n° 2019-01-0177, apr 2019.
- [72] Gore M., Theaker M., Howell-Smith S., Rahnejat H. and King P. “Direct measurement of piston friction of internal-combustion engines using the floating-liner principle”. *Proceedings of the Institution of Mechanical Engineers, Part D: Journal of Automobile Engineering*, Vol. 228 n° 3, pp. 344–354, feb 2014.
- [73] Tabata H., Kaneko N. and Mihara Y. “Improvement in Accuracy of Piston frictional force measurement using floating liner engine”. *Tribology Online*, Vol. 12 n° 3, pp. 141–146, jul 2017.
- [74] Tian T., Wong V. and Heywood J. “A piston ring-pack film thickness and friction model for multigrade oils and rough surfaces”. *SAE Technical Papers*, 1996.
- [75] Wolff A. “Numerical Analysis of the System Piston-Ring-Cylinder of an Automotive IC Engine”. *SAE Technical Papers*, n° 2020-01-2160, sep 2020.
- [76] Mahmoud K., Knaus O., Parikyan T., Offner G. and Sklepik S. “An integrated model for the performance of piston ring pack in internal combustion engines”. *Proceedings of the Institution of Mechanical Engineers, Part K: Journal of Multi-body Dynamics*, Vol. 232 n° 3, pp. 371–384, sep 2018.
- [77] Delprete C. and Razavykia A. “Piston ring-liner lubrication and tribological performance evaluation: A review”. *Proceedings of the Institution of Mechanical Engineers, Part J: Journal of Engineering Tribology*, Vol. 232 n° 2, pp. 193–209, feb 2018.

- [78] Greenwood J. and Tripp J. “The contact of two nominally flat rough surfaces”. *Proceedings of the Institution of Mechanical Engineers*, Vol. 185, pp. 625–633, 1970.
- [79] Zhu D. and Ren N. “Roughness Effect on Elastohydrodynamic Lubrication”. In *Encyclopedia of Tribology*, pp. 2955–2967. 2013.
- [80] Grützmacher P., Profito F. and Rosenkranz A. “Multi-scale surface texturing in tribology-current knowledge and future perspectives”. *Lubricants*, Vol. 7 n° 11, 2019.
- [81] Checo H., Ausas R., Jai M., Cadalen J., Choukroun F. and Buscaglia G. “Moving textures: Simulation of a ring sliding on a textured liner”. *Tribology International*, Vol. 72, pp. 131–142, apr 2014.
- [82] Tian T. “Dynamic behaviours of piston rings and their practical impact. Part 2: Oil transport, friction and wear of ring/liner interface and the effects of piston and ring dynamics”. *Proceedings of the Institution of Mechanical Engineers, Part J: Journal of Engineering Tribology*, Vol. 216 n° 4, pp. 229–248, apr 2002.
- [83] Cheng C., Kharazmi A., Schock H., Wineland R. and Brombolich L. “Three-dimensional piston ring-cylinder bore contact modeling”. *Journal of Engineering for Gas Turbines and Power*, Vol. 137 n° 11, nov 2015.
- [84] Kirner C., Halbhuber J., Uhlig B., Oliva A., Graf S. and Wachtmeister G. “Experimental and simulative research advances in the piston assembly of an internal combustion engine”. *Tribology International*, Vol. 99, pp. 159–168, jul 2016.
- [85] Gopi E., Saleem M., Chandan S. and Nema A. “Thermal and static analysis of engine piston rings”. *International Journal of Ambient Energy*, 2019.
- [86] Turnbull R., Dolatabadi N., Rahmani R. and Rahnejat H. “An assessment of gas power leakage and frictional losses from the top compression ring of internal combustion engines”. *Tribology International*, Vol. 142, pp. 105991, feb 2020.
- [87] Tan Y. and Ripin M. “Technique to determine instantaneous piston skirt friction during piston slap”. *Tribology International*, Vol. 74, pp. 145–153, jun 2014.
- [88] Meng F., Wang X., Li T. and Chen Y. “Influence of cylinder liner vibration on lateral motion and tribological behaviors for piston in internal combustion engine”. *Proceedings of the Institution of Mechanical Engineers, Part J: Journal of Engineering Tribology*, Vol. 229 n° 2, pp. 151–167, feb 2015.
- [89] Meng X., Ning L., Xie Y. and Wong V. “Effects of the connecting-rod-related design parameters on the piston dynamics and the skirt-liner lubrication”. *Proceedings of the Institution of Mechanical Engineers, Part D: Journal of Automobile Engineering*, Vol. 227 n° 6, pp. 885–898, jun 2013.
- [90] Pelosi M. and Ivantysynova M. “Heat transfer and thermal elastic deformation analysis on the Piston-Cylinder interface of axial piston machines”. *Journal of Tribology*, Vol. 134 n° 4, oct 2012.

-
- [91] Ning L., Meng X. and Xie Y. “Incorporation of deformation in a lubrication analysis for automotive piston skirt-liner system”. *Proceedings of the Institution of Mechanical Engineers, Part J: Journal of Engineering Tribology*, Vol. 227 n° 6, pp. 654–670, jun 2013.
- [92] Forero J., Ochoa G. and Alvarado W. “Study of the Piston Secondary Movement on the Tribological Performance of a Single Cylinder Low-Displacement Diesel Engine”. *Lubricants*, Vol. 8 n° 11, pp. 97, oct 2020.
- [93] Booker J. “Dynamically-Loaded Journal Bearings: Numerical Application of the Mobility Method”. *Journal of Lubrication Technology*, Vol. 93 n° 1, pp. 168, 1971.
- [94] Goenka P. “Analytical Curve Fits for Solution Parameters of Dynamically Loaded”. *Journal of Tribology*, Vol. 106 n° 83, pp. 421–427, 1984.
- [95] Booker F. “Dynamically loaded journal bearings: Mobility method of solution”. *Journal of Fluids Engineering, Transactions of the ASME*, Vol. 87 n° 3, pp. 537–546, sep 1965.
- [96] Kälvelid F. *Numerical Modeling of Plain Journal Bearings within a Heavy-Duty Engine Oil System using GT-SUITE*. 2016.
- [97] LaBouff G. and Booker J. “Dynamically Loaded Journal Bearings: A Finite Element Treatment for Rigid and Elastic Surfaces”. *Journal of Tribology*, Vol. 107 n° 4, pp. 505–513, oct 1985.
- [98] Allmaier H., Sander D. and Reich F. “Simulating friction power losses in automotive journal bearings”. *Procedia Engineering*, Vol. 68, pp. 49–55, jan 2013.
- [99] Ai X., Cheng H., Hua D., Moteki K. and Aoyama S. “A finite element analysis of dynamically loaded journal bearings in mixed lubrication”. *Tribology Transactions*, Vol. 41 n° 2, pp. 273–281, jan 1998.
- [100] Van der Tempel L., Moes H. and Bosma R. “Numerical simulation of dynamically loaded flexible short journal bearings”. *Journal of Tribology*, Vol. 107 n° 3, pp. 396–401, jul 1985.
- [101] Beaman J. “Thermohydrodynamic analysis of laminar incompressible journal bearings”. *Tribology Transactions*, Vol. 29 n° 2, pp. 141–150, 1986.
- [102] Khonsari M. and Wang H. “On the fluid-solid interaction in reference to thermoelastohydrodynamic analysis of journal bearings”. *Journal of Tribology*, Vol. 113 n° 2, pp. 398–404, apr 1991.
- [103] Souchet D., Hoang L. and Bonneau D. “Thermoelastohydrodynamic lubrication for the connecting rod big-end bearing under dynamic loading”. *Proceedings of the Institution of Mechanical Engineers, Part J: Journal of Engineering Tribology*, Vol. 218 n° 5, pp. 451–464, may 2004.

- [104] Chamani H., Karimaei H., Bahrami M. and Mirsalim S. “Thermo-elasto-hydrodynamic (TEHD) analysis of oil film lubrication in big end bearing of a diesel engine”. *Journal of Computational and Applied Research in Mechanical Engineering*, Vol. 5, pp. 13–24, 2015.
- [105] Dyson A. and Naylor H. “Application of the Flash Temperature Concept to Cam and Tappet Wear Problems”. *Proceedings of the Institution of Mechanical Engineers: Automobile Division*, Vol. 14 n° 1, pp. 255–280, jan 1960.
- [106] Dyson A. “Kinematics and wear patterns of cam and finger follower automotive valve gear”. *Tribology International*, Vol. 13 n° 3, pp. 121–132, jun 1980.
- [107] Kushwaha M. and Rahnejat H. “Transient elastohydrodynamic lubrication of finite line conjunction of cam to follower concentrated contact”. *Journal of Physics D: Applied Physics*, Vol. 35 n° 21, pp. 2872–2890, nov 2002.
- [108] Teodorescu M., Kushwaha M., Rahnejat H. and Taraza D. “Elastodynamic transient analysis of a four-cylinder valvetrain system with camshaft flexibility”. *Proceedings of the Institution of Mechanical Engineers, Part K: Journal of Multi-body Dynamics*, Vol. 219 n° 1, pp. 13–25, mar 2005.
- [109] Teodorescu M., Balakrishnan S. and Rahnejat H. “Integrated tribological analysis within a multi- physics approach to system dynamics”. *Tribology and Interface Engineering Series*, Vol. 48, pp. 725–737, jan 2005.
- [110] Wu W., Wang J. and Venner C. “Thermal Elastohydrodynamic Lubrication of an Optimized Cam-Tappet Pair in Smooth Contact”. *Journal of Tribology*, Vol. 138 n° 2, apr 2016.
- [111] Dowson D. and Higginson G. *Elasto-Hydrodynamic Lubrication*. 1977.
- [112] Staron J. and Willermet P. “An analysis of valve train friction in terms of lubrication principles”. *SAE Technical Papers*, 1983.
- [113] Shirzadegan M., Almqvist A. and Larsson R. “Fully coupled EHL model for simulation of finite length line cam-roller follower contacts”. *Tribology International*, Vol. 103, pp. 584–598, nov 2016.
- [114] Habchi W., Eyheramendy D., Vergne P. and Morales-Espejel G. “A full-system approach of the elastohydrodynamic line-point contact problem”. *Journal of Tribology*, Vol. 130 n° 2, pp. 1–10, apr 2008.

Chapter 3

Experimental tools and theoretical model

Contents

3.1	Introduction	63
3.2	Experimental tools	63
3.2.1	Steady state: Engine and test cell characteristics	63
3.2.2	Transient state: Vehicle and test cell characteristics	66
3.3	Engine friction: steady state theoretical models	68
3.3.1	Piston-ring model	68
3.3.1.1	Gas pressure force: blow-by model .	70
3.3.1.2	Ring tension force	72
3.3.1.3	Piston assembly temperature	72
3.3.1.4	Hydrodynamic friction force	74
3.3.1.5	Asperity friction force	76
3.3.1.6	Coefficient of friction measurement .	77
3.3.2	Piston skirt model	81
3.3.3	Bearings	82

3.3.3.1	Mobility method	83
3.3.3.2	Reynolds equation	84
3.3.4	Valvetrain	85
3.3.5	Auxiliaries	87
3.3.5.1	Coolant pump	87
3.3.5.2	Oil pump power	88
3.3.5.3	Fuel pump power	89
3.4	Engine friction: transient theoretical model	90
	Bibliography	93

3.1 Introduction

In the research works, the use of experimental and theoretical models is necessary to get a consolidated work and relevant results. Especially in this doctoral thesis, both experimental tools and a theoretical model have been used to study the phenomenon of tribology in an Internal Combustion Engine. For this reason, in this chapter the tools used will be detailed, as well as the hypotheses assumed for the theoretical model development.

This chapter will be structured in two sections:

- First section will describe the experimental setup used to perform the experimental tests under both stationary and transient conditions
- Second section will include a detailed description of the model used to study the tribology phenomenon

3.2 Experimental tools

3.2.1 Steady state: Engine and test cell characteristics

The engine used in this study is a 4 stroke high-speed direct injection Diesel engine with a displacement of 400 cm^3 per cylinder following Euro 6 emissions regulations. In table 3.1 the main engine characteristics are described.

The engine operational parameters were measured in a test cell. The engine was instrumented with different instrumentation. To measure the intake temperatures type "K" thermocouples were used. 8 of them for intake temperatures from air filter to inlet of intake manifold. 2 for intake temperatures (each one of the both parts of intake manifold). 8 intake pipes inlet temperatures and 2 for WCAC coolant inlet and outlet temperature. Also, for exhaust temperatures the same type "K" thermocouples were used. 4 at the outlet of each exhaust pipe. 3 for

Table 3.1: Engine tested characteristics

Type	HSDI Diesel engine
Displacement	1598 (cm^3)
Bore	80 mm
Stroke	79.5 mm
Compression ratio	14.5:1
Number of valves	4/cylinder
Number of cylinders	4
Air management	VGT, HPEGR, LPEGR
Maximum power @ speed	96 kW @ 4000 rpm
Maximum torque @ speed	320 Nm @ 1750 rpm

turbine inlet and outlet and Diesel Particle Filter (DPF) outlet. 4 for LP EGR inlet and outlet (gas and coolant). 1 for LP EGR valve outlet and 1 for HP EGR outlet. Finally, to measure the engine operating temperatures more thermocouples were used. 2 for engine coolant inlet and outlet. 2 for oil at the oil cooler and crankcase. 1 for block temperature and finally, 1 for fuel temperature at the inlet of the high pressure injection pump.

In different parts, the mean pressure was also measured using piezo resistive transducers. 4 of them were installed at compressor inlet and outlet and intake manifold. 2 for turbine inlet and outlet. 1 for FAP outlet and 4 for LP and HP EGR gas upstream and downstream of EGR valves. 1 for oil pressure at the outlet of oil pump and 1 for engine coolant pressure. Finally, in order to estimate the FMEP through the IMEP method, 4 in-cylinder pressure transducers were integrated on the glow plugs. Figure 3.1 shows the pressures sensors installed on the engine.

All the mean variables were acquired at a frequency of 10 Hz with Horiba Stars test automation system, while instantaneous signals were measured at 0.5° Crank Angle Degree (CAD). Table 3.2 shows the test cell instrumentation main characteristics.

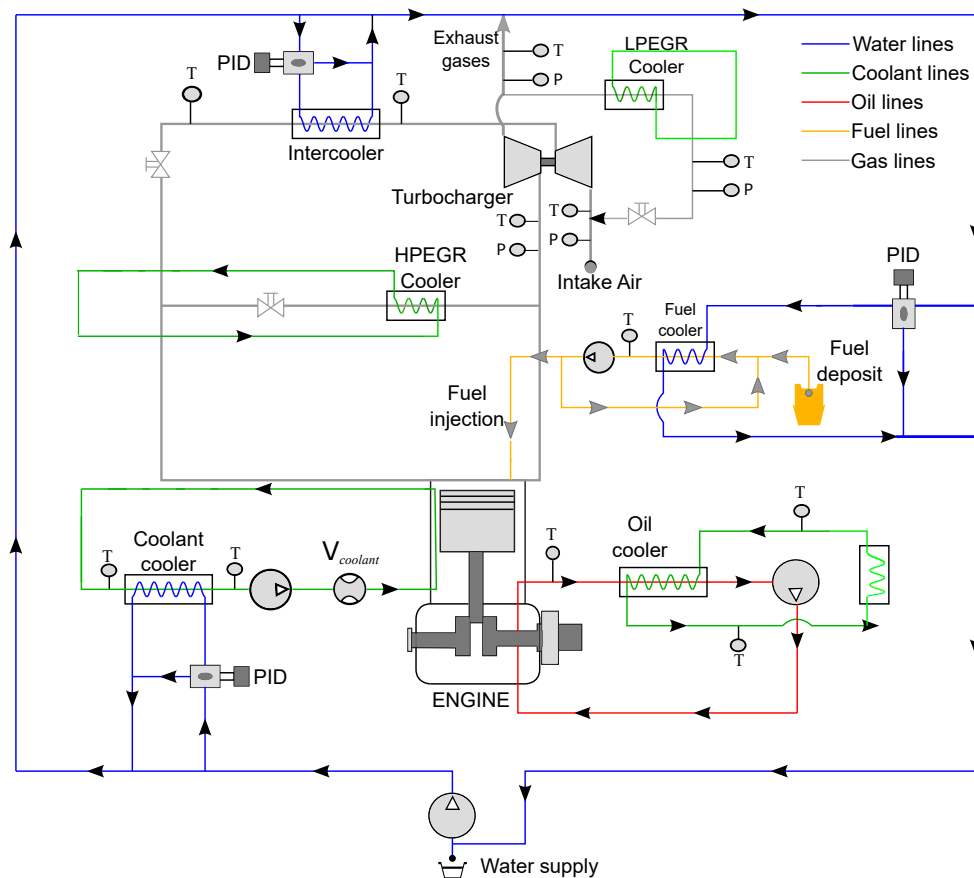


Figure 3.1: Scheme of pressure sensors installed in the engine

Table 3.2: Test cell instrumentation

Variable	Instrument	Range	Accuracy
Crank Angle	Encoder	0 - 360 ^o	$\pm 0.02^o$
Torque	Dynamometer	0 - 400 N m	± 0.5 N m
Gas/wall temperature	K-type thermocouple	70 - 1520K	± 2 K
Oil pressure	Piezoresistive transducer	0 - 10 bar	± 25 mbar
In-cylinder pressure	AVL GH13P	0 - 200 bar	Linearity 0.3%

3.2.2 Transient state: Vehicle and test cell characteristics

The experimental test have been performed with a factory standard SUV. It is a vehicle equipped with a turbocharged Euro 6 compression ignited engine, featuring HP-EGR and LP-EGR used sequentially at the factory calibration and a combination of DOC, DPF and LNT. The vehicle specification is described in table 3.3.

Table 3.3: Tested vehicle specifications

Feature	Description	Feature	Description
Mass [kg]	1580	Tire diameter [mm]	700
Drag Coefficient [-]	0.35	Vehicle Wheelbase [m]	2.705
Frontal area [m^2]	2.2	Gear Ratio 1st [-]	3.727
Friction coefficient [-]	0.01	Gear Ratio 2nd [-]	2.043
Engine Type	Euro 6, inline-four, CI	Gear Ratio 3rd [-]	1.322
Displacement [cm^3]	1598	Gear Ratio 4th [-]	0.947
Max power [kW]	96 @ 4000 rpm	Gear Ratio 5th [-]	0.723
Max Torque [Nm]	320 @ 1750 rpm	Gear Ratio 6th [-]	0.596
Breathing method	turbocharger, intercooler, VGT	Final Drive Ratio [-]	4.428
Emissions control	HP-EGR, LP-EGR, DOC, DPF, LNT	Transmission Efficiency [-]	0.9

The vehicle, with the engine described in previous section, has been set up in a convectional SUV FWD vehicle installed in a transient test cell ROTOTEST Energy 260 2WD. The chassis dynamometer system support a maximum of 262 momentary power and 124 kW as a continuous power. In terms of wheel torque the maximum instantaneous support arise up to 2500 Nm and 1180 Nm as a constant torque. The maximum wheel speed achieves the 2500 rpm and the equivalent vehicle speed, with a wheel diameter of 650 mm can be 250 km/h. With all this characteristics, the system is able to simulate road conditions such as, track grade and vehicle dynamics, while keeping the vehicle standstill in a laboratory under controlled conditions with additional sensors and peripherals. The ROTOTEST test cells can work under two different modes:

- Constant speed where the braking torque is modulated such that vehicle runs at constant speed

- Road load simulation, where a speed-dependent braking torque is applied at the wheels in order to recreate the vehicle dynamics in a predefined road profile

Moreover, the vehicle has been instrumented with an additional rapid prototyping dSpace system in order to acquire fuel consumption, emissions and performance measurements. This setup gathers information from both the factory in-vehicle sensors-by accessing to the ECU variables in real time through ETK port-and custom instrumentation at additional CAN networks. Figure 3.2 shows the test cell described.

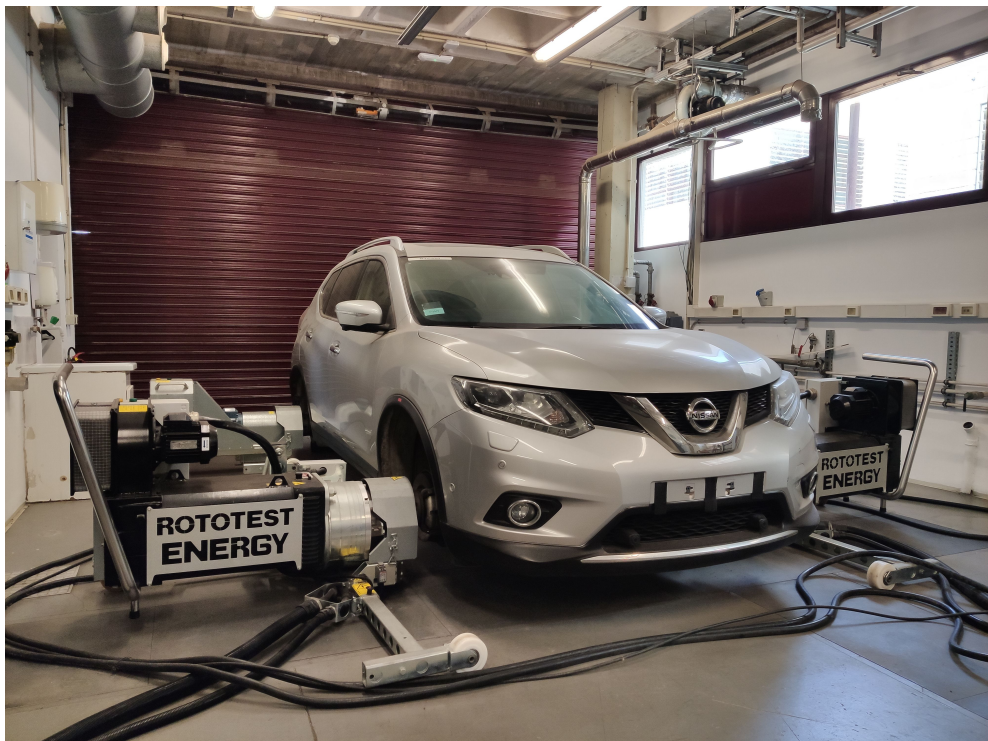


Figure 3.2: ROTOTEST Transient vehicle test cell

3.3 Engine friction: steady state theoretical models

As described in Chapter 2, models for studying tribology in the engine are varied and can be specific to study a particular phenomenon occurring in a certain part of the tribological couple, or they can be more generalist in nature and describe all tribology phenomena occurring throughout the engine. This doctoral thesis has focused on developing a generalist model that addresses all parts of the engine related to friction and, from there, is useful when addressing a more specific problem that requires a greater level of detail.

3.3.1 Piston-ring model

The lubrication model of the piston ring assembly begins with a force balance in the interface of ring and cylinder. This force balance is made by applying the second Newton law in terms of forces and ring moments, to consider the toroidal twist motions, ring oil film hydrodynamics and ring-cylinder asperity contact pressure. Figure 3.3 shows the main forces that interact between ring and cylinder.

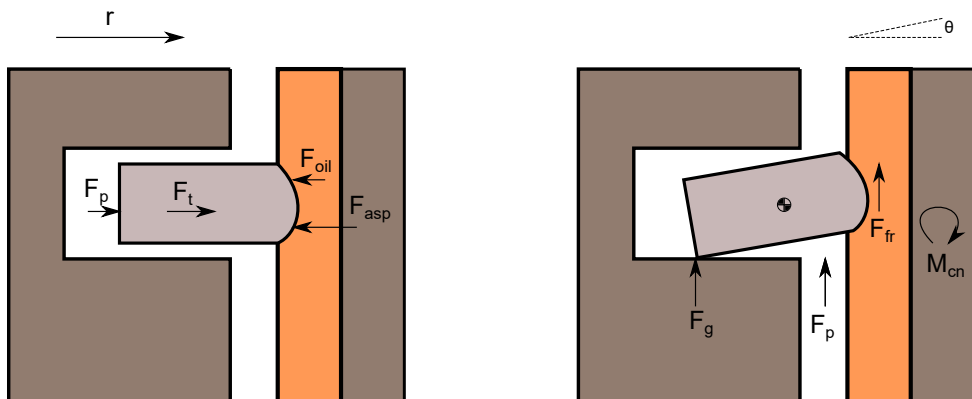


Figure 3.3: Force balance in piston ring assembly

Applying quasi-static force balance in radial direction:

$$M \frac{d^2 r}{dt^2} = F_p + F_t + F_{oil} \left(\frac{dh}{dt} \right) - F_{asp} \approx 0 \quad (3.1)$$

Where

- M : Is the piston mass
- F_p : Is the force caused by the gas coming from the combustion chamber (blow-by) in the groove of the piston-ring
- F_t : Is the force produced by the ring tension as a function of initial tension, ring stiffness, bore distortion and ring thermal expansion
- F_{oil} : Is the force produced by the oil film whose solution is given by Reynolds equation.
- F_{asp} : Is the force produced by the direct interaction of the ring asperity and cylinder asperity. The solution is carried out by integrating the Greenwood-Tripp model.

Also, to obtain the twist motion of the ring, a moment balance is applied to the ring:

$$I_{ring} \frac{d^2 \theta}{dt^2} = F_g(R_g - R_r) + F_p(R_g - R_r) + F_{cf}(R_c - R_r) + M_{cn} - K_t \theta - C_t \frac{d\theta}{dt} \approx 0 \quad (3.2)$$

Being:

- $F_g(R_g - R_r)$: The moment of the groove bottom reaction
- $F_p(R_g - R_r)$: The moment of bottom land pressure
- $F_{cf}(R_c - R_r)$: The moment of cylinder friction force (hydrodynamic plus asperity)
- M_{cn} : The moment of cylinder normal force
- K_t : The ring internal elastic moment
- C_t : The ring internal damping moment.

Each of the forces described above are calculated from developed submodels, whose initial conditions come from the tests carried out on the engine test bench.

3.3.1.1 Gas pressure force: blow-by model

The gas pressure force is calculated through the blow-by model. For this purpose, a model has been adopted from [1]. The author considers instantaneous flow through each ring gap, applying some hypothesis and simplifications:

- Neither the deformation nor the relative motion of the ring is taken into account.
- Gas leakage is assumed to occur only through the annulus gap and is modeled as a nozzle.
- The gas flow is modeled as an isentropic nozzle.
- The temperature of each inter-ring volume is considered as the average of the ring temperature and the liner temperature.
- The pressure behind the ring is considered the pressure immediately upper the volume, thus for the top compression ring the pressure behind the ring is equal to the pressure in combustion chamber.

The model consists on 4 volumes and 3 nozzles. The first volume is considered the combustion chamber, the second volume is the volume between the top compression ring and the second compression ring, the third volume is the volume between the second compression ring and oil control ring and, finally, the fourth volume is considered the crankcase. Figure 3.4 shows the scheme of the blow-by volumes considered.

As said before, the gas in the different volumes is considered isothermal, so the continuity equation for each volume can be expressed as:

$$\frac{dp_i}{dt} = \frac{RT_i}{V_i} \cdot (\dot{m}_{i,in} - \dot{m}_{i,out}) \quad (3.3)$$

where i represents each different volume, R is the gas constant, T_i is the gas temperature, V_i is the volume and $\dot{m}_{i,in}$ and $\dot{m}_{i,out}$ is the instantaneous mass flow rates.

The mass flow through the ring is calculated considering the isentropic nozzle model:

$$\dot{m}_{i,j}(\alpha) = c_{bb} \cdot A_{gap,i} \cdot p_u \cdot \sqrt{\frac{x_i}{RT_u}} \quad (3.4)$$

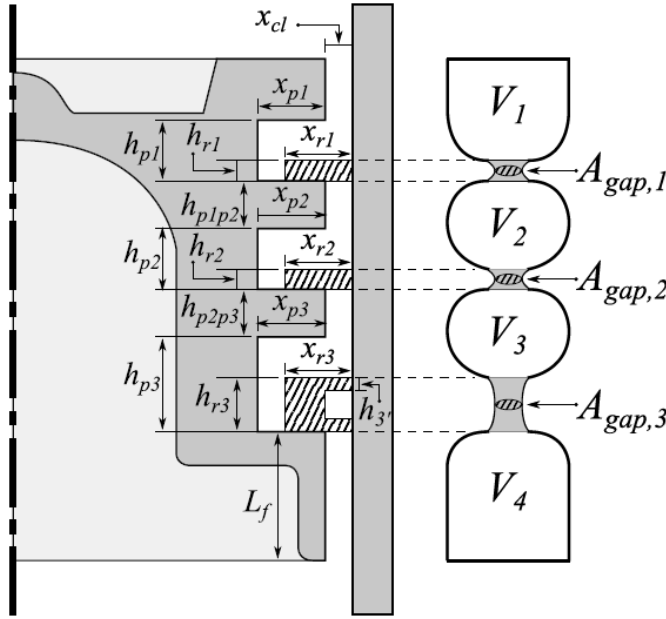


Figure 3.4: Blow-by model scheme. Source: [1]

j is the downstream volume, c_{bb} is the discharge coefficient adjusted in [1], $A_{gap,i}$ is the gap area of the ring, p_u the upstream pressure, T_u the upstream temperature, p_d discharge pressure and x_i :

$$x_i = \frac{2\gamma}{(\gamma - 1)} \left[\left(\frac{p_d}{p_u} \right)^{\frac{2}{\gamma}} - \left(\frac{p_d}{p_u} \right)^{\frac{\gamma+1}{\gamma}} \right] \quad (3.5)$$

If the ratio of the pressures comply the condition:

$$\frac{p_d}{p_u} < \left(\frac{2}{\gamma + 1} \right)^{\frac{\gamma}{\gamma-1}} \quad (3.6)$$

The mass flow is at sonic conditions, using critical pressure (p_{cr}) instead of p_d :

$$p_{cr} = p_u \cdot \left(\frac{2}{\gamma + 1} \right)^{\frac{\gamma}{\gamma-1}} \quad (3.7)$$

Figure 3.5 depicts the pressure calculated in the groove of the different rings of the model.

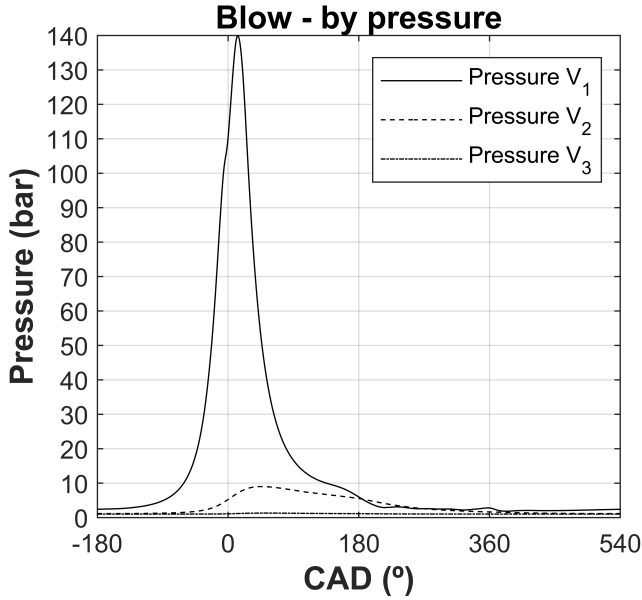


Figure 3.5: Groove pressure in different ring volumes

3.3.1.2 Ring tension force

The tension force produced by the ring is followed by next expression:

$$F_T = \frac{T_0 + K_T(R_0 + \Delta R_{th} + h_0(t))}{R_b} \quad (3.8)$$

In the equation, T is the instantaneous ring tension in N per length unit, T_0 is the reference tension at ring radius, K_T is the ring stiffness, R_0 the initial ring radius, ΔR_{th} is the change in ring radius due to thermal expansion and $h_0(t)$ is the instantaneous minimum oil film thickness. In the model, the installed tension of each ring has been considered following the manufacturer data as shown in table 3.4.

3.3.1.3 Piston assembly temperature

Obtaining the operating temperature of the piston in reciprocating internal combustion engines is a rather difficult task due to the difficulty of installing sensors on the piston during operation. However, in order

Table 3.4: Rings installed tension

Component	Tension (N)
Top compression ring	12
Second compression ring	10
Oil Control Ring	32

to calculate the friction losses in such an assembly, it is necessary to have relevant information about the operating temperature, since the temperature of the oil film will depend on it and, as it has a strong effect on viscosity, it becomes a key variable in the calculation. In this doctoral thesis, the model developed by Salvador [2] was employed.

Salvador divides the piston into different areas, called nodes. Each of these nodes, represented in the figure 3.6, corresponds to a part of the piston and, therefore, will have an associated temperature. The temperature of the three rings correspond to nodes 2, 3 and 4 in the figure respectively. The liner was divided into 4 nodes of the same length. The oil temperature in the simulation would be the averaged temperature between the liner and the piston-ring.

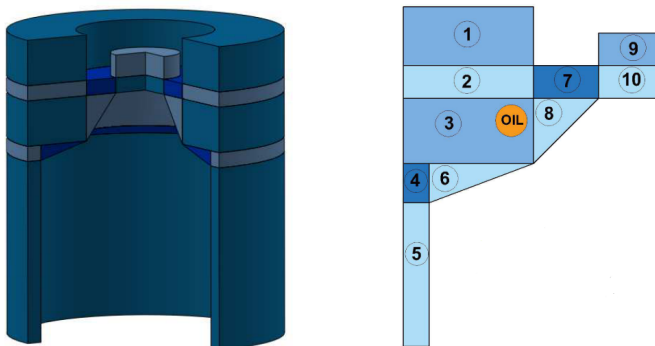


Figure 3.6: Piston nodes distribution

An example of the calculated temperature distribution is shown in Figure 3.7. For the case of the cylinder, three engine speeds and full

load have been selected as a function of the axial length. On the other hand, in the case of the rings and the skirt, a constant speed has been considered and the engine load has been varied.

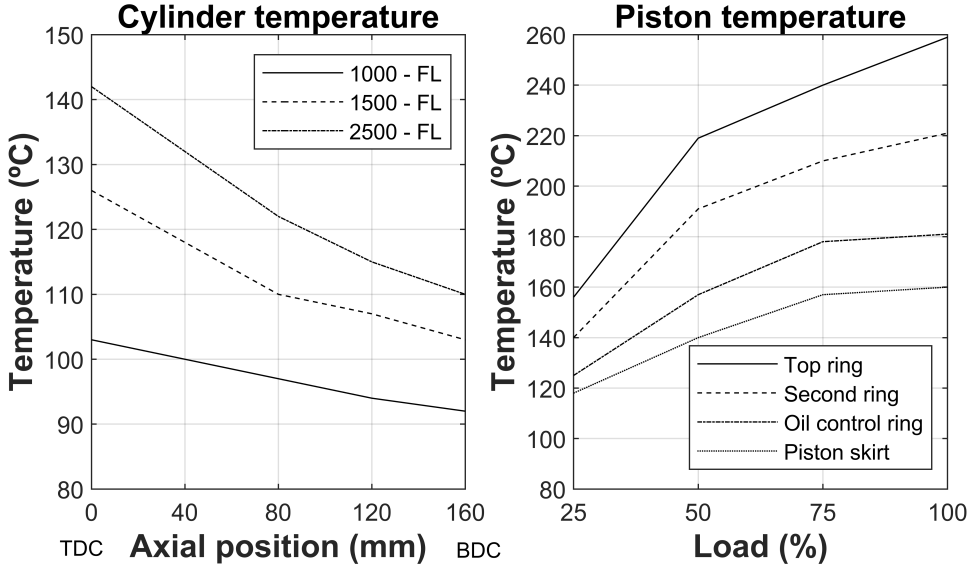


Figure 3.7: Temperature distribution on piston assembly. Left: Cylinder temperature at different axial position and full load. Right: Piston-rings assembly at different engine loads

3.3.1.4 Hydrodynamic friction force

To calculate the friction force of the oil film, the pressure distribution along the ring and throughout the engine cycle must be calculated. For the calculation of the pressure field, the average Reynolds equation with the Patir and Cheng flow factors are used.

$$\frac{\partial}{\partial x} \left(\phi_p h^3 \frac{\partial p}{\partial x} \right) = 6U\mu \left(\frac{\partial \bar{h}_t}{\partial x} + \sigma \frac{\partial \phi_s}{\partial x} \right) + 12\mu \frac{\partial \bar{h}_t}{\partial t} \quad (3.9)$$

From the calculated oil film pressure, the hydrodynamic friction force is obtained through shear stress:

$$\bar{\tau} = \frac{\mu(U_2 - U_1)}{h} (\phi_f \pm \phi_{fs}) \pm \phi_{fp} \frac{h}{2} \frac{\partial \bar{p}}{\partial x} \quad (3.10)$$

Being:

$$F_{oil} = \int_0^x \bar{\tau} dx \quad (3.11)$$

In equation 3.9, ϕ_p is the pressure flow factor that represents the surface impedance to flow in the direction of entraining motion. ϕ_s is the shear flow factor that it accounts the extra lubricant transport as a consequence of the shearing effects, induced by surface roughness. According to equation 3.10, ϕ_f and ϕ_{fs} directly affect the mean shear stress (Couette flow) and ϕ_{fp} is related with the horizontal forces induced by local hydrodynamic pressure in rough contacts (Poiseuille flow). The Patir and Cheng flow factors varies with the Peklenik number, that is, with the surface roughness orientation [3–5].

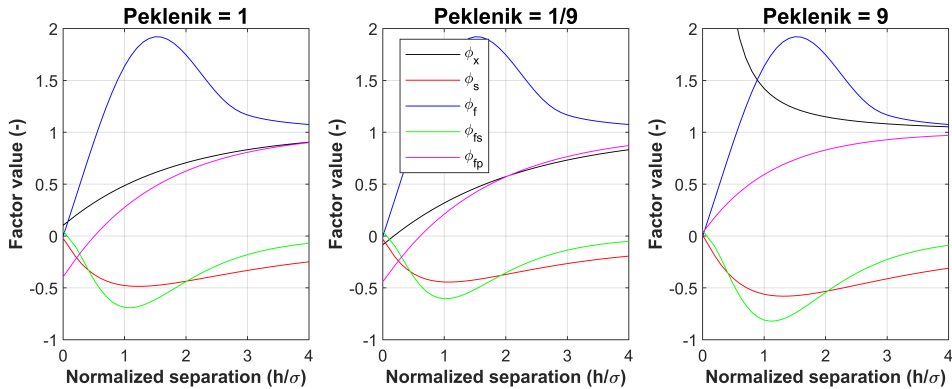


Figure 3.8: Variation of Patir and Cheng flow factors with Peklenik number

As figure 3.8 shows, the Patir and Cheng flow factors are different in function of the surface orientation. Along this model developed, the orientation will be considered isotropic, that is, with a Peklenik number equal to 1. The rings shape is depicted in figure 3.9. The rings profile

were taken from the original engine rings and before the engine running-in. The evaluation of the friction changes with running-in would be proposed as future work [6]. The oil control ring has been rounded in the corner to consider the equivalent hydrodynamic pressure generated by the asperity [7].

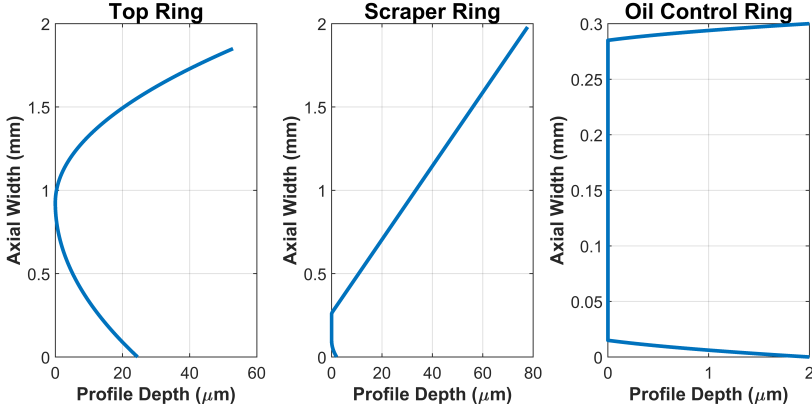


Figure 3.9: Piston ring profiles

3.3.1.5 Asperity friction force

To calculate the contact pressure in the piston-ring, the Greenwood-Tripp Model [8] is used. In the Greenwood-Tripp model spherical shape of the asperity is assumed with constant radius β . Moreover the peaks are uniformly distributed with density η of peaks per area unit. Taking into account the assumptions proposed by G-T, the pressure contact is calculated as:

$$p_{asp} = \frac{16\sqrt{2}}{15} \pi (\sigma\beta_0\eta)^2 E \sqrt{\frac{\sigma}{\beta_0}} f_{\frac{5}{2}} \left(\frac{h}{\sigma} \right) \quad (3.12)$$

and

$$f_{\frac{5}{2}} = \frac{1}{\sqrt{2\pi}} \int_x^\infty (s-x)^{5/2} e^{\left(\frac{-s^2}{2}\right)} ds \quad (3.13)$$

Where h is the local film thickness between both surfaces. σ is the composite roughness height desviation $\sigma = \sqrt{\sigma_1^2 + \sigma_2^2}$; $\eta = \frac{\eta_1 + \eta_2}{2}$; $\beta_0 = \left(\frac{1}{\beta_1} + \frac{1}{\beta_2}\right)^{-1}$ and E is the elasticity modulus combined with the Poisson ratio of the material ν such as: $\frac{1}{E} = \left(\frac{1-\nu_1^2}{E_1} + \frac{1-\nu_2^2}{E_2}\right)$. It is assumed that the height of the asperities is fitted by Gaussian distribution.

Finally, to obtain the friction force coming from the asperity contact, the asperity pressure must be integrated along the face of the ring.

$$F_{asp} = CoF \cdot \int_0^x p_{asp} dx \quad (3.14)$$

Being CoF the boundary friction coefficient of the tribological pair. The Greenwood and Tripp model considers that the summit heights have a gaussian distribution. However, the most ICE cylinder has a non-gaussian height distribution, to correct that, the assumption of Tomanik et al. has been considered [9]. To obtain the Greenwood-Tripp parameters, the parameters shown in Table 3.5 have been taken according to the work previously mentioned.

Table 3.5: Parameters used in Greenwood-Tripp model

	$\sigma\beta\eta$	σ/β	$\eta(1/m^2)$	E (GPa)	ν
Top Compression ring	0.059	0.0028	1.02e9	200	0.285
Second Compression ring	0.044	0.0021	1.02e9	200	0.285
Oil control ring	0.044	0.0021	1.02e9	200	0.285
Cylinder	0.093	0.0069	1.02e9	126.5	0.25

3.3.1.6 Coefficient of friction measurement

The boundary coefficient of friction was measured in SRV Reciprocating Tribometer (see Figure 3.10) as a part of the research stay made in the LFS - Laboratório de Fenômenos de Superfície POLI/USP of Universidade de São Paulo, Brazil. The experimental assembly was performed with ball on flat configuration. This configuration was chosen

due to its easy assembly and test execution. However, this configuration can be more representative of the camshaft assembly than piston-ring assembly. The material geometry and properties are shown in Table 3.6.



Figure 3.10: SRV Reciprocating Tribometer.

Table 3.6: SRV experimental assembly characteristics

	Material	Diameter (mm)	Hardness (HV)	Young Modulus (GPa)	Poisson Ratio	Roughness Sa (μm)
Ball	AISI 52100	10	813	210	0.3	0.042
Plate	AISI H13	24	615	210	0.3	0.012

Attending that the experimental condition to measure the friction is steady-state, warm condition, the temperature of the test was set at

120^oC. This condition is representative of the oil temperature in the cam contact and piston ring/cylinder bore interface. The load during the test was representative of that found in the tribocouples mentioned. In piston-ring the contact load is carried out by the asperity contact pressure, which is between [0.4 - 0.6] MPa [10, 11] and 1.2 GPa in camshaft [12]. The load applied to the test was calculated with Hertz Contact Pressure theory considering the material used during the experiment, showed in Table 3.6. The load that is representative of the piston-ring and camshaft contact is 10N and 100N respectively. The test stroke was fixed at 5 mm with a frequency of 5 Hz. The maximum velocity of the experiment is achieved in the mid-stroke and zero velocities at the reversal points. Finally, each step had a duration of 15 min and repeated 3 times. The parameters used in the experimental test are summarized in Table 3.7.

Table 3.7: SRV experimental test characteristics

Feature	Value	
Load (N)	10	100
Temperature (^o C)	120	120
Stroke (mm)	5	5
Frequency (Hz)	5	5
Time (min)	15	15

To calculate the coefficient of friction it has been considered the last 5 minutes of the experiment to have a steady-state measurement. The instantaneous curves generated during the test in the 3 repetitions, have been averaged to an unique curve that represent the entire stroke. The resultant averaged curves for each step is depicted in Figures 3.11 and 3.12.

The comparison between the two averaged coefficient of friction is shown in Figure 3.13. Moreover, the final coefficient of friction introduced in the model, is the averaged values of the curves presented in Figure 3.13.

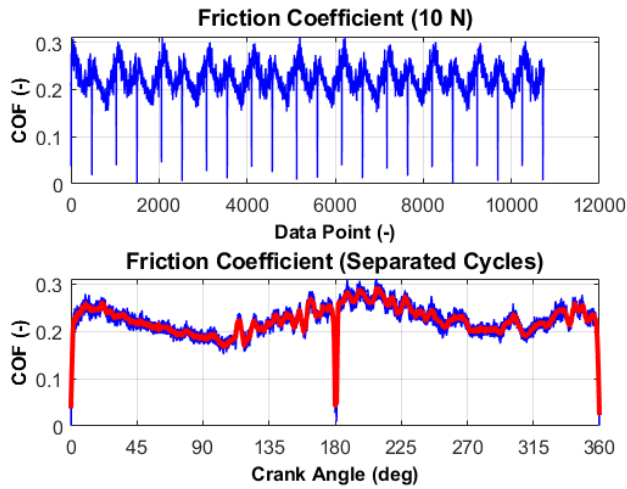


Figure 3.11: Averaged Coefficient of Friction for load equal to 10N

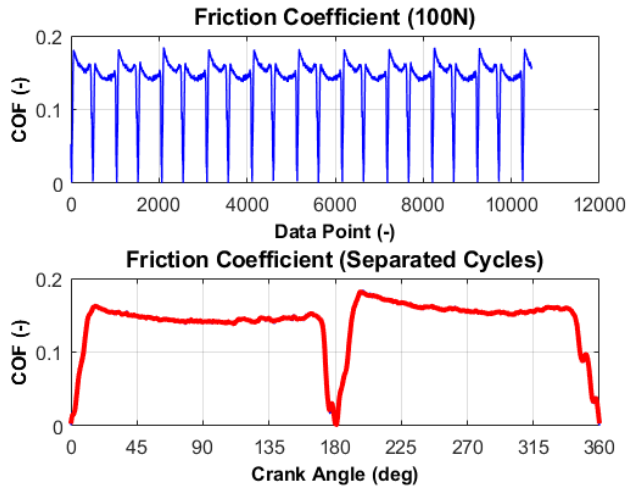


Figure 3.12: Averaged Coefficient of Friction for load equal to 100N

This values, for the piston ring assembly are fixed in 0.22 and 0.15 for the camshaft contact.

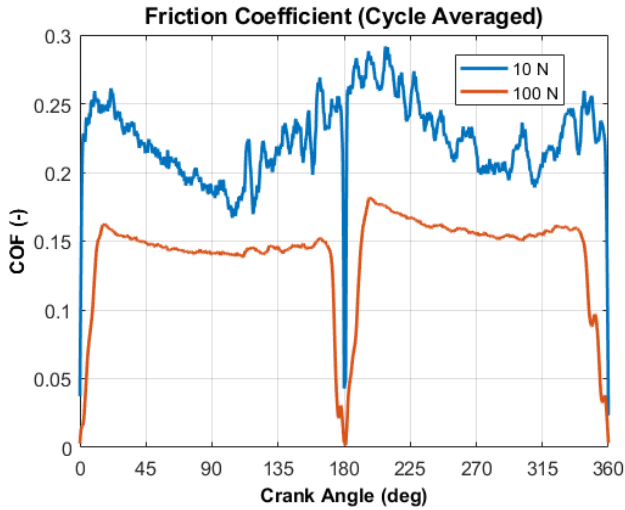


Figure 3.13: Averaged Cycle Coefficient of Friction for both load

3.3.2 Piston skirt model

In piston skirt model, the secondary motion of the piston is solved in order to predict the eccentricity and tilt motion as depicted in figure 3.14.

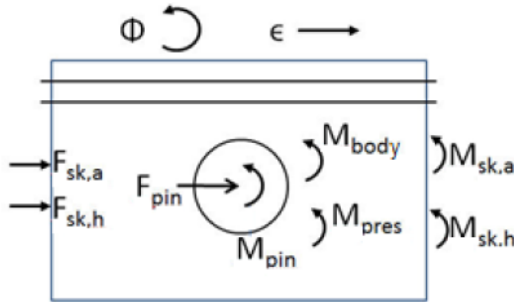


Figure 3.14: Force and moment balance in piston

Applying the second Newton law considering the lateral acceleration:

$$M_p \frac{d^2 \epsilon}{dt^2} \approx 0 = F_{pin} + F_{sk,h} + F_{sk,a} \quad (3.15)$$

and a moment balance:

$$I_p \frac{d^2 \Phi}{dt} \approx 0 = M_{body} + M_{press} + M_{pin} + M_{sk,h} + M_{sk,a} \quad (3.16)$$

Where M_p is the piston mass. The variable ϵ refers to the piston eccentricity and Φ to the piston tilt. F_{pin} is the lateral force caused by the secondary motion of the piston. $F_{sk,h}$ is the hydrodynamic friction force produced in the skirt. $F_{sk,a}$ is the asperity friction force. Both of them are calculated as presented in section 2.4.2. I_p is the piston inertial moment and M_i represent the moment produced by the force i in equation 3.16.

The skirt has a pad angle associated since it is not a fully 360 degree skirt. In the model developed, the piston skirt has a pad angle θ_{MN} and θ_{MJ} , according with figure 3.15 equal to 107° .

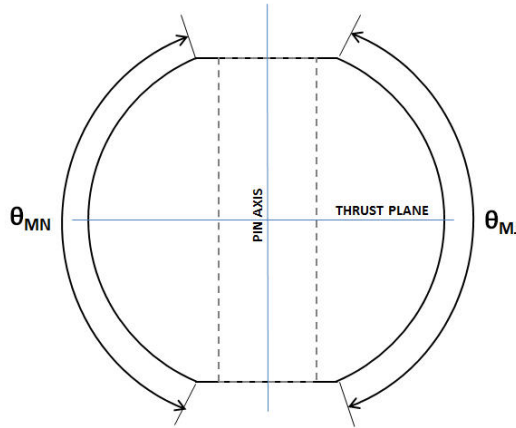


Figure 3.15: Skirt pad angles

The deviations of skirt axial on major and minor thrust and the ovality deviation is considered equal to 0 in the model.

3.3.3 Bearings

In this thesis, the solution of the oil film in bearings is solved with two models:

- The camshaft bearings, for saving computational time are solved with the mobility method
- The main engine bearings, con-rod and journal, are solved by average Reynolds equation

3.3.3.1 Mobility method

Rigid bearing model with parallel axis (no tilt) is used here. This model considers that three are the factors which contribute to total torque and friction power loss in the bearing including shear, squeeze and contact whose expression is:

$$N_{total} = N_{shear} + N_{squeeze} + N_{contact} \quad (3.17)$$

The shear term is the power required to shear the fluid due to relative rotation between the journal and shell and is calculated with next relation.

$$N_{shear} = \frac{2\pi R^3 L \mu |\omega_j - \omega_b|^2}{\sqrt{c^2 - \epsilon^2}} + (\epsilon_x F_y - \epsilon_y F_x) \left(\frac{\omega_j + \omega_b}{2} \right) \quad (3.18)$$

First term of the equation represent the effect described above, where R represents the bearing radius ; L represents the bearing width; μ is the lubricant viscosity at work temperature; ω_j and ω_b are the angular velocity of the journal and bearing respectively; c is the radial clearance between the journal and bearing and ϵ is the eccentricity calculated. Second term of the expression 3.18 is generated due to the journal and bearing center misalignment. Since the reaction forces are equal and opposite but applied at different locations, they generates a moment couple located at the midpoint of the journal center and bearing center [13].

The squeeze term in Eq. 3.17 is due to the force of the journal moving with a certain linear velocity as well as a consequence of this phenomena no torque is generated [14].

$$N_{squeeze} = \frac{d\epsilon_x}{dt} F_x + \frac{d\epsilon_y}{dt} F_y \quad (3.19)$$

Finally the contact force generated in the journal bearing is calculated with the Greenwood-Tripp model previously described

3.3.3.2 Reynolds equation

The film problem is solved by the average Reynolds equation considering the Patir and Cheng flow factors. It is considered the rotation and 2D planar motion of the journal but the tilt of the journal it is not considered. The bearing is divided in different elements in order to apply on each of them the Reynold equation as shown in figure 3.16. This discretization is used in connecting rod and main crankshaft bearings.

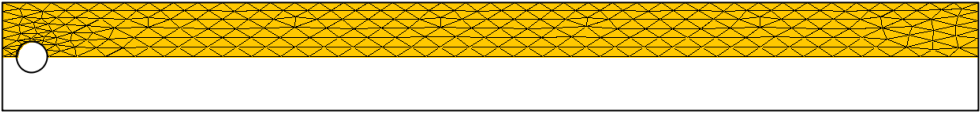


Figure 3.16: Journal Bearing nodes with symmetric half bearing assumption

Finally, a thermal balance is made in the bearing in order to consider the oil temperature rise during the operation. A simple thermal balance as expressed in next equation is used:

$$\rho_{oil} \cdot C_{p,oil} \cdot Q \cdot (T_f - T_i) = P \cdot (1 - F_h) \quad (3.20)$$

Where ρ_{oil} represents the oil density as a function of temperature. $C_{p,oil}$ is the heat capacity of the oil. Q is the volumetric flow rate. T_i the initial oil temperature and T_f the final oil temperature calculated. Finally, P is the bearing friction force and F_h is a coefficient that indicates the portion of the friction losses that is lost to the atmosphere and it is not considered to increase the oil temperature. In the model a value of 0.15 is used.

The geometry characteristics of the crankshaft bearings are shown in table 3.8

For both the mobility method and the Reynolds equation, friction losses due to asperities are taken into account. As explained in a previous section, the asperity losses have been calculated with the Greenwood-Tripp model, the model parameters for the bearings are those shown in table 3.9:

Table 3.8: Bearings geometry

	Main Bearings	Con-rod Bearings
Diameter (mm)	51.48	51.58
Width (mm)	17.8	21.1
Clearance (mm)	0.025	0.025
Material	Al-Sn-Cu-Ni	Al-Sn-Cu-Ni

Table 3.9: Parameters used in Greenwood-Tripp model

	$\sigma\beta\eta$	σ/β	$\eta(1/m^2)$	E (GPa)	ν
Bearings	0.061	0.0012	4e9	71	0.33

3.3.4 Valvetrain

In the valvetrain, the predominating lubrication regime is EHD. The main part of the friction losses is due to the direct contact between the cam and follower, which during the most of the cycle is given under mixed and boundary lubrication regime. To simulate the pressure contact the Hertzian model is used. The Hertzian model assumes two cylinders in contact with an uniform pressure distribution in the axial direction [15].

$$p_{hertz} = 0.399w^{0.5}E^{0.5}l^{-0.5}r^{-0.5}\sqrt{1 - \left(\frac{x}{1.598w^{0.5}r^{0.5}l^{-0.5}E^{-0.5}}\right)^2} \quad (3.21)$$

Where p is the pressure along width x ; w is the total normal load applied; l is the axial length of the contact; r is the combined radius of both surfaces and E is the Young's modulus. Figure 3.17 represents the Hertz contact area.

Also, a contact deformation model is used to predict the deformation between both surfaces:

$$\delta = 1.2599w^{2/3}E^{-2/3}r^{-1/3} \quad (3.22)$$

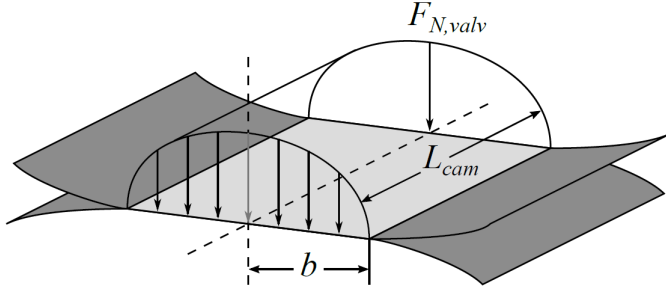


Figure 3.17: Hertz contact area

The friction force carried by the camshaft can be expressed as the sum of the viscous friction force and asperity friction force:

$$F_{fr,v} = F_b + F_v \quad (3.23)$$

Where F_b , the boundary component can be written as:

$$F_b = \tau_0 A_a + m P_a \quad (3.24)$$

Being τ_0 the Eyring Shear Stress considered 2.5 MPa in the thesis model. m represents the pressure coefficient of the boundary: 0.17 [16]; A_a and P_a are the area and pressure carried out by the asperities. The pressure and area of contact in the boundary regime are modeled as explained in section 3.3.1.5.

On the other hand, the viscous component, F_v , is modeled as:

$$F_v = \tau (A - A_a) \quad (3.25)$$

where τ is the shear stress of lubricant. Depending on the oil film thickness, Newtonian or non-Newtonian behavior oil film will occur. The limit is the Eyring Shear. If the shear stress is lower than this value, it can be evaluated as:

$$\tau = \frac{\mu_{roeland} u_s}{h_0} \quad (3.26)$$

Where u_s is the sliding velocity, $\mu_{Roeland}$ is the Roelands equation effect of pressure on viscosity expressed as:

$$\mu_{Roeland} = \mu_{ambient} e^{[(1 + \frac{p}{pr})^z - 1] \ln(\frac{\mu_{ambient}}{\mu_{\infty}})} \quad (3.27)$$

Being

$$z = \frac{\alpha p_r}{\ln\left(\frac{\mu_{ambient}}{\mu_\infty}\right)} \quad (3.28)$$

Where α is the pressure-viscosity coefficient $15 \cdot 10^{-9} 1/Pa$. p is the oil film pressure; p_r is a constant pressure $1.96 \cdot 10^8 Pa$; μ_∞ is the viscosity constant $6.315 \cdot 10^{-5} Pa \cdot s$ according to [17].

In the case that τ would be higher than Eyring Shear, it is modeled as:

$$\tau = \tau_0 + \kappa \frac{F_{N,valu} - P_a}{A - A_a} \quad (3.29)$$

Being κ the rate of change of shear stress with pressure, taking a value of 0.08 [18] and $F_{N,valu}$ the normal force acting in the contact.

Finally, the solution adopted to calculate the minimum oil film thickness can be carried out by models developed by different authors, however, the model used in this thesis is the proposed by Moes [19]

$$h_{ctr} = \left[(H_{RI}^{2.333} + H_{EI}^{2.333})^{0.429s} + (H_{RP}^{3.5} + H_{EP}^{3.5})^{0.286s} \right]^{s^{-1}} \quad (3.30)$$

The Moes equation take into account the four limits present in the equation. Subscript RI is the rigid-viscous limit; Subscript RP is the rigid-piezoviscous limit; Subscript EI is the elastic-isoviscous limit and the subscript EP is the elastic-piezoviscous limit of the oil.

3.3.5 Auxiliaries

The auxiliaries model in this thesis work is the same that developed by Tormos et. al [20]. The authors developed a model for each auxiliaries components in the engine: coolant pump, oil pump and fuel pump.

3.3.5.1 Coolant pump

The energy consumption of the coolant pump can be approximated assuming that coolant is flowed by a centrifugal pump with straight blades:

$$N_{cool} = \frac{\Delta p \cdot \dot{V}_{cool}}{\eta_{cool}} \quad (3.31)$$

where \dot{V}_{cool} is the coolant flow rate, η_{cool} is the pump efficiency and Δp_{cool} is the coolant pressure drop. These parameters can be determined as follows:

$$\Delta p_{cool} = k_{1,cool} \cdot \dot{V}_{cool}^2 \quad (3.32)$$

In this case, $k_{1,cool}$ is a value that has been determined experimentally.

The experiments realized in [1] showed that it is reasonable to assume that

$$\dot{V}_{cool} = k_{2,cool} \cdot n \quad (3.33)$$

where $k_{2,cool}$ is the proportionality constant between coolant flow and engine speed.

By combining all the above equations, the coolant pump power can be calculated as:

$$N_{cool} = \frac{k_{1,cool} \cdot k_{2,cool}^2 \cdot n^3}{\eta_{cool}} \quad (3.34)$$

3.3.5.2 Oil pump power

The common oil pump in ICEs is the gear or lobe pumps. As coolant pump, the oil pump power can be modeled as:

$$N_{oil} = \frac{\Delta p_{oil} \cdot \dot{V}_{oil}}{\eta_{oil}} \quad (3.35)$$

being η_{oil} the pump efficiency, Δp_{oil} the oil pressure drop and \dot{V}_{oil} is the oil flow rate. Since the oil pump is a volumetric machine, the oil flow rate can be obtained as a function of engine speed:

$$\dot{V}_{oil} = k_{1,oil} \cdot n \quad (3.36)$$

where $k_{1,oil}$ is the proportionality between oil flow and engine speed.

Due to the pump has a relief valve, Δp_{oil} depends on oil flow rate a certain engine speed ($n_{\Delta p,max}$) where the maximum oil pressure is achieved ($\Delta p_{oil,max}$). If the oil pressure values are lower than ($\Delta p_{oil,max}$), Δp_{oil} is determined considering the pressure losses in a pipe with a simplified model. That model depends on a factor obtained with the Darcy-Weisbach equation:

$$\Delta p_{oil} = k'_{2,oil} \cdot f_{pipe} \cdot \dot{V}_{oil}^2 \quad (3.37)$$

Where f_{pipe} is obtained from the empirical formula of Moody [21]:

$$f_{pipe} = 0.001375 \left[1 + \left(200\sigma_r + \frac{\pi \cdot D_{pipe} \cdot \mu_{oil} \cdot 10^6}{4 \cdot \dot{V} \rho_{oil}} \right)^{1/3} \right] \quad (3.38)$$

being D_{pipe} the pipe diameter, σ_r the pipe roughness. μ_{oil} the oil viscosity and ρ_{oil} the oil density. However, due to the difficulty of finding the values of σ_r and D_{pipe} , Carreño [1] proposes the following expression:

$$f_{pipe} = \left(\frac{k'_{3,oil} \cdot \mu_{oil}}{\dot{V}_{oil}} \right)^{k_{3,oil}} \quad (3.39)$$

Replacing and reordering the expression of Δp_{oil} is:

$$\Delta p_{oil} = \left(\frac{k'_{3,oil} \cdot \mu_{oil}}{k_{1,oil} \cdot n} \right)^{k_{3,oil}} \cdot (k_{1,oil} \cdot n)^2 \quad (3.40)$$

Depending of the operating oil pressure during the engine operation, the oil pump power can be determined as:

$$N_{oil} = \frac{k_{1,oil} \cdot \Delta p_{oil,max}}{\eta_{oil}} \quad (3.41)$$

in the case that $\Delta p_{oil} = \Delta p_{oil,max}$. On the other case the expression is:

$$N_{oil} = \frac{(k_{1,oil} \cdot n)^3}{\eta_{oil}} \cdot \left(\frac{k_{2,oil} \cdot \mu_{oil}}{k_{1,oil} \cdot n} \right)^{k_{3,oil}} \quad (3.42)$$

3.3.5.3 Fuel pump power

The normal pump to increase the fuel pressure in engines is piston, thus, the total amount of fuel compressed depends on the pump rotating speed and pump size (volumetrics), being proportional to the engine speed, therefore the fuel pump power depends on the engine speed and the pressure drop. Due to the rail pressure is much higher than fuel tank pressure, the pressure drop will be considered equal to rail pressure (p_{rail}), so, fuel power pump can be expressed as:

$$N_f = \frac{\dot{V} \Delta p_f}{\eta_f} = \frac{k'_{1,f} \cdot n \cdot \Delta p_f}{\eta_f} \quad (3.43)$$

In the pump installed in the engine studied, the fuel pump power consumption depends on p_{rail} , n and the quantity of fuel injected. As determining \dot{V}_{fuel} it is a difficult task, a solution were adopted:

$$\dot{V}_f = k_{1,f} \cdot \dot{m}_f^{k_{2,f}} \quad (3.44)$$

Replacing the expression in the equation above, the total power consumption of the fuel pump can be estimated as:

$$N_f = \frac{k_{1,f} \cdot \dot{m}_f^{k_{2,f}} \cdot p_{rail}}{\eta_f} \quad (3.45)$$

For the constants of the auxiliaries model, in this thesis next constants have been used:

Table 3.10: Auxiliaries coefficients

	Oil	Coolant	Fuel
k_1	1.700583	$3.97 \cdot 10^{-5}$	$1.41 \cdot 10^{-3}$
k_2	$8.07 \cdot 10^{-3}$	0.05657	-
k_3	0.64	-	-

3.4 Engine friction: transient theoretical model

To study the effect of friction during transients condition, the development of the internal equation of motion will be shown. The model will be made with 2 Free Driveline Clusters. One of them is the engine components and the other one represents the kinematics of the driveline, from transmission until road characteristics. This two Free Driveline Clusters are connected by means of a clutch. In this model, the differential equations of motion are integrated in time. With this methodology it is possible to calculate the transient speed and torque in

the system. The mechanical engine output is function of BMEP and/or accelerator position, previously introduced from the experimental steady-state test. In addition, from the stationary maps and depending on the mechanical engine output, the instantaneous fuel consumption of the engine is obtained. When studying different lubricants, the BMEP of the engine will vary according to the increase or decrease of the mechanical losses. This increase/decrease will cause a change in the mechanical engine output and hence the instantaneous fuel consumption. Moreover, the resistance to motion depends on the vehicle speed and driveline, vehicle and environment characteristics.

The engine equation of motion can be expressed as:

$$\tau_{eng} = I_{eng} \cdot \frac{d\omega_{eng}}{dt} \quad (3.46)$$

Where I_{eng} represents the engine inertia, ω_{eng} is the engine speed and τ_{eng} is the engine torque. The Driveline equation is a force balance of different vehicle elements:

$$\tau_{drv,v} = \tau_{eff,iner} + \tau_{trans,rat} + \tau_{ext} \quad (3.47)$$

Where, the first term of the equation ($\tau_{eff,iner}$) is referred to the torque required to accelerate the effective inertia evaluated at the clutch of the entire drivetrain. Each of the inertias are reduced to the square of the gear ratio since they are passed along towards engine. Thus, the vehicle and axle inertia are reduced both the final drive ratio and the transmission ratio:

$$\tau_{eff,iner} = \left(I_{trans,1} + \frac{I_{trans,2}}{R_t^2} + \frac{I_{dsh}}{R_t^2} + \frac{I_{axl}}{R_d^2 \cdot R_t^2} + \frac{M_{veh} \cdot r_{whl}^2}{R_d^2 \cdot R_t^2} \right) \cdot \frac{d\omega_{drv}}{dt} \quad (3.48)$$

Where $I_{trans,1}$ is the input side transmission moment of inertia, that in this case, has been considered equal to transmission inertia divided by 2, $I_{trans,2}$ is the output side transmission moment of inertia. As in the case before, it has been considered equal to transmission inertia divided by 2, I_{axl} is the different axes moment of inertia in the vehicle, included the wheels and I_{dsh} is the driveshaft inertia. R_t represents the transmission ratio and R_d is the final drive ratio. M_{veh} is the vehicle mass and r_{whl} the wheel radius. Finally, ω_{drv} is the driveline speed on vehicle.

The second term of the equation represents the load induced by a transient gear ratio. During the gear shifts the gear ratio is changed linearly between the discrete ratios. So an additional term is included. The additional term is derived from the effective inertia equation where the effective inertia before the transmission ratio includes all items in the previous term excluding the input moment of inertia of the transmission.

$$\tau_{trans, rat} = - \left(\frac{I_{trans,2}}{R_t^3} + \frac{I_{dsh}}{R_t^3} + \frac{I_{axl}}{R_d^2 \cdot R_t^3} + \frac{M_{veh} \cdot r_{whl}^2}{R_d^2 \cdot R_t^3} \right) \cdot \omega_{drv} \cdot \frac{dR_t}{dt} \quad (3.49)$$

Finally, the external forces that vehicle overcomes, that is, the third term of the equation, is calculated as follow:

$$\tau_{ext} = \left(\frac{F_{aer} + F_{rol} + F_{grd}}{R_d \cdot R_t} \right) \cdot r_{whl} \quad (3.50)$$

Where F_{aer} is the aerodynamic force that the vehicle overcome expressed as:

$$F_{aer} = \frac{1}{2} \cdot \rho \cdot A \cdot C_d \cdot v^2 \quad (3.51)$$

Being ρ the aire density, A the vehicle frontal area, C_d the vehicle drag coefficient and v the vehicle speed.

The rolling resistance, F_{rol} is calculated as follow:

$$F_{rol} = c_r \cdot m_{eq} \cdot g \cdot \cos \alpha \quad (3.52)$$

Where c_r is the rolling friction coefficient, typically between 0.01 - 0.015 [22]. m_{eq} is the total vehicle mass included the passengers and additional loads. g is the earth gravity acceleration and α is the road angle.

Finally, the force due to road slope is given as:

$$F_{grd} = m_{eq} \cdot g \cdot \sin \alpha \quad (3.53)$$

Bibliography

- [1] Carreño Arango R. *A comprehensive methodology to analyse the Global Energy Balance in Reciprocating Internal Combustion Engines*. Universitat Politècnica de València, 2016.
- [2] Salvador Iborra J. *A Contribution to the Global Modeling of Heat Transfer Processes in Diesel Engines*. Universitat Politècnica de València, 2020.
- [3] Tomanik E., Profito F., Sheets B. and Souza R. “Combined lubricant - surface system approach for potential passenger car CO₂ reduction on piston-ring-cylinder bore assembly”. *Tribology International*, Vol. 149 n^o July, pp. 1–12, 2020.
- [4] Patir N. and Cheng H. “An Average Flow Model for Determining Effects of Three-Dimensional Roughness on Partial Hydrodynamic Lubrication”. *Journal of Tribology*, Vol. 100, pp. 12–17, 1978.
- [5] Patir N. and Cheng H. “Application of Average Flow Model to Lubrication Between Rough Sliding Surfaces”. *Journal of Lubrication Technology*, Vol. 101 n^o 2, pp. 220–229, 1979.
- [6] Priest M., Dowson D. and Taylor C. M. “Predictive wear modelling of lubricated piston rings in a diesel engine”. *Wear*, Vol. 231, pp. 89–101, 1999.
- [7] Profito F., Tomanik E. and Zachariadis D. “Effect of cylinder liner wear on the mixed lubrication regime of TLOCs”. *Tribology International*, Vol. 93, pp. 723–732, 2016.
- [8] Greenwood J. and Tripp J. “The contact of two nominally flat rough surfaces”. *Proceedings of the Institution of Mechanical Engineers*, Vol. 185, pp. 625–633, 1970.
- [9] Tomanik E., Chacon H. and G.Teixeira. “A simple numerical procedure to calculate the input data of Greenwood-Williamson model of asperity contact for actual engineering surfaces”. *Tribological Research and Design for Engineering Systems*, pp. 205–215, 2003.
- [10] Johansson S., Nilsson P., Ohlsson R. and Rosen B. “Experimental friction evaluation of cylinder liner piston ring contact”. *Wear*, Vol. 271, pp. 625–633, Jun 2011.
- [11] Akalin O. and Newaz G. “Piston Ring-Cylinder Bore Friction Modeling in Mixed Lubrication Regime: Part I Analytical Results”. *Journal of Tribology*, Vol. 123, pp. 211–218, Jan 2001.
- [12] Orgeldinger C. and Tremmel S. “Understanding Friction in Cam-Tappet Contacts: An Application-Oriented Time-Dependent Simulation Approach Considering Surface Asperities and Edge Effects”. *Lubricants*, Vol. 9, Nov 2021.

- [13] Raimondi A. A. and Boyd J. “A Solution for the Finite Journal Bearing and its Application to Analysis and Design: I”. *ASLE Transactions*, Vol. 1, pp. 159–174, 1958.
- [14] Taylor C. M. *Engine Tribology*. Elsevier, 1993.
- [15] Hertz H. “Über die Berührung fester elastischer Körper (On the contact of elastic solids)”. *Journal für die reine und angewandte Mathematik*, Vol. 92, pp. 156–171, 1882.
- [16] Teodorescu M., Taraza D., Henein Naeim A. and W.Bryzik. “Simplified Elastohydrodynamic Friction Model of the Cam-Tappet Contact”. *SAE Technical Paper*, n° 2003-01-0985, 2003.
- [17] Roelands C. *Correlational aspects of the viscosity-temperature-pressure relationship of lubricants oils*. 1966.
- [18] Guo J., Zhang W. and D.Zou. “Investigation of dynamic characteristics of a valve train system”. *Mechanism and Machine Theory*, Vol. 46, pp. 1950–1969, 2011.
- [19] Moes H. “Optimum similarity Analysis with applications to Elastohydrodynamic Lubrication”. *Wear*, Vol. 159, pp. 57–66, 1992.
- [20] Tormos B., Martín J., Carreño R. and Ramírez L. “A general model to evaluate mechanical losses and auxiliary energy consumption in reciprocating internal combustion engines”. *Tribology International*, Vol. 123, pp. 161–179, jul 2018.
- [21] Fernández Feria R. and Ortega Casanova J. *Mecánica de fluidos. Notas de clase: Teoría, problemas y prácticas*. Universidad de Málaga, 2014.
- [22] Tormos B., Pla B., Bastidas S., Ramírez L. and Pérez T. “Fuel economy optimization from the interaction between engine oil and driving conditions”. *Tribology International*, Vol. 138, pp. 263–270, 2019.

Chapter 4

Model results

Contents

4.1	Introduction	97
4.2	Steady-state model	97
4.2.1	Methodology and boundary conditions	97
4.2.2	Global results	100
4.2.3	Piston-ring assembly	103
4.2.4	Piston skirt	107
4.2.5	Bearings	109
	4.2.5.1 Connecting rod bearing	110
	4.2.5.2 Journal bearing	112
4.2.6	Camshaft	114
4.3	Transient model	117
4.3.1	Introduction	117
4.3.2	Methodology	117
4.3.3	Results and model validation	118
	4.3.3.1 Model validation: Drive cycle fuel consumption	118
	4.3.3.2 Mechanical losses and its distribution during driving cycles	124
4.4	Conclusions	132

Bibliography	133
---------------------------	------------

4.1 Introduction

In this chapter, the main results obtained from the stationary and transient models will be detailed. On one hand, the chapter will start showing the settings obtained in stationary mode and the main characteristics of each tribological pair such as: minimum oil film thickness, friction forces caused by asperities and by the hydrodynamic film, determination of the lubrication regime as a function of the operating points...

On the other hand, in the transient model, the adjustment made will be detailed and an analysis will be made of the energy consumed by each tribological pair during the real driving cycle, as well as the main operating points where each pair acts.

From both models, main conclusions of the strategies to be followed for fuel consumption reduction will be obtained, starting the next chapter of the thesis.

4.2 Steady-state model

4.2.1 Methodology and boundary conditions

To validate the mechanical losses model, 20 experimental engine map points were measured, with a total of 5 engine speed steps and 4 different engine loads. In table 4.1 the points measured are shown, where the column torque is the brake torque of the engine. This operating points are represented in figure 4.1 where x-axis is the engine speed and y-axis the brake torque.

For each operating point, the same methodology to calculate FMEP is used and performed using the "net-IMEP" method. The FMEP presented through this equation correspond to the rubbing losses and auxiliaries losses, the pumping losses are not considered as FMEP. On the one hand, 50 cycles of chamber pressure are measured in each of the cylinders, being the average of these cycles the indicated pressure used for the FMEP calculation. On the other hand, BMEP is measured and averaged to obtain the average effective torque of the engine for that

Table 4.1: Experimental engine operating points

Case Number	Engine speed (RPM)	Torque (Nm)	Load (%)	Case Number	Engine speed (RPM)	Torque (Nm)	Load (%)
1	1000	31.63	25	11	1500	209.65	75
2	1000	63.94	50	12	1500	291.86	100
3	1000	85.54	75	13	2500	80.68	25
4	1000	108.13	100	14	2500	139.19	50
5	1250	27.60	25	15	2500	230.96	75
6	1250	51.85	50	16	2500	330.94	100
7	1250	102.03	75	17	3500	69.12	25
8	1250	154.92	100	18	3500	131.51	50
9	1500	68.59	25	19	3500	199.39	75
10	1500	136.09	50	20	3500	273.76	100

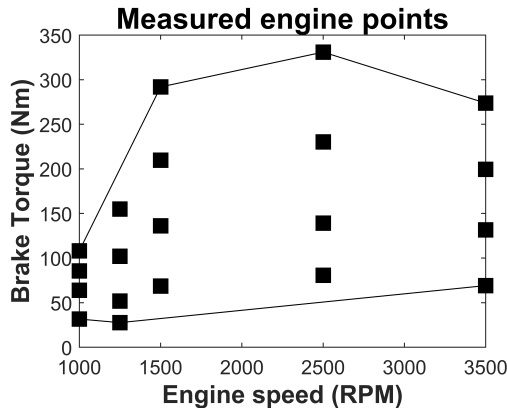


Figure 4.1: Engine measured points

operating point. Experimental mechanical friction losses are calculated as follows:

$$FMEP = nIMEP - BMEP = gIMEP - PMEP - BMEP \quad (4.1)$$

The term $gIMEP$ correspond to the gross indicated mean effective pressure calculated as:

$$gIMEP = \frac{\int_{BDC_{int}}^{BDC_{exh}} P dV}{V_d} \quad (4.2)$$

And the term $PMEP$ correspond to the pumping losses calculated as:

$$PMEP = \frac{\int_{BDC_{exh}}^{BDC_{int}} P dV}{V_d} \quad (4.3)$$

Being V_d the engine displacement

Engine oil considered

Experimental tests were conducted with a commercial 5W-30 oil. However, due to the importance of considering the effect of the shear rate in the estimation of friction losses in the engine a Non-Newtonian oil behaviour has been considered [1]. The oil used for the simulation was the one measured by Taylor et al. [2] since it presents the same SAE Grade that the used in the experimental test. The main characteristics of the engine oil selected is shown in figure 4.2:

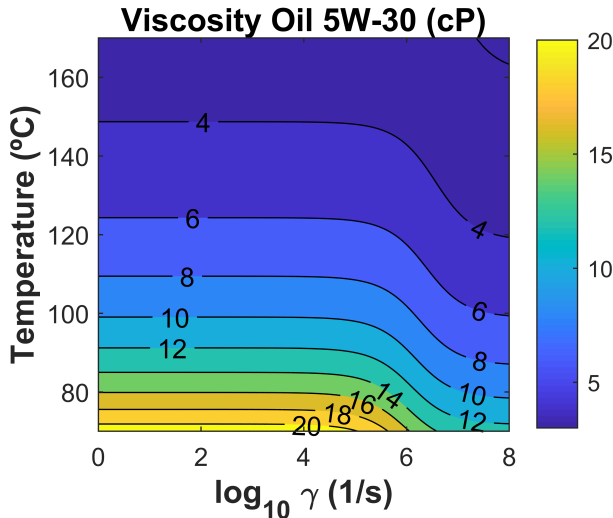


Figure 4.2: Dynamic viscosity of 5W-30 used for model validation

As it will be seen in later sections, considering the variation of viscosity with shear rate will be of high importance, especially in the piston ring and cam-follower contact tribological pairs, since the difference that can be obtained in terms of friction are similar to consider an oil with a different SAE grade.

4.2.2 Global results

This section will show the overall results obtained from the model. Starting with the validation with respect to the experimental results, and, in later sections, each tribological pair will be analyzed according to the results obtained.

Thus, in figure 4.3, the model results against the experimental results are depicted.

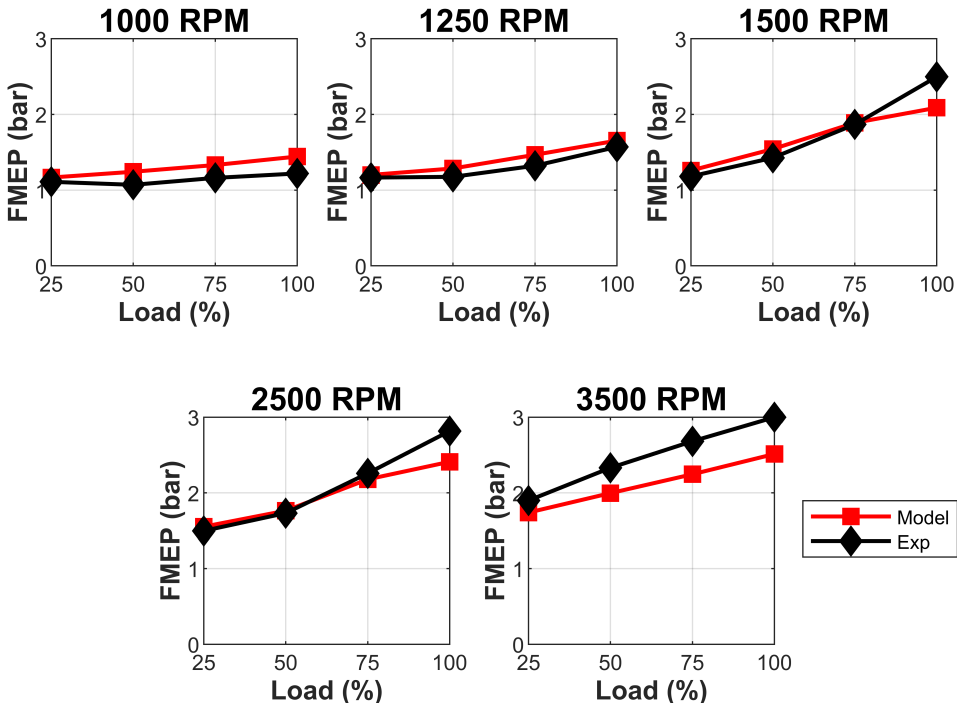


Figure 4.3: Steady state model validation

As can be seen, at 3500 RPM the model follows the trend of the mechanical friction losses, however it underestimates the values obtained experimentally with a 9% of difference. On the contrary, at 1000 RPM the model overestimates the value of the mechanical losses obtained, in this case, a 4% of difference is found. Once the model has been validated, the great advantage of modeling is to obtain tribology-related data that cannot be obtained experimentally or the cost associated with obtaining them is very high. The proof of this is the ability to separate the tribological pairs and to be able to represent them as a function of torque and engine speed as shown in figure 4.4:

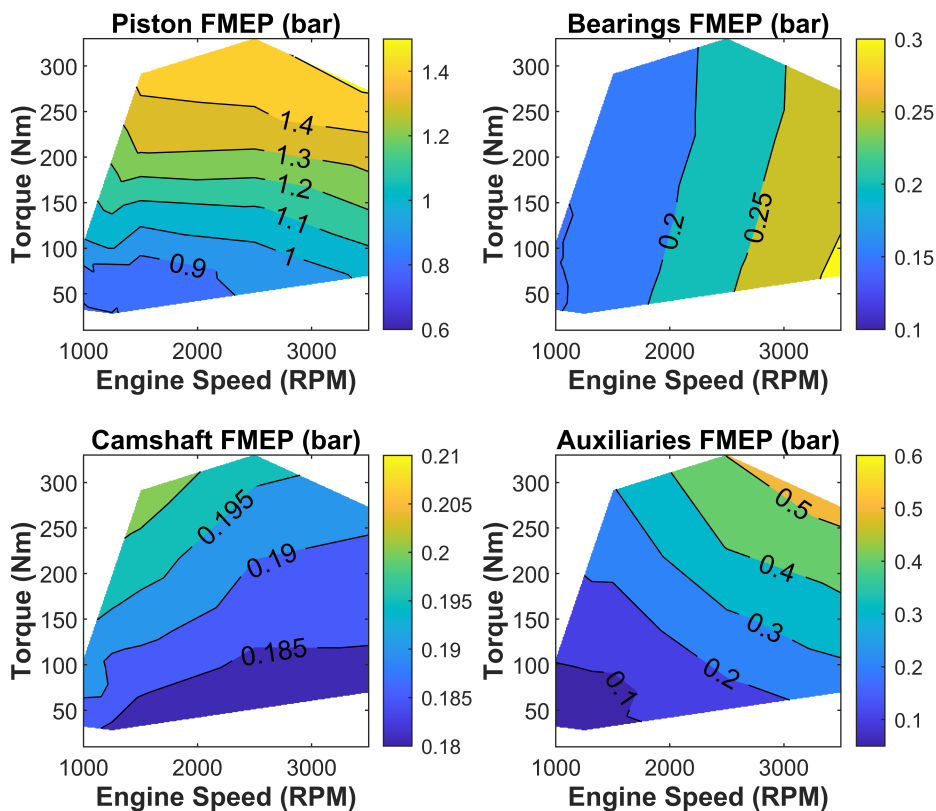


Figure 4.4: Friction engine maps for each tribological pair

The figure shows the friction for each component and its dependence on the engine speed and the associated torque. Thus, for example, for the

piston-ring assembly, if the engine torque keeps constant and increases the engine speed, it can be seen how the friction is smoothly attenuated. According to the Stribeck curve, this is an indication that the average operating lubrication regime of the rings is predominantly mixed. In the case of the bearings, increasing the engine speed, however, implies a direct increase in friction losses, characteristic of the hydrodynamic regime. Moreover, for a constant speed, increasing the load slightly decreases the FMEP, since increasing the load decreases the oil film and, therefore, the hydrodynamic losses. Finally, in the representative maps of the camshaft, at constant load, increasing the speed leads to a decrease in friction losses, even more accentuated than in the piston, therefore, the predominant lubrication regime is boundary/mixed. These maps are really useful to estimate, in a first approximation, the order of magnitude of mechanical losses in each component and in which lubrication regime is working in order to propose an optimal strategy to reduce mechanical friction losses in internal combustion engines.

However, the distribution of mechanical losses, in percentage, can also be estimated as shown in figure 4.5.

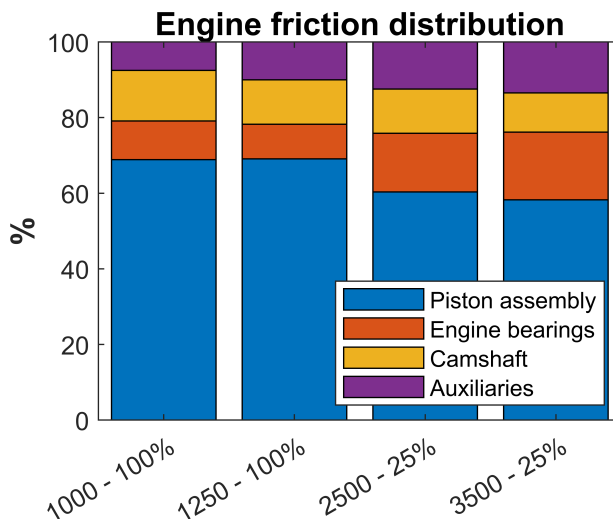


Figure 4.5: Mechanical losses distribution

As can be seen on Figure 4.5, 4 extreme operating points, from the point of view of the lubrication regime, have been represented. The

first two points would correspond, according to the Stribeck curve, to limit/mixed lubrication regimes, i.e. low speed and high load. The other two points are the opposite, i.e. high speed and low load, with the hydrodynamic regime predominating. In the first two operating points, the friction distribution has a greater effect coming from the piston and camshaft assembly because its operating characteristics make it predominate in this speed. However, the friction in bearings has a greater weight in the hydrodynamic part of the engine, being its distribution in almost 30%, at the expense of reducing the friction contribution from piston and camshaft. This overview of mechanical losses is useful when it is necessary to optimize the engine friction, since knowing the most representative points in a homologation cycle, it is known which lubrication regime predominates and what would be the optimal strategy to reduce fuel consumption.

4.2.3 Piston-ring assembly

As shown in figure 4.5, the piston ring assembly is the largest contributor to mechanical frictional losses in an internal combustion engine. If the distribution of friction losses is discretized in each of the rings of the piston assembly, it is obtained that the largest contributor to friction is the Oil Control Ring (OCR), followed by the Top Compression Ring (TCR) and finally the Second Compression Ring (SCR). This is depicted in figure 4.6. Different authors also show a similar trend in different works [3–5].

Friction losses in piston rings are closely linked to the surface finish of the liner, the ring itself and, in the case of the OCR, mostly to the tangential tension force. All this will determine the lubrication regime in which most of the cycle operates and, therefore, the strategy to be followed to reduce friction. There are different ways to determine the prevailing lubrication regime in any of the rings. One is through the minimum film thickness that exists between the ring and the cylinder. To estimate the limits between different lubrication regimes the classical approach is considered. Taking the λ ratio, defined as averaged film thickness divided by composite square roughness. If λ is lower than 1, then the lubrication regime is boundary. When the parameter is between

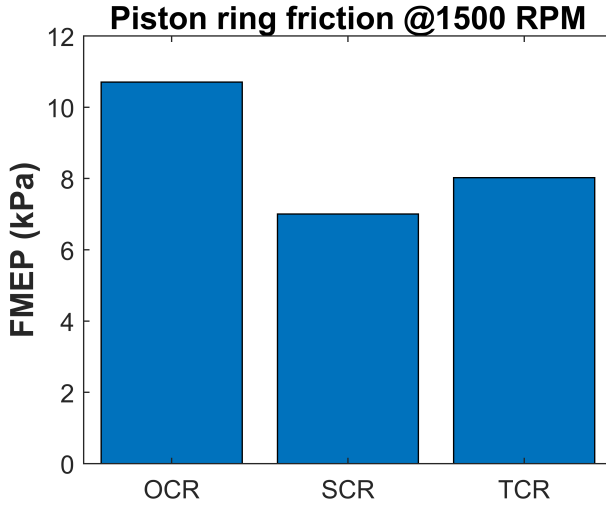


Figure 4.6: Friction losses in piston rings - Low load

1 and 3, the lubrication regime corresponds to mixed lubrication and for $\lambda > 3$ the lubrication regime is hydrodynamic [6].

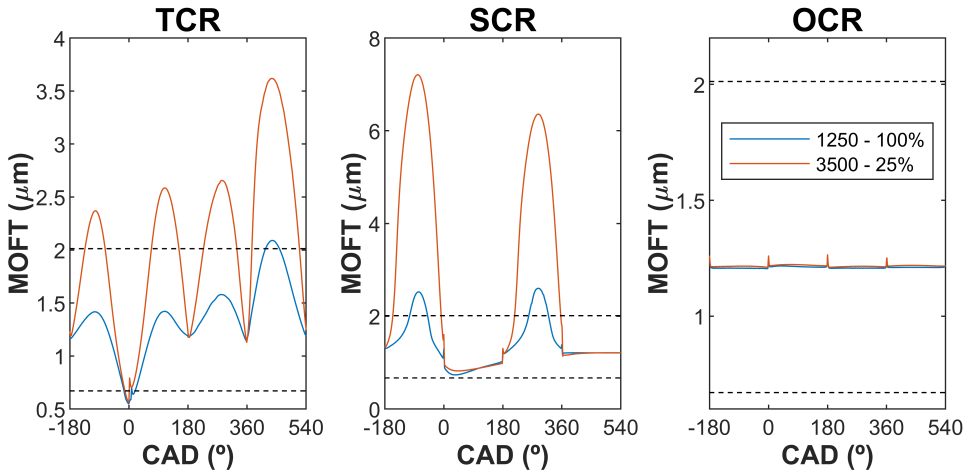


Figure 4.7: MOFT on piston-ring assembly

As shown in the figure 4.7, two engine operating points have been represented, one at high load and low speed (1250 - 100%) and the other at low load and high speed (3500 - 25 %). The consideration of the lubrication condition is starved for the rings. In addition, the limits of lubrication as a function of the oil film have been plotted in an orientative manner. The upper dashed line represents the transient between the hydrodynamic lubrication regime and the mixed lubrication regime. The second lower line represents the transition between the mixed lubrication regime and the boundary lubrication regime.

The three lubrication regimes are found in the piston ring assembly. The top compression ring reaches the boundary regime around top dead center in the compression stroke. This is because the boundary regime is favored at these points of the cycle due to the low instantaneous speed of the ring, in addition to the load supported by the pressure of the blow-by gases. The opposite case can be found at mid-stroke during the expansion stroke since the load supported by the ring is minimal and the maximum speed is given at mid-stroke, thus favoring the hydrodynamic lubrication regime. As previously mentioned, the major contributor to friction in the piston ring assembly is the oil control ring. Because its shape is flat to control the amount of oil reaching the upper rings, from the point of view of the Reynolds equation it does not form an oil film due to the shape of the face, although some hydrodynamic pressure is generated by the shape of the asperities. Therefore, its predominant regime, regardless of the operating conditions of the engine is boundary/mixed, being the largest ring contribution to mechanical frictional losses.

The effect of the lubrication regime can also be seen in the power dissipated by both hydrodynamic friction and asperity friction. Figure 4.8 shows the instantaneous power dissipated by friction in each of the rings. It should be emphasized that the in-cylinder pressure at high speed and low load is higher than for low speed and high load. Therefore, in spite of being in a more hydrodynamic regime, the frictional power due to asperity is higher at the point of high engine speed. However, the effect that occurs when representing the minimum film thickness is observed. At low rotational speed, the total contribution of frictional losses is substantially higher due to asperities than due to the hydrodynamic regime. On the other hand, at high rotational speed, although the contribution due to asperities is greater than the other point of the engine

represented, the contribution due to hydrodynamic losses also increases in greater proportion than in the previous point.

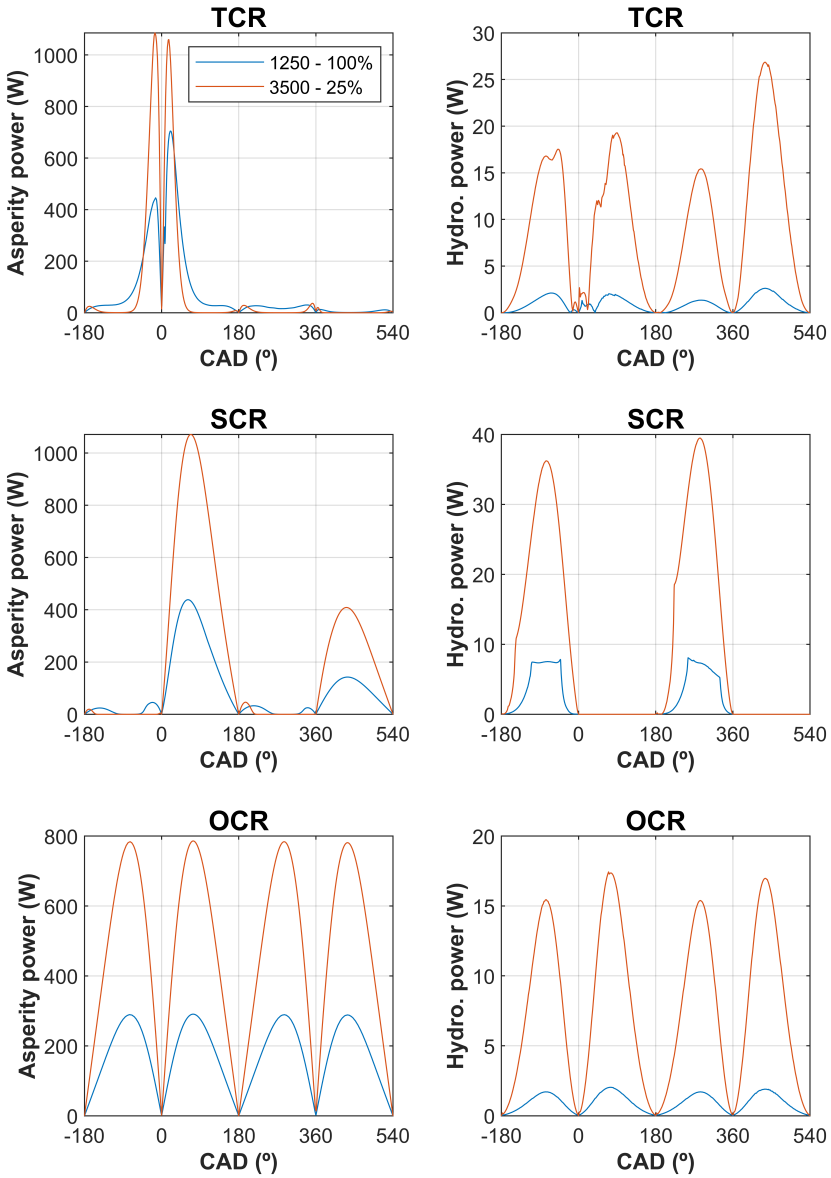


Figure 4.8: Friction power on piston rings

Finally, to complete the information on the operating regime in which, in this case, the rings are found, the Stribeck curve is plotted, first instantaneous during the compression stroke. As can be seen, the hydrodynamic lubrication zone is entered instantaneously at 3500 rpm, something that had already been observed in Figure 4.9. Moreover, being in the compression stroke, once the top dead center is reached, the boundary lubrication regimen becomes more noticeable at low speed than at high speed.

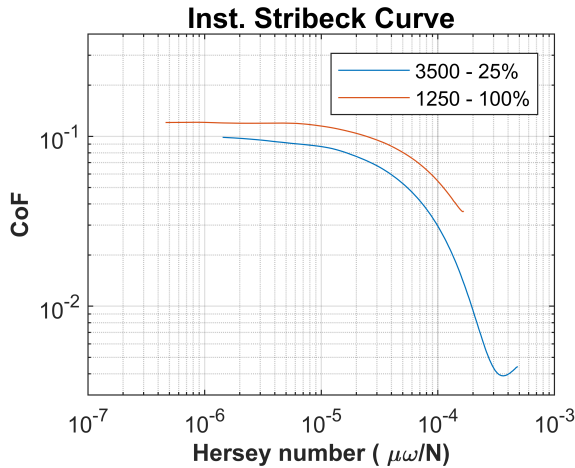


Figure 4.9: Instantaneous Stribeck curve for piston-rings.

Finally, the average Stribeck curve for the 20 simulated points can be plotted. The average friction coefficient over the cycle, the average viscosity over the cycle, the average instantaneous speed over the cycle and finally the average force applied, in this case to the ring, is used to calculate the Stribeck curve. The result is as shown in the figure 4.10.

The conclusion is that, on average, the rings, according to engine characteristics and boundary conditions, work in mixed lubrication regime.

4.2.4 Piston skirt

The skirt is one of the major contributors to friction in internal combustion engines. However, it is commonly known that its working

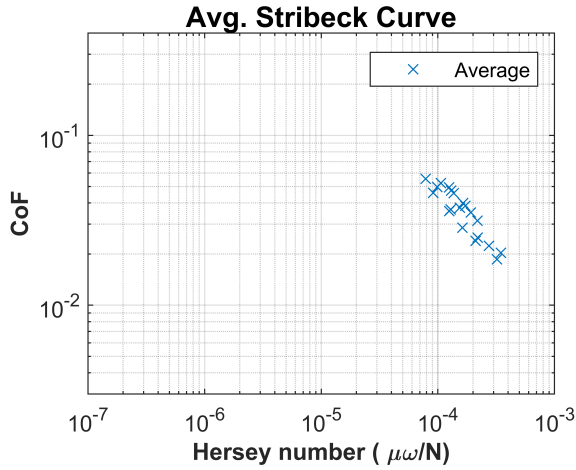


Figure 4.10: Average Stribeck curve por piston-rings.

lubrication regime is purely hydrodynamic, unless the oil viscosity decreases excessively. Therefore, it is to be expected that as engine speed increases, friction losses will increase, and conversely as engine load increases.

The instantaneous Stribeck curve for the compression stroke is represented as follows in Figure 4.11.

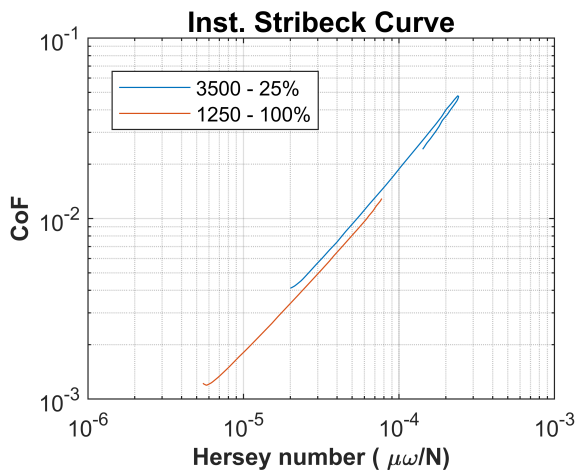


Figure 4.11: Inst. Stribeck curve for piston skirt.

Both operating points are under hydrodynamic conditions, so the oil film formed is much higher than λ equal to 3. Therefore, the decrease in liner friction is achieved by reducing the viscosity of the used oil. In terms of frictional power, due to the hydrodynamic regime, it is expected that for high rotational speed the power dissipated will be higher than for lower rotational speed tending more towards the minimum coefficient of friction. Figure 4.12 represents the friction force of each engine operating point.

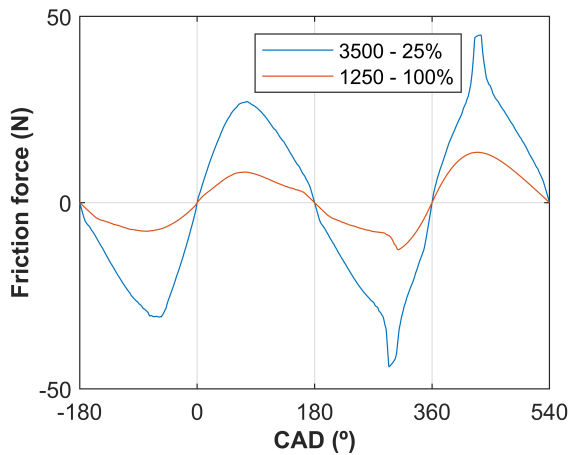


Figure 4.12: Piston skirt friction force curves at two different engine operating points.

4.2.5 Bearings

There are two types of bearings in the engine: connecting rod and journal bearings. For the analysis of the connecting rod bearings it will take the one of the first cylinder since, assuming that the chamber pressure is the same for each of the cylinders, the force distribution is the same. However, for the journal bearings it will take the one located between cylinder 2 and 3, since it will be the one with the highest load and, from the friction point of view, the one with the highest interest to study.

4.2.5.1 Connecting rod bearing

The connecting rod bearings support the load coming from the combustion chamber. Since it is a bearing, the predominant lubrication regime is hydrodynamic, therefore, it is expected that as the load supported by the bearing increases at the same engine speed, friction will decrease. However, this decrease in friction force is due to a decrease in the coefficient of friction and can enter a mixed lubrication regime. However, if the number of Hersey is reduced too much, the bearing may enter the boundary/mixed regime, which may cause increased wear. Figure 4.13 shows the instantaneous Stribeck curve 30 degrees before and after the maximum in-cylinder pressure.

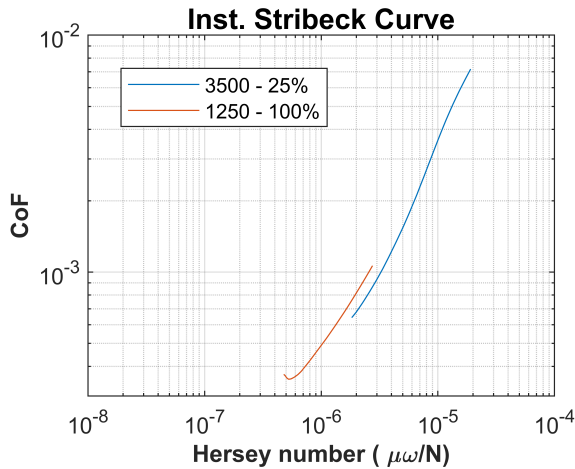


Figure 4.13: Inst. Stribeck curve con-rod bearing.

To corroborate that the lubrication regime can become mixed, figure 4.14 represents the minimum oil film thickness in the bearing, where the dashed lines represent the entry from the hydrodynamic regime to the mixed regime and from the mixed regime to the boundary regime.

Once past top dead center, the film thickness withstands the maximum load, eventually entering the mixed regime. If the bearing works close to the mixed regime, it has the advantage, on the one hand, of optimizing the mechanical losses due to friction but, on the other hand, there may be a risk of bearing wear due to the asperity force that it may be generated.

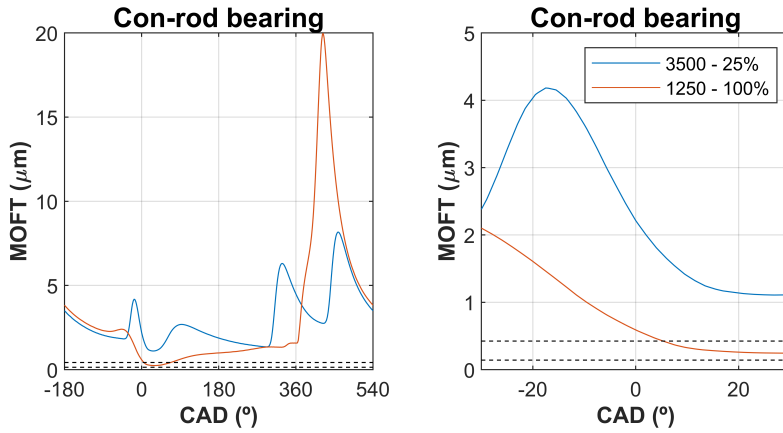


Figure 4.14: MOFT con-rod bearing.

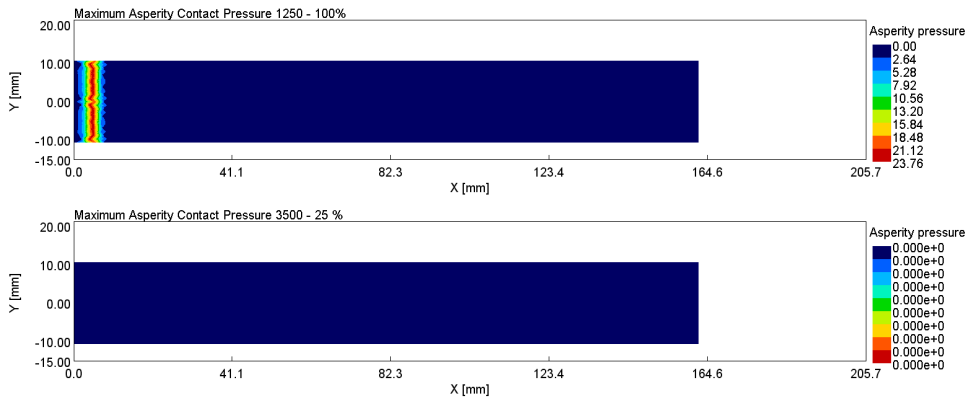


Figure 4.15: Asperity pressure con-rod bearing.

Finally, the maximum asperity pressure achieved by con-rod bearing at different engine speed and load has been represented in figure 4.15. As shown, the maximum asperity pressure is achieved in the 1250 engine speed and 100% load. The interaction between the surfaces occurs. On the other hand, as the rotational speed increases and the load decreases, there are no pressures due to the interaction of the surface roughnesses.

4.2.5.2 Journal bearing

The main difference between con-rod bearings and journal bearings lies in the load carried by each one. As mentioned in the previous section, con-rod bearings support the direct load coming from the combustion chamber; however, journal bearings, since they are not connected to the connecting rod, but to the crankshaft, do not support the direct load of a piston, but the load of the pistons that are closer to it. For example, the main bearing, which is located in the middle of the crankshaft, supports to a greater extent the load of pistons 2 and 3, and to a lesser extent, because it is farther away, the load of pistons 1 and 4. The journal bearings do not carry as high a load as the con-rod bearings and, therefore, the risk of wear is lower. Figure 4.16 represents the load supported by each main bearing.

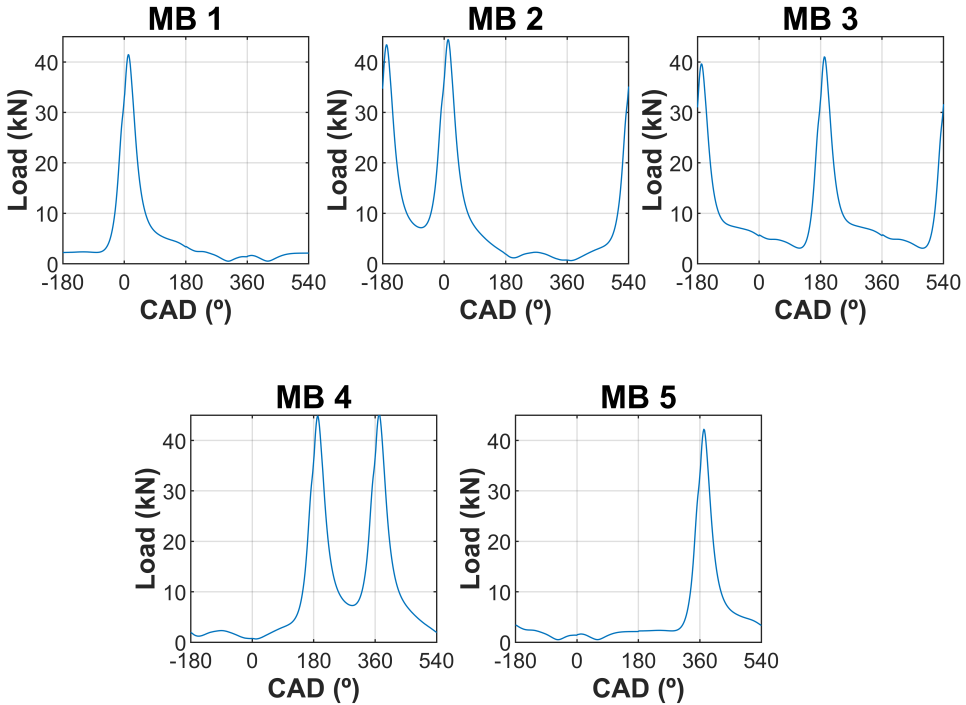


Figure 4.16: Load supported by main bearings.

Each of the bearings supports a load according to its place in the crankshaft. The bearing that supports the greatest load is MB 3, therefore, the analysis will be carried out on this bearing, as it is the one that contributes most to the friction of the 5 that make up the crankshaft. A first representation of the lubrication regime in which the bearing operates can be made by plotting the instantaneous Stribeck curve in the vicinity of the point of maximum bearing load together with the instantaneous coefficient of friction.

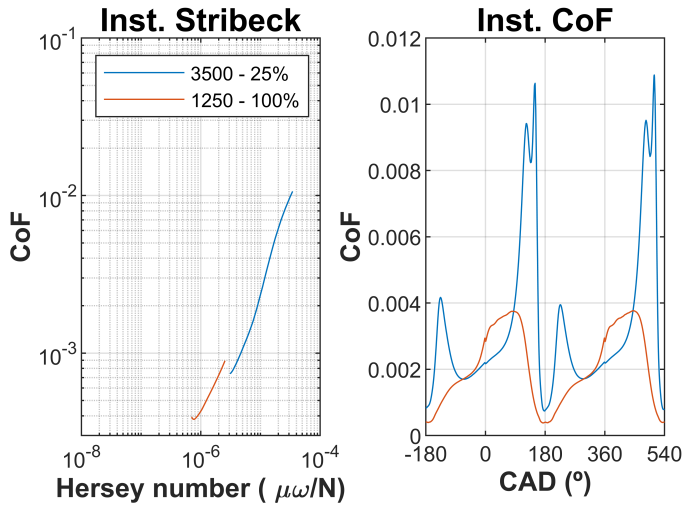


Figure 4.17: Instantaneous Stribeck curve and CoF for MB 3.

As can be seen in figure 4.17, the lower the rotational speed and the higher the load, the lower the coefficient of friction, i.e. the bearing is mostly working in the valley of the Stribeck curve. However, for a higher engine speed, the coefficient of friction increases but due to the increase of the minimum oil film thickness, increasing the viscous friction force and, therefore, the coefficient of friction.

As in the case of the conrod bearing, as it represents the minimum film thickness (figure 4.18), the lowest rotational speed enters the mixed speed. However, as the rotational speed increases, the film thickness is so high that it remains in the hydrodynamic regime, so the friction coefficient shown in the figure above corresponds to a viscous friction coefficient produced by the shearing of the oil film.

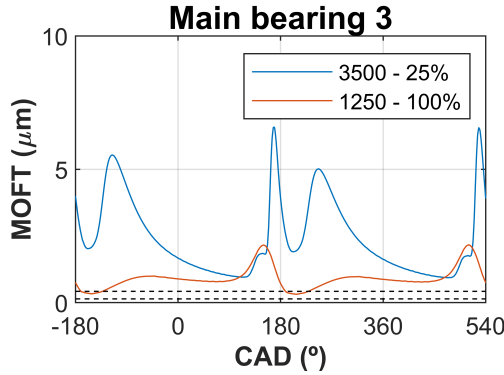


Figure 4.18: MOFT for MB 3.

4.2.6 Camshaft

In the model made in this doctoral thesis, not only the cam-follower contact on the camshaft has been considered, but also the bearings and the sliding of the valve during opening and closing. The figure 4.19 shows the total friction produced in each component and its percentage within the friction produced in the camshaft.

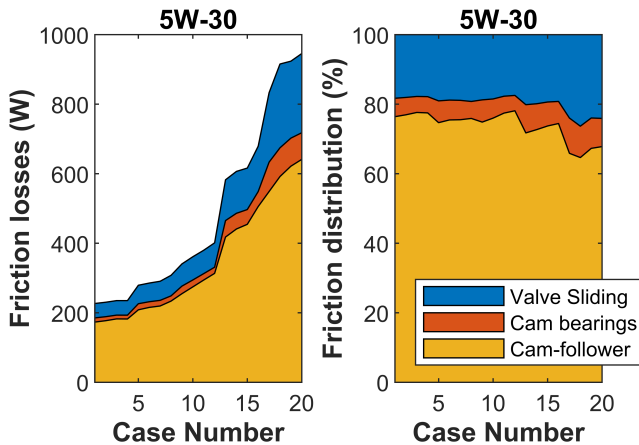


Figure 4.19: Friction losses in camshaft

As can be seen, depending on the operating point, the friction produced at the cam contact can range from 80% of the friction produced

in the camshaft to 70% produced at high speeds. As discussed in the previous section, due to the dependence on engine speed, the bearings increase their contribution as the engine speed increases. Finally, as valve slippage follows Coulomb's law, the higher the engine speed, the higher the load and the higher the friction produced. Since the main interest from a tribological point of view lies in the cam-follower contact, this section will carry out a tribological analysis focused on this tribological pair.

As said, the major friction production is given in the cam-follower contact mechanism. The cam-follower contact is dominated by the theory of elastohydrodynamic lubrication due to the high pressures of the oil film and the interaction between the materials, which increases, for example, the stress on the parts when they come into contact with each other. Figure 4.20 shows the part of the cam and the roller which are under higher stress, being in the order of 1 GPa.



Figure 4.20: Hertz Stress in lobe and roller.

Figure 4.21 plots the average Stribeck curve for the cam-follower set. The average friction coefficient and the average Hersey number during the contact time of the cam with the follower have been taken.

According to lubrication theory, the cam-roller mechanism tends to work in a boundary lubrication regime at the moment of contact, as shown in Figure 4.22. If its plotted the film thickness for two different rotational regimes, it can be seen that it remains within the boundary regime.

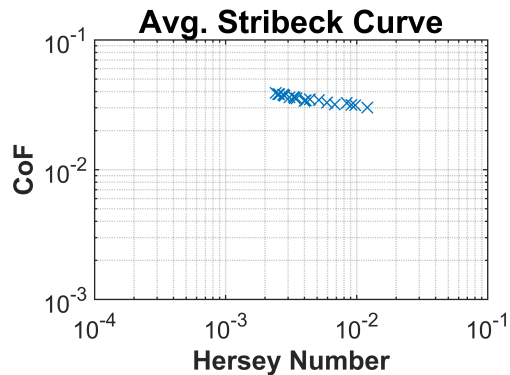


Figure 4.21: Average Stribeck curve for cam-roller contact.

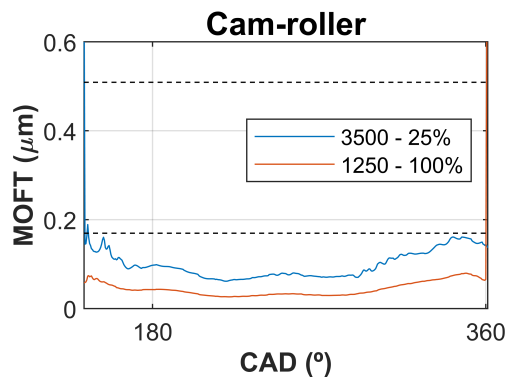


Figure 4.22: MOFT in cam-roller contact.

Despite being at two opposite operating points from the point of view of the lubrication regime, when contact occurs, at both points we are at the limit part of the regime. Therefore, the optimal solution to reduce friction is to include friction modifiers in the oil to reduce the coefficient of friction and to apply a polished surface finish to the cam surface.

4.3 Transient model

4.3.1 Introduction

This part of chapter 4 shows the model developed under transient conditions to estimate the energy dissipated by friction in each of the components that make up the engine during a real driving cycle. For this purpose, the boundary condition imposed has been that the engine has to start in hot conditions to avoid the dependence of the mechanical losses on temperature, which will be considered in a later section.

4.3.2 Methodology

To validate the model under transient conditions, experimental results have been compared against results obtained from the model. To validate the complete powertrain, the instantaneous torque measured at the wheel as well as the wheel speed during the driving cycle were taken, thus validating the gearbox ratio and performance. On the other hand, to validate the engine model, the fuel consumption has been taken as a reference, whose experimental data were taken from the engine ECU. In addition, the engine speed of the modeled engine has also been compared against the experimental one, so that once these variables coincide, the consideration is made that the experimental mechanical losses are equal to the mechanical losses obtained by the model and, therefore, the energy dissipated by each tribological torque in real driving cycles can be obtained.

The chosen route is a 33 km daily commute between two cities in Spain, consisting of urban sections, highway driving and rural roads. The urban section corresponds to the first 180 seconds of the cycle. Then, in the second section of the cycle and the most durable corresponds to the highway. Finally, the cycle ends with a rural road. This route has been tested with three different driver profiles, simulating standard operating conditions. The speed profile for each driving condition is shown in Figure 4.23. In addition to the speed profile, the altitude of the route is also considered and represented. The route present a positive height difference of 289 meters.

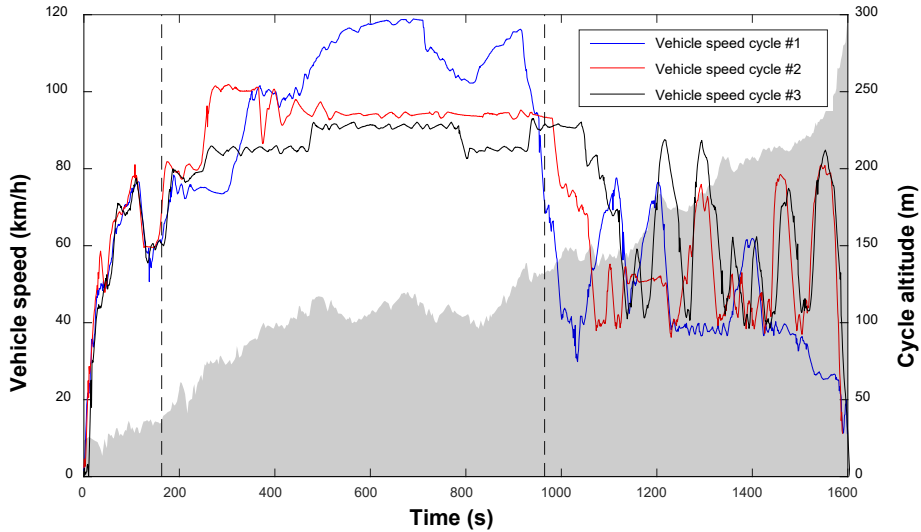


Figure 4.23: Speed profiles real driving cycle

4.3.3 Results and model validation

This section will show the results obtained experimentally against those obtained from the simulation model, in addition to other parameters obtained from the model that are not easily obtained from the experimental analysis.

4.3.3.1 Model validation: Drive cycle fuel consumption

The model has been fitted for driving cycle number 1 and validated in cycles 2 and 3, so that the vehicle speed are different in the cycles and the engine operating area differs in each one. Some parameters measured in the transients tests have been taken to assess the validity of the model. To validate the simulated powertrain, the energy expended by the driven wheel in the test and instantaneous engine speed during all cycles has been compared with respect to the simulation in GT-Drive. The energy expended at the driven wheels (EWE) has been calculated according to

the following expression:

$$EWE(kWh) = \int_{t_{ini}}^{t_{fin}} \frac{T_{wheel}(t) \cdot \omega_{wheel}(t)}{3.6 \cdot 10^6} \cdot dt \quad (4.4)$$

Where $T_{wheel}(t)$ is the instantaneous torque developed by the two driven wheels during the cycle; $\omega_{wheel}(t)$ the instantaneous wheel speed during the cycle and $3.6 \cdot 10^6$ is the conversion factor to obtain the expended energy in kWh . In Figure 4.24, the energy available at driven wheels in the three cycles is represented. The graph compares the energy available obtained by the simulation and the experimental test.

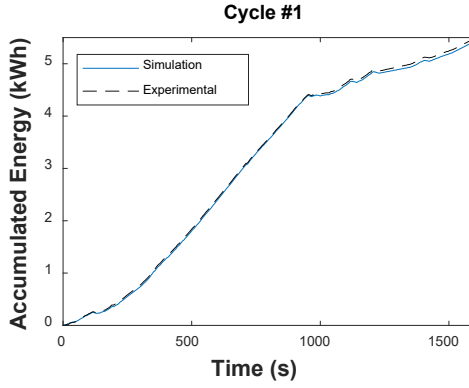
Also in Figure 4.25 the engine speed obtained from the experimental test and the engine speed obtained from the simulation are compared.

To validate the simulated engine model, the accumulated fuel consumption of the engine during the cycles has been taken as a reference. Figure 4.26 compares the accumulated fuel consumption measured experimentally and the fuel consumption obtained by simulation.

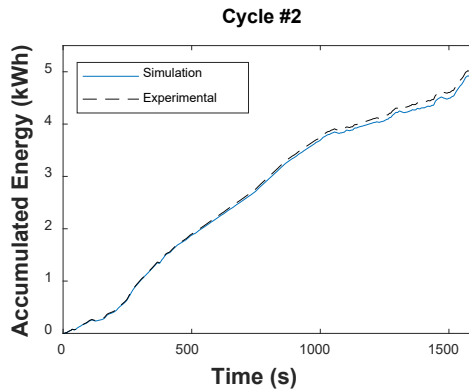
As shown, there are slight differences between the experimental result and the result obtained from the simulation. However, the trend is parallel. Depending on the engine operating points the results are more accurate, since the map interpolation can introduce errors in the simulation.

As a summary, table 4.2 shows the percentage error obtained between the experimental results and the results obtained by the simulation. This comparison shows the difference between the accumulated fuel consumption values at the end of the cycle and the total energy expended at the driven wheels at the end of the cycle.

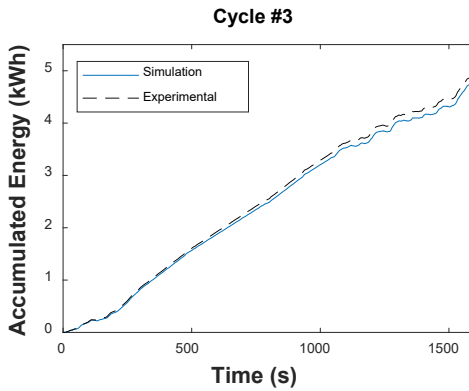
The differences are small between the measured and the simulated cycles thus, it can be concluded that the model performs well in the driving cycles studied. Hence, it is interesting for studying variables that cannot be obtained experimentally during a driving cycle, such as: the bivariate histogram which allows to determine the operating area of the engine during the cycles. In Figure 4.27, the different bivariate histograms for the three driving cycles are represented. These histograms are useful in order to justify the engine performance in terms of fuel consumption, mechanical losses and engine efficiency.



(a) Cycle 1

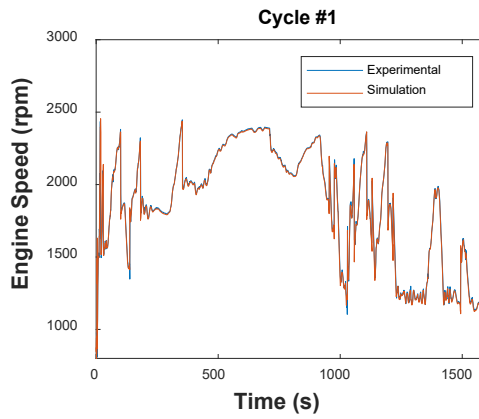


(b) Cycle 2

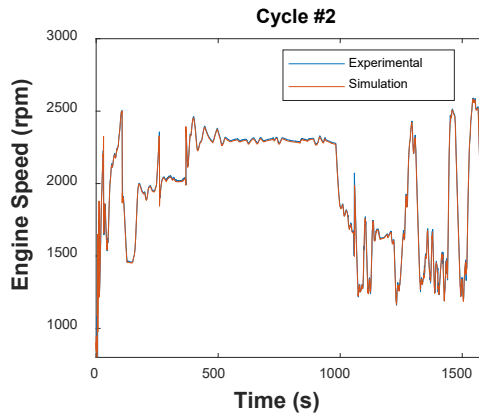


(c) Cycle 3

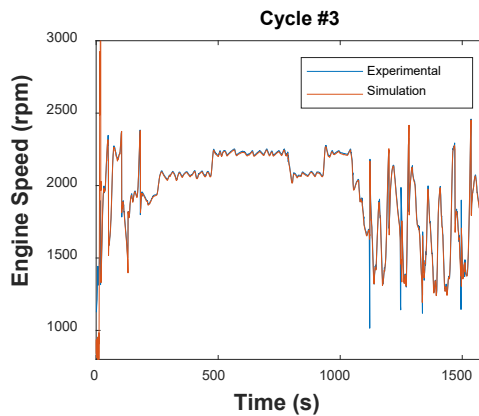
Figure 4.24: Accumulated energy in the vehicle wheel.



(a) Cycle 1

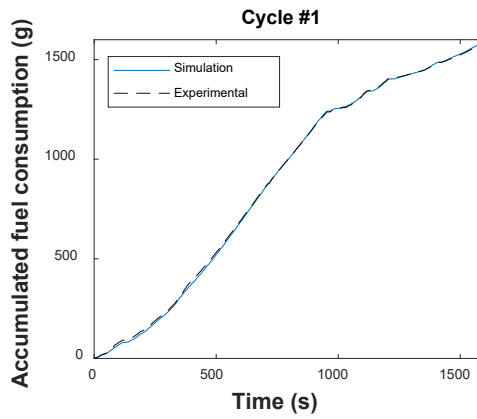


(b) Cycle 2

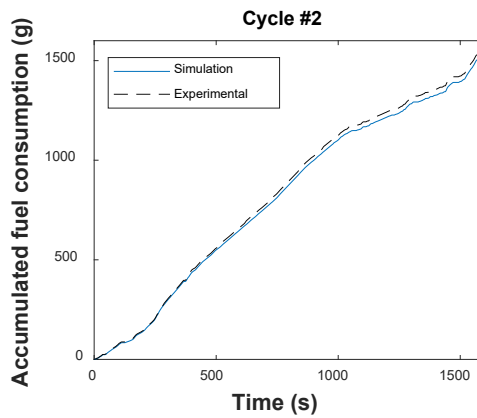


(c) Cycle 3

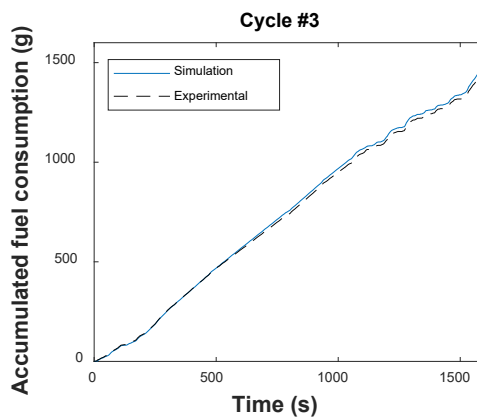
Figure 4.25: Comparison between experimental engine speed and theoretical engine speed.



(a) Cycle 1

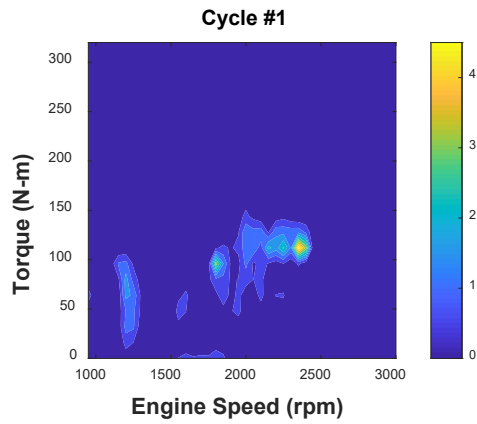


(b) Cycle 2

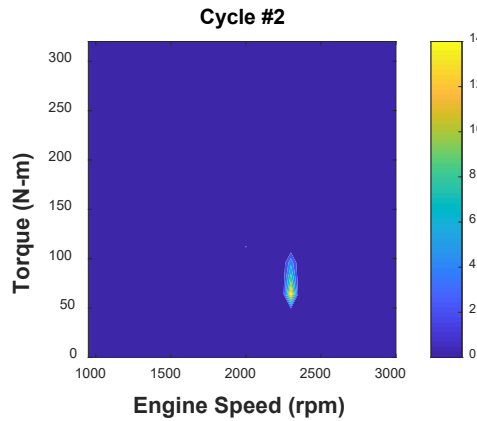


(c) Cycle 3

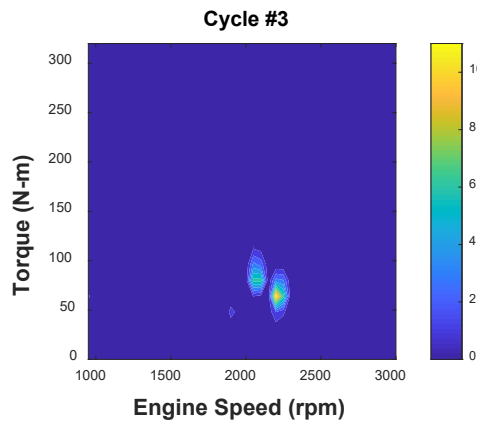
Figure 4.26: Comparison between experimental fuel consumption and theoretical fuel consumption.



(a) Cycle 1



(b) Cycle 2



(c) Cycle 3

Figure 4.27: Time distribution in each cycle measured.

Table 4.2: Experimental vs. simulation results

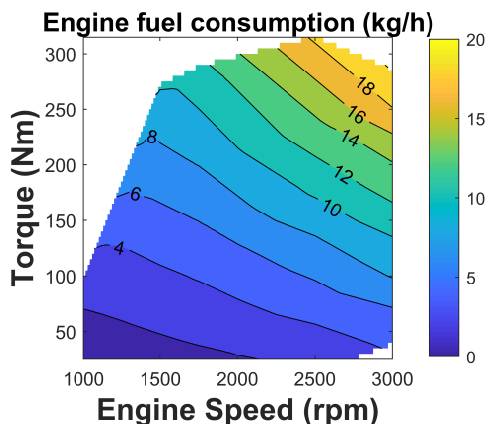
		Fuel consumption (g)	Expended wheel energy (kWh)
Cycle N ^o 1	Experimental	1578.26	5.44
	Simulation	1583.02	5.39
	Difference (%)	0.30	-0.96
Cycle N ^o 2	Experimental	1534.34	5.01
	Simulation	1509.39	4.91
	Difference (%)	-1.62	-2.02
Cycle N ^o 3	Experimental	1429.70	4.87
	Simulation	1457.43	4.74
	Difference (%)	1.94	-2.52

In this way, the different fuel consumption of each cycle can be justified. Before that, engine consumption map and specific fuel consumption map are shown in Figure 4.28 derived from previous work.

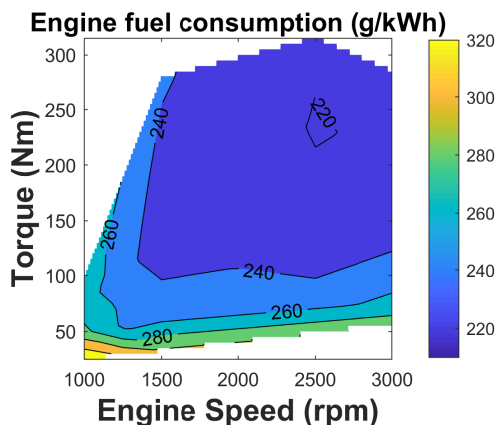
As shows Figure 4.27, cycle number 2 and cycle number 3 have very similar operating area. Thus, during both cycles the average specific fuel consumption are quite similar. However, the total fuel consumed is different. As the powertrain efficiency is the same for both cycles, the higher expended energy in driven wheels is the higher fuel consumption in the cycle for that reason the fuel consumption in cycle 3 is 7% higher than in cycle 2. The same analysis would be made in order to explain the mechanical losses in the engine and its distribution during the driving cycles.

4.3.3.2 Mechanical losses and its distribution during driving cycles

This section shows the calculation of the energy dissipated by engine mechanical losses during driving cycles. As demonstrated, the fitted model performs in a similar way to the engine and vehicle performance during experimental testing. Since in driving cycles the energy released in engine mechanical losses cannot be directly measured, it has been



(a) Fuel consumption



(b) Brake specific fuel consumption

Figure 4.28: Engine fuel consumption maps.

assumed that the mechanical losses calculated in the simulation (obtained from experimental map) is those that occur in the cycles tested. As demonstrated in [7], using steady-state friction engine maps in order to estimate the friction losses in a transient cycle is a good general agreement. That methodology is more accurate if the engine temperature at cycle start is warm conditions. In cold starting, thermal dynamic effect in engine friction are more significant due to the exponential increase of the viscosity with the temperature and the model accuracy decrease. In this work, the mechanical losses maps introduced into the model

were measured under warm conditions and fixed engine oil temperature. During the driving cycle measured, the engine starting was in warm conditions, but the engine temperature differs 10 °C approximately during the test, and therefore, the friction dynamic effects could appear. Consequently, the friction losses distribution variate. However, to justify the phenomenon of non-dependence on temperature in this methodology several points of the stationary map of the engine have been assessed under two conditions:

- The distribution of mechanical losses for the experimental measured oil temperature, in the stationary tests has been calculated
- The oil temperature has been decreased 10 °C from the experimental temperature measured for each point, and the friction losses distribution has been simulated under this new temperature condition.

Figure 4.29 shows that the mechanical losses distribution does not change a lot according to the temperature variation in the cycles when the engine starts in warm conditions, so, the effect of the reduced temperature variations can be neglected in this work. In the carried out driving cycle tests, the initial engine cooling system temperature was around 90°C. Subsequently and as developed in the stationary model, individual maps of each pair of engine friction elements, including auxiliary losses, are used. These maps have been introduced into the software to obtain an estimation of frictional losses during driving cycles in terms of: Engine bearings, valvetrain, piston-ring assembly and auxiliaries. In Figure 4.30, the distribution of the mechanical losses in function of engine speed and load is presented. In piston-ring assembly, the friction losses have a strong dependence with engine load and lubricant temperature. The higher engine load and temperature, the higher the contribution of piston-ring assembly to global mechanical losses is. In engine bearings, the friction losses increase faster with engine speed variation than with engine load variation. Also, the lowest lubricant temperature, the higher friction losses are due to the increase of dynamic viscosity of the engine oil. This condition is given at high engine speed and low load, it can be seen that the contribution of engine bearings to global mechanical losses is maximum in this operating

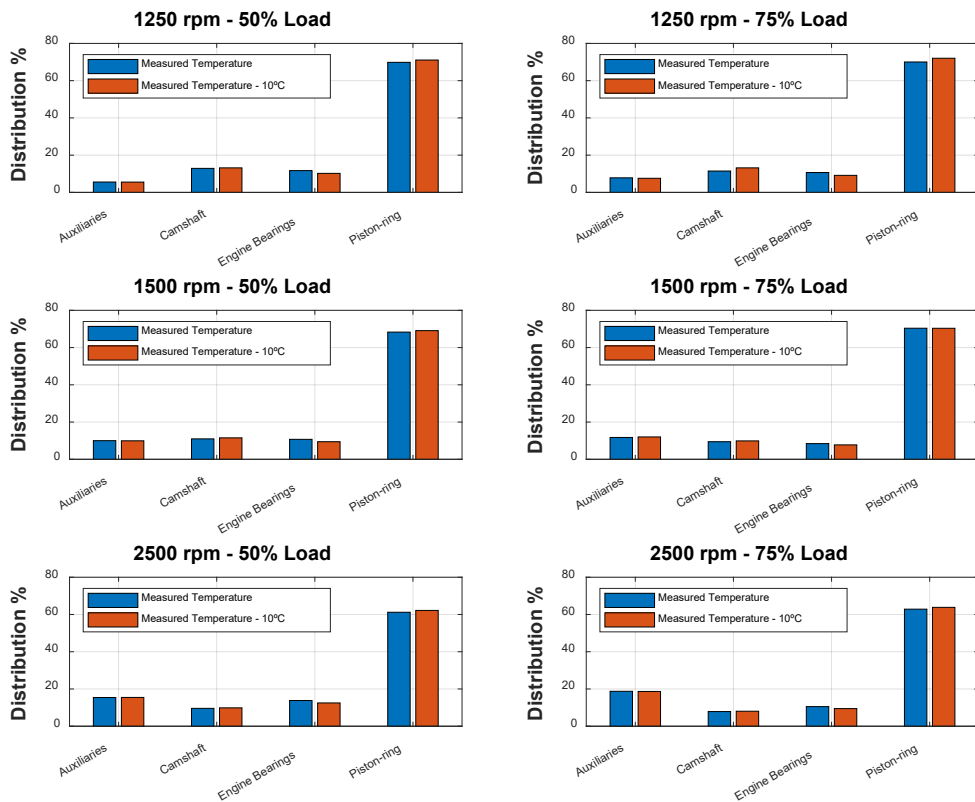


Figure 4.29: Variation of mechanical losses distribution with temperature

point. Finally, the friction losses in camshaft is closely bounded to the lubricant temperature. If the lubricant temperature increase, the viscosity, and consequently the oil film thickness in the lobe decreases. In this point, the boundary lubrication regime appears and the friction losses in the camshaft increases. However, in comparison with the piston-ring assembly and bearings, the variation of the total friction losses in the camshaft does not suffer a great change along the engine map. Thus, the maximum contribution of the camshaft friction losses in the global mechanical losses occurs at low load and speed.

Figure 4.31 shows the comparison between the energy lost by experimental friction, obtained from the interpolation of the mechanical

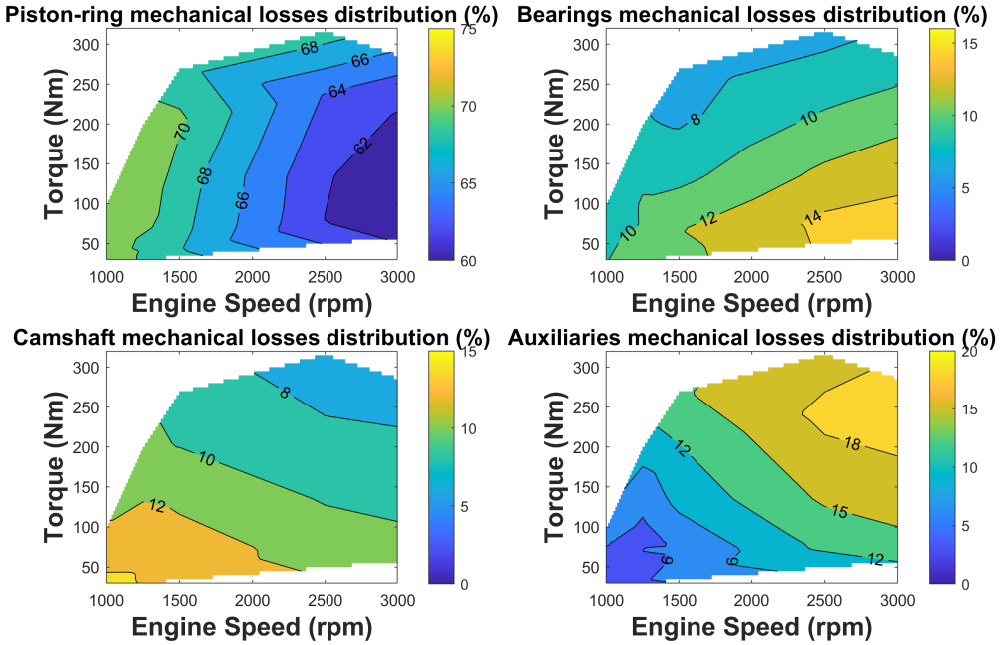
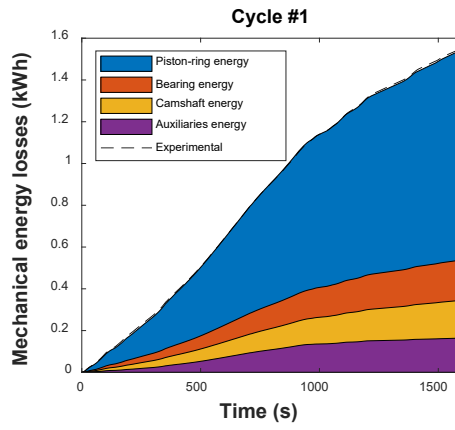


Figure 4.30: Friction engine maps in %

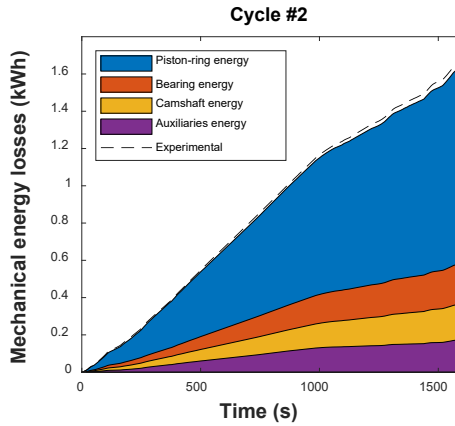
losses engine maps in stationary conditions, and simulated energy friction losses obtained from interpolating the individual friction maps of each frictional element. Due to the fitting presented, it has been considered that the model reproduces the mechanical losses during the driving cycle. As can be seen, most of the lost energy corresponds to the piston-ring assembly. Their contribution is 65% of the total energy lost. Due to the operating area of the engine in the cycles number 2 and 3 are quite similar as shown before, the distribution of the mechanical losses are similar. However, the operating area of the cycle number 1 is different in comparison to others. As the engine load is slightly higher in cycle 1 the distribution of the mechanical losses differs, increasing the proportion of the auxiliaries losses and decreasing the bearings and camshaft losses.

In Table 4.3 the obtained values and energy distribution of each frictional element during the two cycles are summarized.

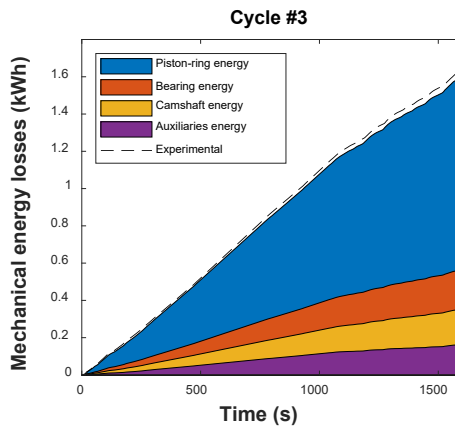
The lower friction energy losses are given for cycle number 1.



(a) Cycle 1



(b) Cycle 2



(c) Cycle 3

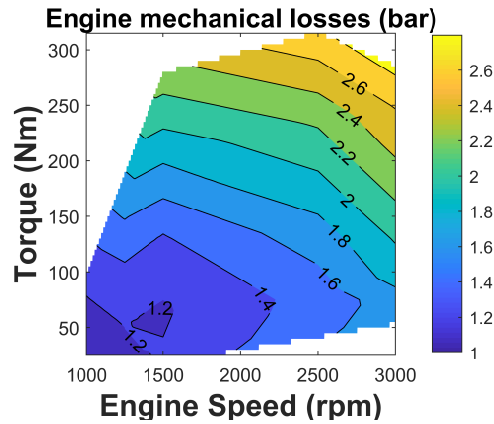
Figure 4.31: Energy dissipated by friction in the driving cycle.

Table 4.3: Mechanical losses distribution during driving cycles

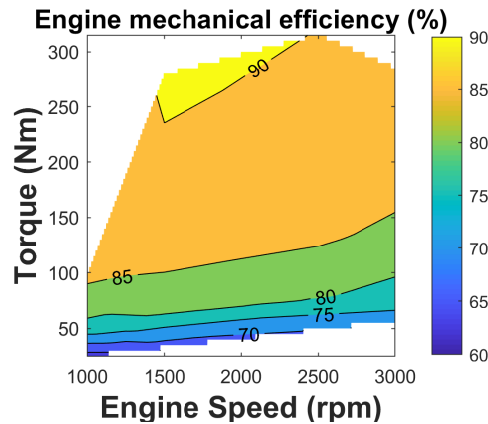
	Cycle N ^o 1		Cycle N ^o 2		Cycle N ^o 3	
	kWh	%	kWh	%	kWh	%
Piston-ring assembly	1.002	65.15	1.047	64.47	1.032	64.74
Engine bearings	0.192	12.48	0.216	13.30	0.211	13.24
Camshaft	0.180	11.70	0.190	11.70	0.190	11.92
Auxiliaries	0.164	10.67	0.171	10.53	0.161	10.10
Total	1.538	-	1.624	-	1.594	-

But the cycle N^o3 needs less energy to travel the same trip during the same time. This effect results in savings in the effective power required of the engine in cycle N^o3. However, the saving produced in the effective power is not proportional to that produced at the indicated power, because the engine operates at a point where the mechanical efficiency is lower for this cycle. In Figure 4.32 the engine mechanical losses and its efficiency are represented. The higher engine load, the higher mechanical efficiency is. As in cycle 2 as in cycle 3, the average load and engine speed are lower than cycle 1, but, the expended energy in the wheels is higher in cycle 1 than cycle 2 and 3 and, consequently the fuel consumption is the highest in cycle number 1. However, the mechanical losses in cycle number 3 is higher than cycle number 1 in spite of the fact the fuel consumption is minimal in cycle number 3, so, it can be concluded that minimal fuel consumption is not directly minimal engine mechanical losses.

Based on the figure 4.30, friction losses in the piston-ring assembly increase faster with increased engine load than with engine speed. The cycle number 1 has a higher average load than the other two cycles, so, the piston-ring distribution in that cycle is major than the other two cycles. Moreover, due to the similar operating area of the cycle number 2 and 3, the friction distribution in both cases is similar. As shown in Table 4.3.



(a) Engine mechanical losses (bar)



(b) Engine mechanical efficiency (%)

Figure 4.32: Engine mechanical maps.

However, for cycle N^o3, the total percentage of energy lost by friction decreases, increasing the percentage lost by the engine bearings. For this cycle, the average engine speed is higher. Friction losses in bearings depends basically on the engine speed and therefore the bearing mechanical losses distribution is minor in comparison to the cycle 2 and 3.

4.4 Conclusions

In this chapter, two lines of work are seen when addressing the problem of tribology in reciprocating internal combustion engines.

First, a model has been validated under stationary conditions by contrasting experimental results. One of the main advantages of the stationary model is the variability of parameters related to tribology that it provides and that are difficult to measure from the experimental point of view. These parameters are the minimum oil film thickness, the shear rate at which each tribological pair works and, from there, to estimate at what lubrication regime each part of the engine is working. With this information, it is easy to estimate the strategy to reduce the mechanical losses of the engine and increase its efficiency, either through strategies related to the viscosity of the lubricating fluid, or through the use of metallic components with a better surface finish, or both options.

On the other hand, a model has also been validated to estimate the energy consumed by friction during a real driving cycle. This tool is particularly useful for estimating the fuel consumption saved thanks to the tribological improvements that have been implemented. In addition, they give you the advantage of being able to estimate the energy consumed in each of the engine components through the model's stationary maps. In the next chapter, the model is further developed to consider that the engine temperature starts at ambient conditions and not at hot conditions as before.

Bibliography

- [1] Sander D., Allmaier H., Priebisch H., Reich F., Witt M., Füllenbach T., Skiadas A., Brouwer L. and Schwarze H. “Impact of high pressure and shear thinning on journal bearing friction”. *Tribology International*, Vol. 81, pp. 29–37, 2015.
- [2] Taylor R. I. and De Kraker B. R. “Shear rates in engines and implications for lubricant design”. *Proceedings of the Institution of Mechanical Engineers, Part J: Journal of Engineering Tribology*, Vol. 231, pp. 1106–1116, 2017.
- [3] Chen H., Li Y. and Tian T. “A novel approach to model the lubrication and friction between the twin-land oil control ring and liner with consideration of micro structure of the liner surface finish in internal combustion engines”. *SAE Technical Papers*, n° 2008-01-1613, 2008.
- [4] Li Y., Chen H. and Tian T. “A deterministic model for lubricant transport within complex geometry under sliding contact and its application in the interaction between the oil control ring and rough liner in internal combustion engines”. *SAE Technical Papers*, n° 2008-01-1615, 2008.
- [5] Profito F., Tomanik E. and Zachariadis D. “Effect of cylinder liner wear on the mixed lubrication regime of TLOCs”. *Tribology International*, Vol. 93, pp. 723–732, 2016.
- [6] Zhu Dong and Wang Q. Jane. “On the λ ratio range of mixed lubrication”. *Proceedings of the Institution of Mechanical Engineers, Part J: Journal of Engineering Tribology*, Vol. 226 n° 12, pp. 1010–1022, 2012.
- [7] Funk T., Ehnis H., Kuenzel R. and Bargende M. “Validity of a Steady-State Friction Model for Determining CO_2 Emissions in Transient Driving Cycles”. *SAE Technical Paper*, n° 2019-24-0054, 2019.

Chapter 5

Optimization of friction losses in ICE

Contents

5.1	Introduction	137
5.2	Friction reduction from the point of view of lubricant	137
5.2.1	Lubricant matrix	137
5.2.2	Results: Total engine friction	139
5.2.3	Results: Piston-ring and skirt assembly	141
5.2.4	Results: Engine bearings	144
5.2.5	Results: camshaft	146
5.2.6	Results: Evaluation of the engine oils in a WLTC cycle	149
5.2.6.1	Methodology	149
5.2.6.2	Main cycle characteristics	151
5.2.6.3	Fuel savings produced	152
5.2.6.4	Results: Total energy balance	155
5.3	Friction reduction from the point of view of surface finishing	157
5.3.1	Boundary conditions	158

5.3.2	Simulation results	158
5.3.2.1	Piston rings	158
5.3.2.2	Piston skirt	160
5.3.2.3	Journal bearings	161
5.3.2.4	Camshaft	163
5.3.2.5	Friction saving in the engine	165
5.4	Conclusions	168
	Bibliography	170

5.1 Introduction

In this chapter it will be studied two different strategies to reduce the friction produced in the engine. In the first part of the chapter, low viscosity engine oils with different rheological characteristics will be introduced in the stationary and transient model previously developed. From the stationary model, the tribocouples main parameters will be analyzed when LVEO are used and how it affects to the engine's performance. From the transient model, the reduction of fuel consumption will be analyzed in a WLTC cycle starting at ambient temperature.

Moreover, the second strategy analyzed will be the usage of different surface finishing on the piston liner assembly, reducing roughness and varying the viscosity of the oil used as well. This strategies will lead to fundamental conclusions for reducing fuel consumption and increasing the efficiency of internal combustion engines from decreasing friction losses.

5.2 Friction reduction from the point of view of lubricant

5.2.1 Lubricant matrix

SAE 5W-30 oil recommended by the engine OEM was used as a reference to assess the effect of low viscosity engine oil. From there, the SAE viscosity grade was reduced and VII viscosity index improver additives were added to enhance the oil's performance. Therefore, this work has 3 candidate oils to be evaluated: two 0W-20's and one 0W-12, whose main characteristics are shown in table 5.1.

Within the 0W-20 viscosity grade oils, the viscosity index has been improved through additivitation. The effect of the viscosity index can be seen in the variation of the dynamic viscosity with shear rate in figure 5.1.

At 40°C, the viscosity of 0W-20 Alternative Viscosity Modifier (ALT VM) is very similar to an oil with a lower SAE grade, in this case 0W-12.

Table 5.1: Lubricants used in the analysis and their properties.

Oil designation	5W-30	0W-20	0W-20 Alt VM	0W-12
SAE grade	5W-30	0W-20	0W-20	0W-12
KV @ 40°C [cSt]	67.84	46.21	28.35	30.20
KV @ 100°C [cSt]	11.87	8.48	7.61	5.89
HTHS @ 150°C [cP]	3.44	2.65	2.64	2.09
Density @ 15°C [kg/m ³]	848.9	829.7	834.9	833.0
Viscosity Index	172	161	285	140

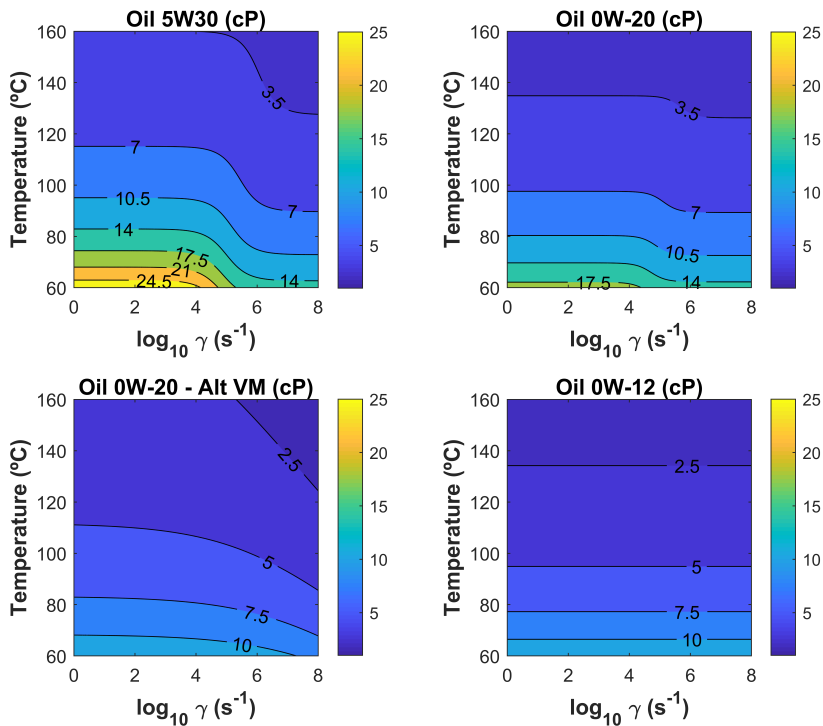


Figure 5.1: Engine oils shear thinning curves.

However, at a temperature of 100°C the viscosity of the oil is within the standard range stipulated by the SAE J300 standard as far as viscosity is concerned. In order to characterize the oil and be able to introduce the main features required by the model, the boundary friction coefficient has been measured with the Mini-Traction Machine (MTM). The specimens used were steel ball on steel disc, and the conditions were 30N load and 100°C for a range of speeds. The friction coefficient value at the boundary regime for the computational simulation was 0.09. This value was the same for both 0W-20s and the 0W-12 since the intention is to study the effect of rheological properties and not the coefficient of friction of these oils. Finally, the engine oil temperature used in the study is depicted in figure 5.2.

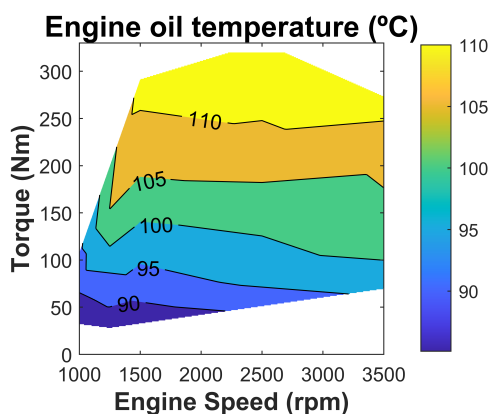


Figure 5.2: Engine oil temperature

5.2.2 Results: Total engine friction

This section will show the results obtained by simulating the friction model with different lubricating oils. Initially, it has been considered that the variation in the auxiliary elements with respect to the lubricating oil will be negligible compared to the main lubrication elements in the engine. Therefore, the FMEP results presented take into account the piston-ring assembly, the engine bearing and the camshaft.

From the model, the total friction produced in the engine is calculated and depicted in a graph related with load and engine speed as can be seen on Figure 5.3.

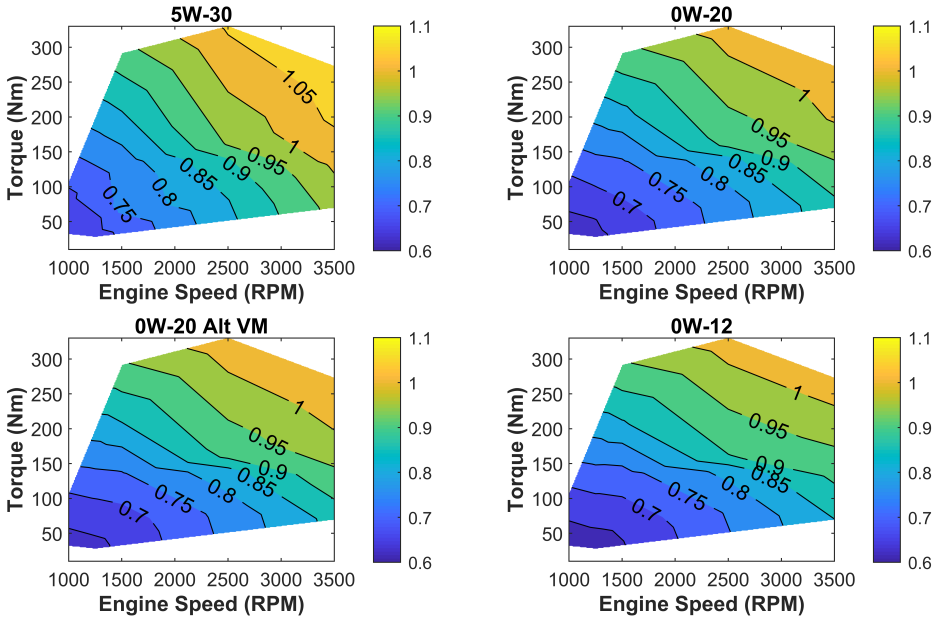


Figure 5.3: Engine friction maps

The lower the oil viscosity grade, the lower the friction losses in the engine are. This should occur in those tribocouples in which the predominant regime is hydrodynamic. If the FMEP savings are represented, taking the 5W-30 oil as a reference, it is obtained that the greatest savings occur with 0W-12 oil. See Figure 5.4.

The higher the engine speed and the lower the viscosity grade, the greater the effect on friction losses is. This can be seen in figure 5.4 where for high engine speed and low load, the friction saved is up to 7% compared to the 5W-30 reference oil¹. On the other hand, decreasing oil viscosity has the advantage of reducing mechanical losses in the hydrodynamic part but penalizes friction in the engine operating points which mixed regime is predominant. At high load and low engine speed

¹Savings are depicted as negative values.

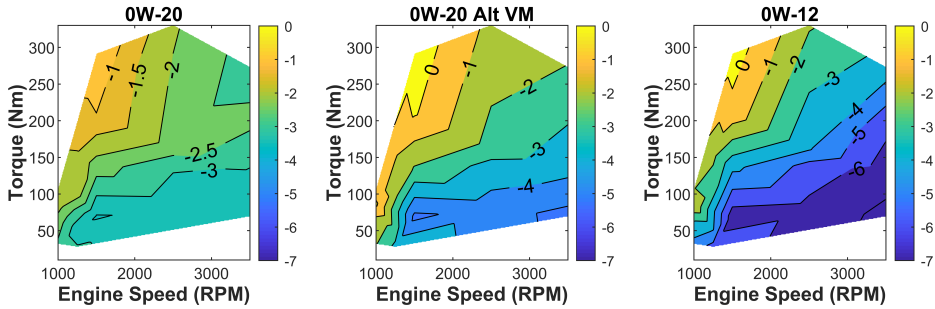


Figure 5.4: Engine friction savings (%)

for the 0W-12 and 0W-20 ALT VM oils, this effect is produced. However, for the 0W-20 oil there are lower savings in the hydrodynamic part of the engine compared to the 0W-12 oil, but there are also savings in the more mixed lubrication regime part of the engine. This effect has already been demonstrated by other authors [1–5]. Depending on the engine operating points, the use of LVEO oils will have a greater effect on the reduction or penalize the friction force.

5.2.3 Results: Piston-ring and skirt assembly

The different lubrication regimes to which the piston ring assembly and piston skirt were exposed during different operating points have already been discussed in sections 4.2.3. and 4.2.4. Beforehand, the use of LVEO would penalize the friction force in the piston ring assembly since, for the most of the operating points, the lubrication regime presented is mixed and, decreasing the viscosity of the oil would increase the asperity contact and, therefore, friction losses. The opposite effect of using LVEOs on the piston skirt would have the contrary trend. One question remains to be answered, however, and that is whether the decrease in skirt friction would compensate for the increase in ring friction.

Figure 5.5 shows the increase and decrease of friction in both piston-ring and piston-skirt when using different LVEO. Four operating points have been shown, two more mixed regimes points (1000 and 1500 RPM full load) and two more hydrodynamic regimes points (2500 and 3500 RPM - 25%). For this 4 points, the piston-ring assembly friction

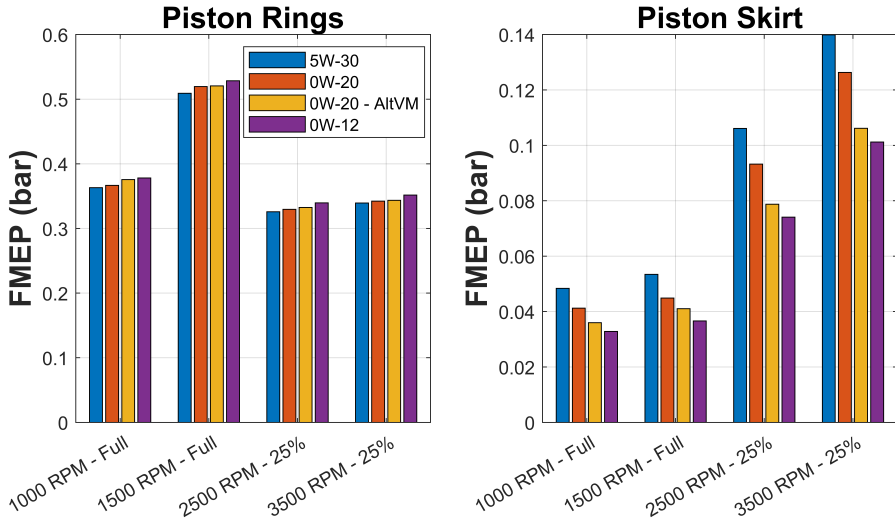


Figure 5.5: Engine friction in piston-rings and skirt

increases when decreasing the oil viscosity, however, for the piston-skirt assembly, decreasing the oil viscosity decreases the friction force, and this decreasing is greater when increasing the engine speed and, consequently, the hydrodynamic friction force. In the more hydrodynamic regimes, the friction decreases in the skirt compensates the increase in friction in the piston ring assembly. To see how it affects each point, Figure 5.6 shows the relative friction in the assembly comparing the different oils.

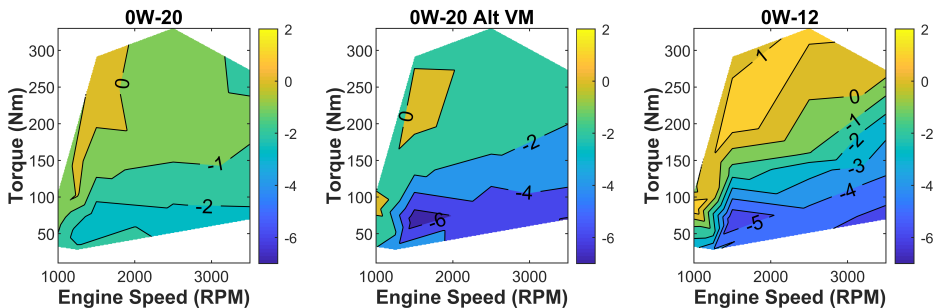


Figure 5.6: Engine friction in piston-rings and skirt.

By representing the minimum film thickness in the top compression ring it can be seen, in a better way, the effect that the viscosity reduction has on the oil. To see the difference between the oils, two extreme engine points have been selected.

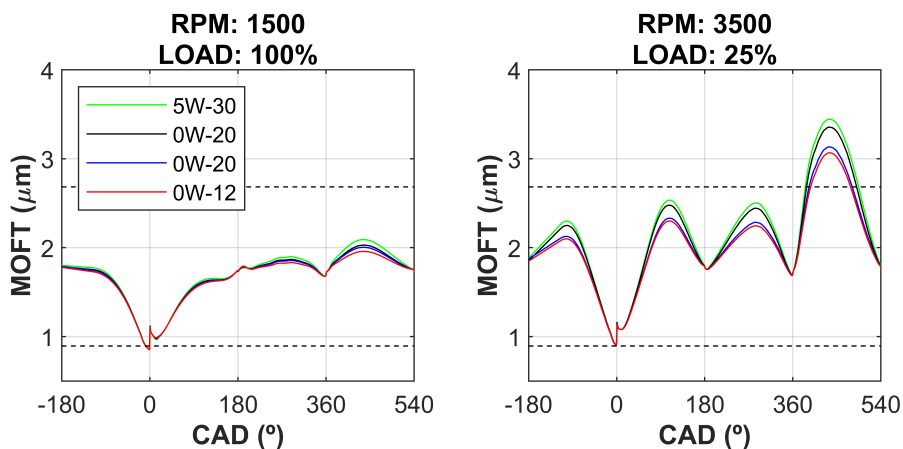


Figure 5.7: Top compression ring MOFT

The decrease in viscosity has a greater effect when the regime tends to be hydrodynamic, that is, at low load. But, as mentioned above, most of the cycle the rings are working under a mixed regime, so a decrease in viscosity increases the asperity friction forces and, therefore, increases the friction in the piston ring assembly. This phenomenon is more clearly reflected if the Stribeck curve is plotted in figure 5.8 for each of the simulated oils.

If the lower viscosity oil is taken, i.e. 0W-12, it tends to have a higher average coefficient of friction than, for example, 5W-30 oil. It is indicative that the lower oil viscosity, the higher the friction coefficient and, therefore, the higher friction produced. On the other hand, in piston skirt, it can be seen that the fact of decreasing too much the oil viscosity, can refer in the appearance of the force of asperity friction by roughness, indicative that, in a certain part of the cycle, the mixed regime is being reached. Although the point where it is reached is at very low speed and very high load, it is a strange point from the point of view of the homologation cycle. Figure 5.9 shows how, in the vicinity of the dead

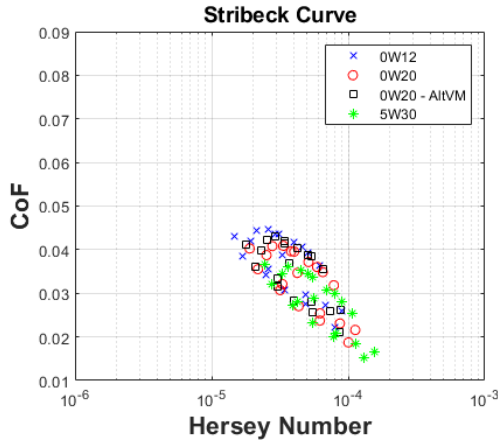


Figure 5.8: Stribeck Curve for TCR.

center, there is an increase in friction due to the appearance of asperities because the oil film decreases.

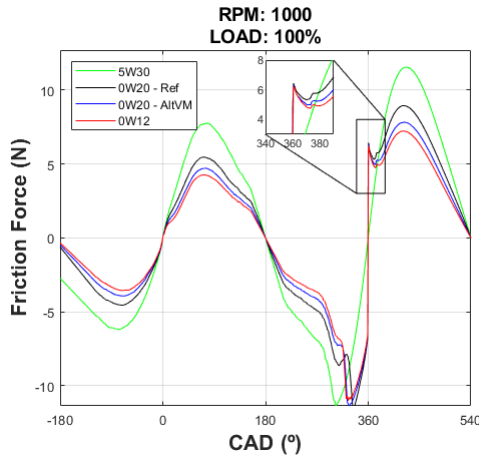


Figure 5.9: Friction forces in piston skirt.

5.2.4 Results: Engine bearings

Bearings are the tribocouples that works, mainly, in hydrodynamic regime and, therefore, it is the tribological pair on which the reduction of

oil viscosity has the greatest effect. Figure 5.10 shows the friction savings produced by using 5W-30 oil as a reference.

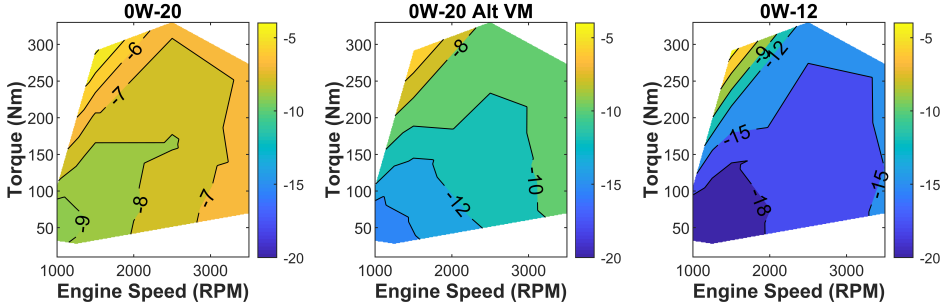


Figure 5.10: Friction savings (%) in engine bearings.

The maximum friction savings, as a percentage, reaches the limit of 18% compared to the use of a SAE 5W-30. However, decreasing the viscosity of the oil in the bearings has, on the one hand, the advantage of decreasing the viscous losses, but on the other hand, it starts to increase the losses due to asperity and potentially, the risk of the wear increases. This behavior is noticeable when very low viscosity oil is used in low speed and high load conditions. If the asperity friction force and the minimum oil film thickness is represented for the main bearing, taking into account the lambda limits to consider the different lubrication regimes, an increase of asperity friction is obtained as shown in Figure 5.11.

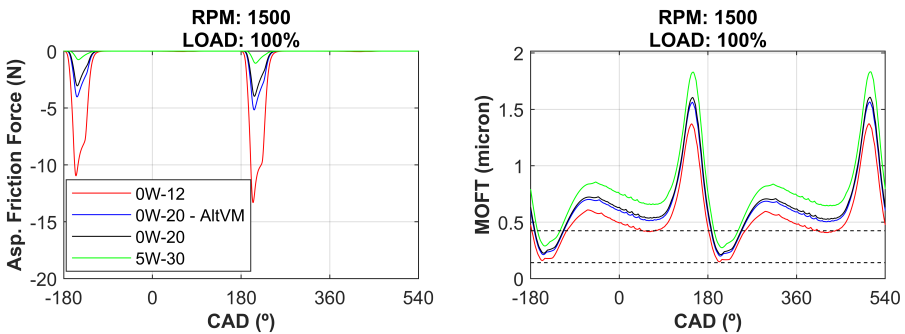


Figure 5.11: Asperity friction force and MOFT in main bearings.

As the viscosity of the oil decreases, the film thickness decreases, favoring the appearance of asperity forces between the journal and the bearing, especially at the points where the bearing supports the highest load. For the 0W-12 oil, the lubrication regime is mixed and even close to the boundary regime. To see how much the roughness pressure has increased, figure 5.12 shows the roughness pressure on the bearing surface with 5W-30 and 0W-12.

Where the asperity pressure has increased twice as much as initially calculated for the 5W-30. This increase in asperity pressure affects, on the one hand, an increase in the average coefficient of friction and, therefore, an increase in mechanical losses in the bearings and, on the other hand, an acceleration of the bearing wear.

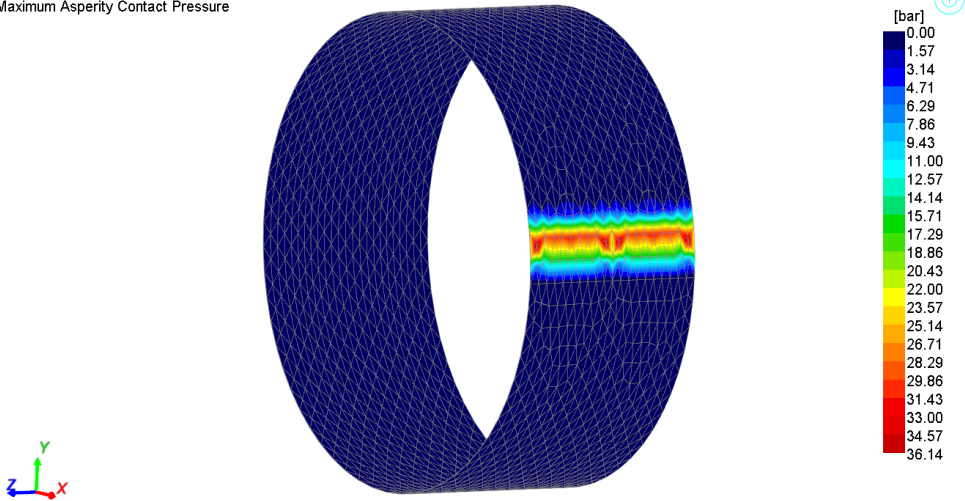
5.2.5 Results: camshaft

In the camshaft contact, the mixed/boundary regime predominates. So, reducing the oil viscosity would increase friction losses at the camshaft. Friction savings of camshaft are depicted in Figure 5.13.

Although decreasing the viscosity directly increases the friction according to the Stribeck curve, it should be noted that the camshaft bearings have also been considered. Thus for the 0W-20 oil, although the viscosity has been decreased, the savings in the camshaft bearings is greater than the increase produced as a consequence of cam-roller contact, also because the viscosity difference at high shear rate between the reference oil and the 0W-20 is not very high under the engine operating conditions in the simulation. On the other hand, it is observed that the 0W-20 ALT VM oil has a greater increase in friction than the 0W-12 oil. This phenomenon is caused by the viscosity of each oil at high shear rate, in the order of $10^7(s^{-1})$ and $10^8(s^{-1})$, where the 0W-20 ALT VM oil has a lower viscosity than the 0W-12 oil, therefore, although the viscosity has decreased and the friction in the camshaft bearings has decreased, it is not enough to compensate the increase in friction in the cam-roller contact, that is why the 0W-20 ALT VM oil is the oil that penalizes more in the camshaft.

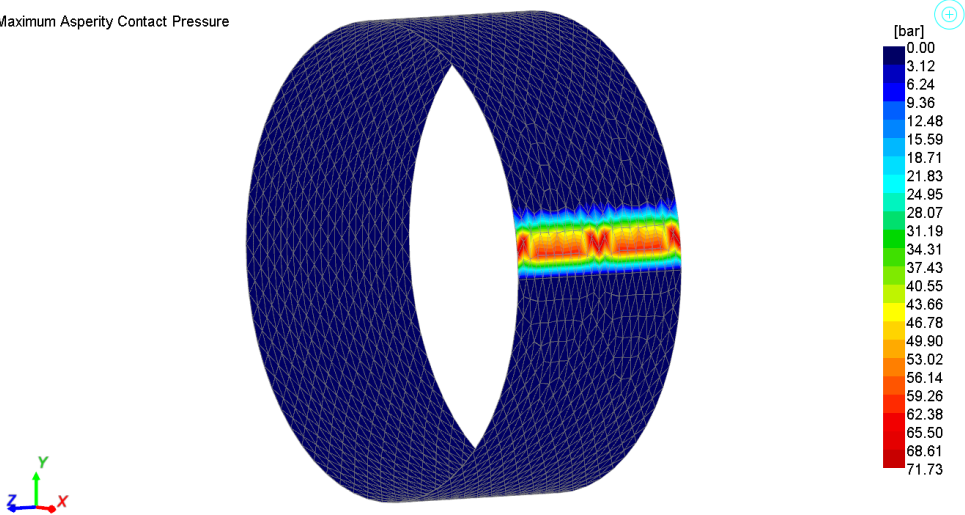
Figure 5.14 shows, for each of the engine operating points, the friction losses in each of the camshaft elements: the cam-roller contact, the

Maximum Asperity Contact Pressure



(a) 5W-30

Maximum Asperity Contact Pressure



(b) 0W-12

Figure 5.12: Maximum asperity pressure in main bearings.

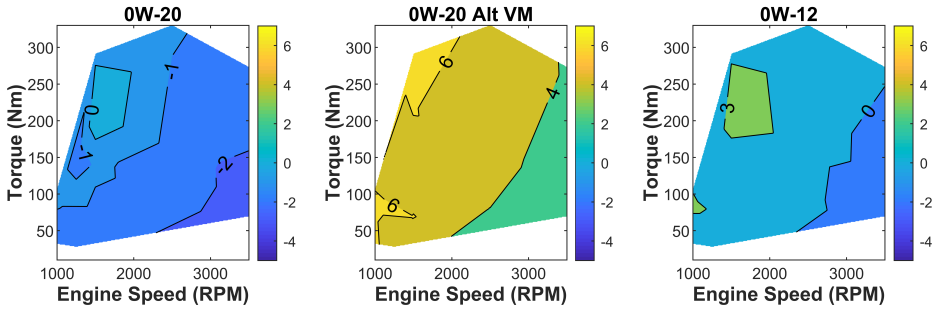


Figure 5.13: Friction savings (%) in the entire camshaft

bearings and the valve guide for the reference oil and for the oil producing the highest friction. The cases numbers are according to table 4.1.

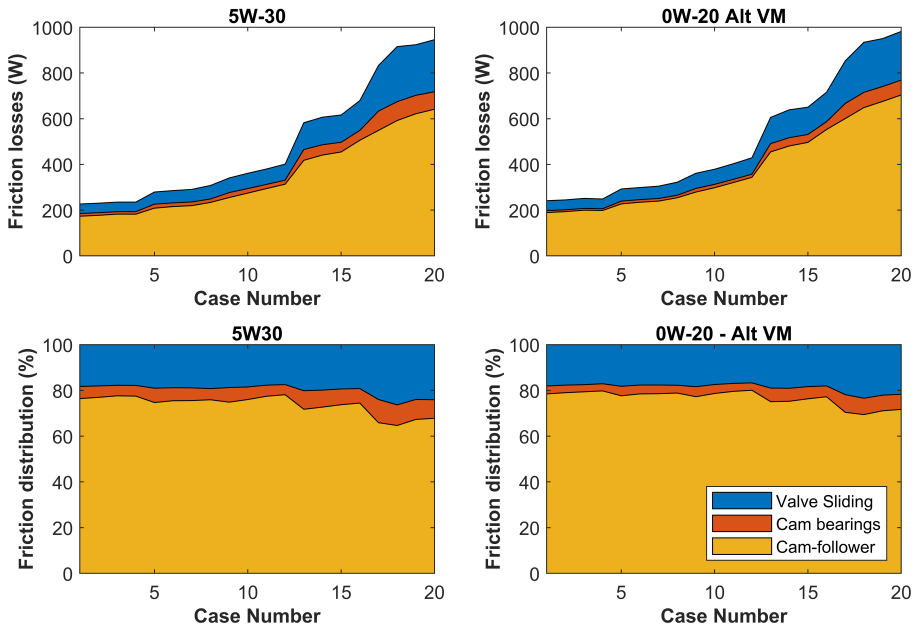


Figure 5.14: Friction in the entire camshaft

The 0W-20 ALT VM oil decreases bearing friction, but, on the other hand, the increase in friction at the actuator contact is greater than the

savings produced in the bearing and consequently increasing total friction in camshaft.

5.2.6 Results: Evaluation of the engine oils in a WLTC cycle

A study is carried out under real driving conditions to see the effect of using low viscosity oils in an reciprocating internal combustion engine. For this purpose, the transient model developed in the previous chapter is used and the speed profile corresponding to a WLTC cycle is introduced. In addition, as shown below, a temperature correction has been applied to take into account the variation of the viscosity of the oils during the cycle.

5.2.6.1 Methodology

The WLTC approval cycle was used to evaluate the different oils. This cycle starts at an ambient temperature approximately equal to 23°C. The engine oil temperature ends at about 90°C at the end of the cycle, which implies an evolution in temperature that will have an effect on the viscosity of the different oils. The oil temperature has been measured on the dynamic engine test bench, as depicted in Figure 5.15.

In this case the friction depends on the temperature, therefore the following expression is applied to correct the friction calculated from the maps with the temperature:

$$FMEP(T, Tor, RPM)_{cycle} = FMEP(Tor, RPM)_{ref} \cdot \left(\frac{\mu(T)}{\mu_{ref}} \right)^n \quad (5.1)$$

Where $FMEP_{cycle}$ is the FMEP during the cycle depending on oil temperature. $FMEP_{ref}$ is the FMEP calculated at reference temperature equal to 90°C. $\mu(T)$ is the dynamic viscosity of the oil simulated in function of the engine cycle temperature and μ_{ref} is the dynamic viscosity of the oil at temperature equal to 90°C. Finally n is the exponential value equal to 0.4 adopted from [6].

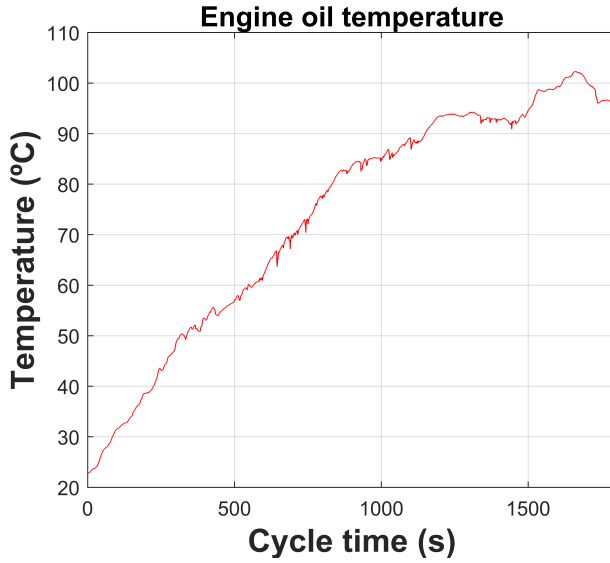


Figure 5.15: Engine oil temperature evolution during the WLTC cycle

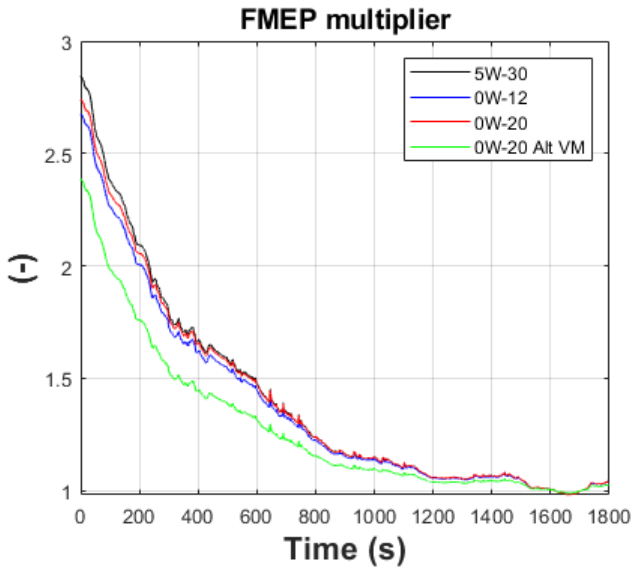


Figure 5.16: Friction correction coefficient.

The FMEP correction coefficient is applied to each oil, with the value that multiplies the reference FMEP. Figure 5.16 depicts the values of correction coefficient along the cycle time.

The lowest coefficient is for the 0W-20 ALT VM oil. This is due to its high viscosity index value which makes the viscosity variation at 100°C with respect to 40°C the lowest of all. So much so, that at 40°C the viscosity of the oil is lower than for a 0W-12, so the correction coefficient is the lowest. Figure 5.17 shows the viscosity of each of the selected oils.

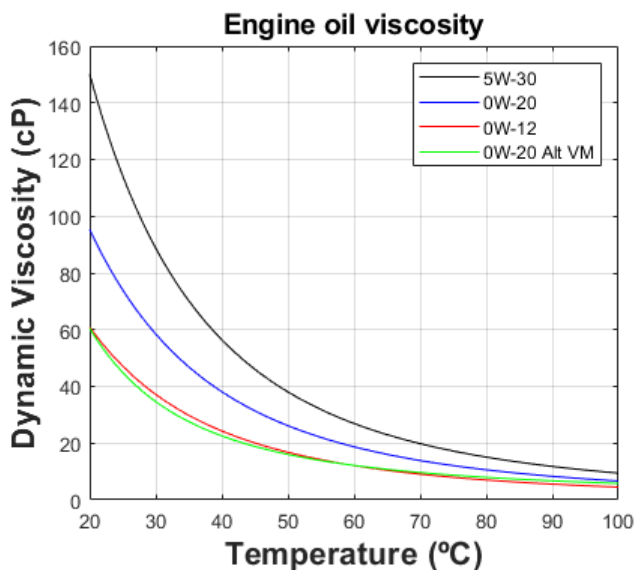


Figure 5.17: Engine oils viscosity tested.

5.2.6.2 Main cycle characteristics

The cycle where the savings in fuel consumption was evaluated oils has been the WLTC, since the vehicle is the same as the one described in the model of the previous chapter. The cycle has the speed profile showed in figure 5.18.

The cycle has a total duration of 1800 seconds, with the vehicle covering a total distance of 23.25 km. Table 5.2 shows the average characteristics of the cycle, as well as the average BMEP and the average engine speed.

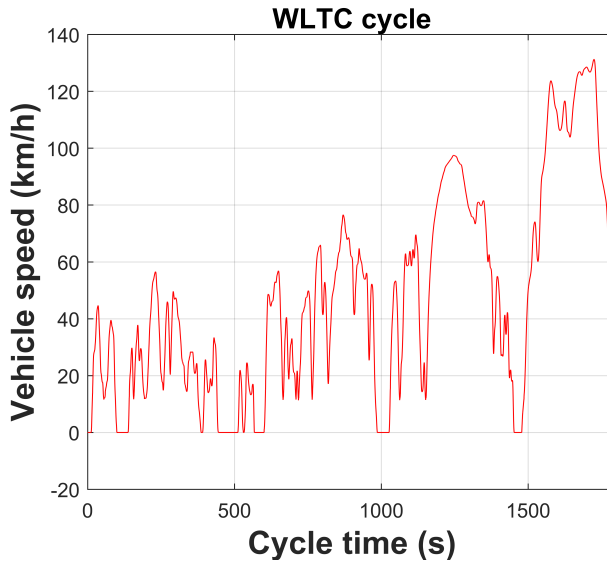


Figure 5.18: WLTC cycle speed profile.

Table 5.2: WLTC cycle characteristics

Cycle characteristics	
Average Engine Speed (RPM)	1261
Average Engine Brake Torque (Nm)	54.2
Average Engine BMEP (bar)	4.26
Time (s)	1800
Distance (km)	23.25

5.2.6.3 Fuel savings produced

Based on the description of the cycle, the behavior of the different lubricating oils in the engine has been evaluated. According to the stationary cycle analysis, the 0W-12 oil would be expected to produce the greatest fuel savings during the whole cycle, but, taking into account that the lowest correction coefficient is for the 0W-20 ALT VM, the following curve is obtained:

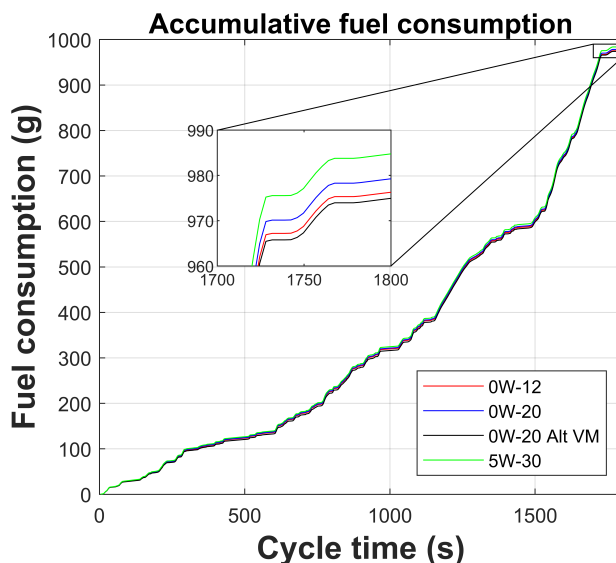


Figure 5.19: Fuel consumption for the cycle depending on the lubricant used.

The one that consumes the least amount of fuel is 0W-20 ALT VM, followed by 0W-12, 0W-20 and finally the oil recommended for the OEM manufacturer. The total fuel consumption for each of the oils is shown in table 5.3.

Table 5.3: Total fuel consumption and fuel savings for the different lubricants used.

Oil	Total fuel consumption (g)	Fuel savings (%)
5W-30	984.75	-
0W-20	979.25	0.55
0W-12	976.28	0.86
0W-20 ALT VM	974.94	1.00

0W-20 ALT VM, attending that it is the oil with the highest viscosity index and the lowest viscosity at low temperature, offers the best

performance in terms of fuel consumption. A more exhaustive analysis has been carried out taking into account that the WLTC cycle can be divided in 4 main parts as shown in figure 5.20. It shows the fuel savings produced by each lubricating oil in each sector in comparison with 5W-30 reference oil.

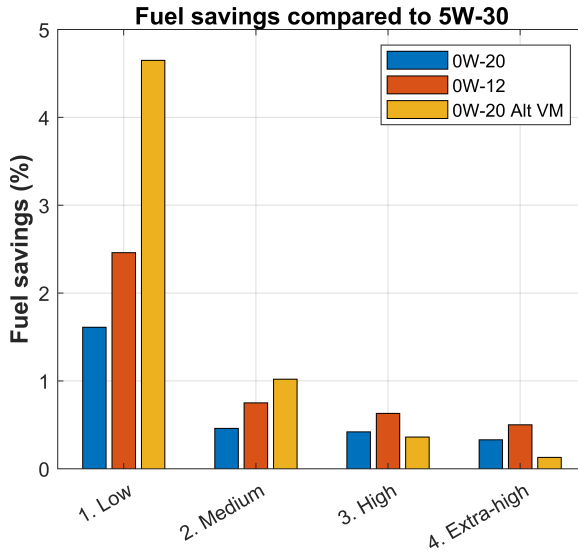


Figure 5.20: Lubricant fuel savings (%) divided in WLTC cycle stages.

Compared to other oils, it is observed that at the beginning of the cycle in the low and medium part, the 0W-20 ALT VM oil has a lower fuel consumption. However, as the engine’s operating temperature increases, and due to the fact that, on average, it works at medium speed and low load (conditions where the 0W-12 oil produces more friction savings), it generates lower fuel consumption savings in the last part and it has a worse behavior from the rheological point of view compared against 0W-12 oil.

For each stage of the cycle, the gross consumption in grams of fuel and the fuel savings produced with respect to 5W-30 are shown below. Table 5.4 shows this values.

Table 5.4: Lubricants fuel consumption by cycle stages

WLTC stages fuel consumption (g)	5W-30	0W-20	0W-12	0W-20 ALT VM
Low (0 - 589 s)	138.85	136.62	135.44	132.39
Medium (590s - 1022 s)	189.79	185.94	185.39	184.89
High (1023 s - 1477 s)	269.1	267.98	267.4	268.14
E-High (1478 s - 1800 s)	390.01	388.715	388.05	389.52
WLTC stages fuel saving (%)	5W-30	0W-20	0W-12	0W-20 ALT VM
Low (0 - 589 s)	-	-1.61%	-2.46%	-4.65%
Medium (590s - 1022 s)	-	-0.46%	-0.75%	-1.02%
High (1023 s - 1477 s)	-	-0.42%	-0.63%	-0.36%
E-High (1478 s - 1800 s)	-	-0.33%	-0.50%	-0.13%

5.2.6.4 Results: Total energy balance

The main advantage of the transient model is the ability to predict the energy consumed in each part of the vehicle. From the energy used to overcome the inertia of the car, to the energy dissipated in the fuel pump. All this is useful to have an order of magnitude of the frictional energy that it has been saved thanks to the use of LVEO. Therefore, figure 5.21 shows the energy accumulated in the cycle for the 5W-30 lubricant and for the lubricant with the lowest fuel consumption, 0W-20 ALT VM.

The decrease in total energy in each of the components is hardly observable. However, Table 5.5 shows the total energy in each of the friction components and the percentage reduction with respect to 5W-30.

In this case, when the engine is hot, the highest energy/friction saving in the piston ring assembly is given for the 0W-12 oil, however, when the temperature correction is applied and due to the higher viscosity index

Table 5.5: Lubricants energy consumption

Total energy (kJ)	5W-30	0W-20	0W-12	0W-20 ALT VM	Energy Saved (%)		0W-20 ALT VM
					0W-20	0W-12	
Piston	1432.4	1395	1386.4	1340.3	Piston	-2.61	-6.43
Bearings	474.59	432.43	383.22	396.66	Bearings	-8.88	-16.42
Camshaft	632.03	624.98	640.91	637.12	Camshaft	-1.12	0.81
Oil pump	121.74	96.78	74.56	82.54	Oil pump	-20.50	-32.20
Water pump		68.48					
Diesel pump		211.67					
Differential		780.51					
Gearbox		784.16					
Acceleration		12101					
Tires		4576.2					
Drag		6724.5					

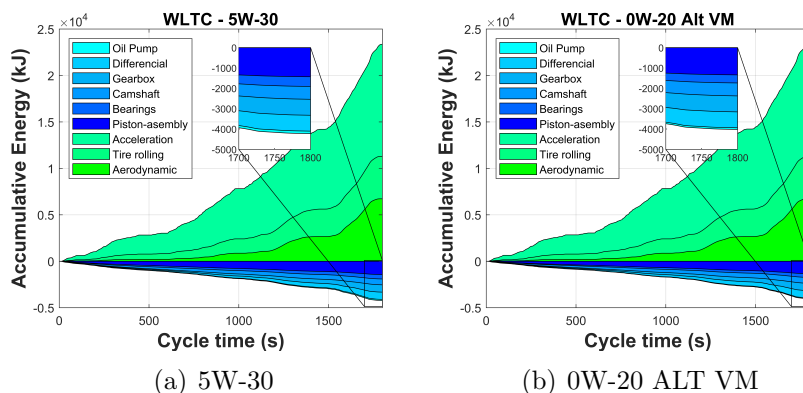


Figure 5.21: Vehicle consumed energy during the WLTC cycle.

of the 0W-20 ALT VM oil, this tendency is reversed. However, this effect does not occur for the bearings, since, although the 0W-20 oil has lower viscosity when cold, when in hot conditions the difference is so great that it does not compensate for the difference in viscosity when cold. Finally, in the camshaft the same thing happens as in the stationary model, the lower the viscosity, the higher the friction energy consumption.

5.3 Friction reduction from the point of view of surface finishing

In previous section, the optimization of friction losses from the lubricant's point of view was studied, focusing on its fundamental rheological properties. In this section, although a study will be carried out with 3 oils of different SAE grade, it is more focused on the FMEP savings produced in the engine by using two cylinders with different surface finishes, taking into account the reduction of the asperity force instead of reducing the hydrodynamic component.

5.3.1 Boundary conditions

For the study of friction savings through different cylinder surface finishes, a matrix of engine operating conditions has been designed. There are two levels of in-cylinder pressure and two levels of temperature, simulating the average values of an urban cycle and a real driving cycle to estimate the savings in terms of fuel. Table 5.6 shows the engine operating condition. In addition to the operating conditions shown, the study was carried out with 3 oils of different SAE grades, all of which were considered to have Newtonian behavior: 10W-40, 5W-20 and 0W-12.

Finally, two cylinders with different surface finishes are included in the study. One of them is a conventional grey cast iron (GCI) and the other one is the Twin Wire Arc Spray (TWAS) finishing.

5.3.2 Simulation results

5.3.2.1 Piston rings

Two strategies have been implemented in the piston-ring assembly to reduce friction losses. Firstly, the simulation has been launched with two surface finishing of different surface roughness and, in addition, low viscosity oils have been used to check the impact on fuel consumption reduction. The GCI surface finishing, having a higher surface roughness, will have higher asperity losses than the TWAS surface finish. On the contrary, the TWAS finish will decrease the asperity friction losses but will increase the hydrodynamic losses. In summary, TWAS surface finish is intended to decrease asperity losses and decreasing oil viscosity is intended to eliminate hydrodynamic friction losses.

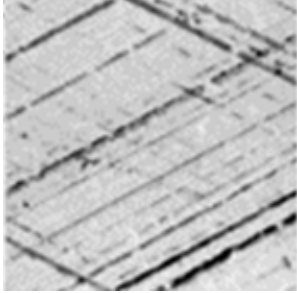
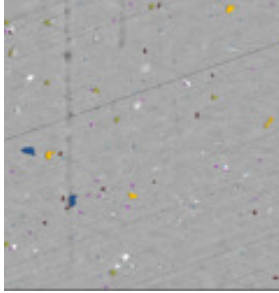
Figure 5.22 shows how using the TWAS cylinder there is a decrease in roughness with respect to the same engine operating conditions. Furthermore, this decrease in roughness reaches almost 0 FMEP when using 10W-40 oil. On the other hand, the complete elimination of roughness suggests an increase in hydrodynamic friction force. However, the combination of decreasing the viscosity and using another cylinder with a lower surface roughness is the best combination, as shown in figure 5.22.

Table 5.6: Engine condition

Operating conditions		
RPM	PCP (bar)	
1000		
2000		
3000	100 bar	52 bar
4000	IMEP = 10.3 bar	IMEP = 2 bar
5000		
Temperature condition		
	Hot ($^{\circ}\text{C}$)	Cold ($^{\circ}\text{C}$)
Top Ring	160	120
Second Ring	130	100
OCR	120	60
Liner (178 mm length)		
1*length	140	80
0.8*length	130	70
0.6*length	120	60
0.4*length	115	50
0.2*length	110	40
0*length	110	40

In this figure, the dashed line represents the friction produced when the surface finish is TWAS and the solid line when the surface finish is GCI. In cold working conditions, it is observed how the TWAS finish is working in hydrodynamic regime for all engine speeds, since the higher the speed, the higher the friction force in the engine. For the same working conditions, for the GCI finish, up to 2000 RPM, the working condition is mixed, reaching the hydrodynamic regime at the highest

Table 5.7: Surface finishing characteristics. Source: [7]

ISO 25178	Conventional GCI honed bore	TWAS mirror-like bore
Surface Roughness Parameters		
$S_a(\mu m)$	0.44	0.08
$S_{pk}(\mu m)$	0.19	0.06
$S_k(\mu m)$	0.63	0.09
$S_{vk}(\mu m)$	1.79	0.37
$S_{mr1}(\%)$	7.8	8.1
$S_{mr2}(\%)$	78.7	84.1

engine speed. On the other hand, when the conditions are hot, the oil viscosity decreases, and this implies, according to the Stribeck curve, that it tends to work more in mixed regime (see Figure 5.23. For the TWAS finish and 0W-12 oil, this lubrication regime begins to appear. However, the shape of the curve for the GCI finish indicates that for the entire engine speed and these conditions, the lubrication regime is mixed. However, the fact that the friction is reduced by means of surface finishing reduces the friction to almost half of the initial value obtained, so that the weight of the asperities in the piston ring assembly is high.

5.3.2.2 Piston skirt

The piston-skirt has a hydrodynamic lubrication regime. This means that by decreasing the viscosity of the fluid between the cylinder and the skirt, friction losses decrease. With the different simulated oils

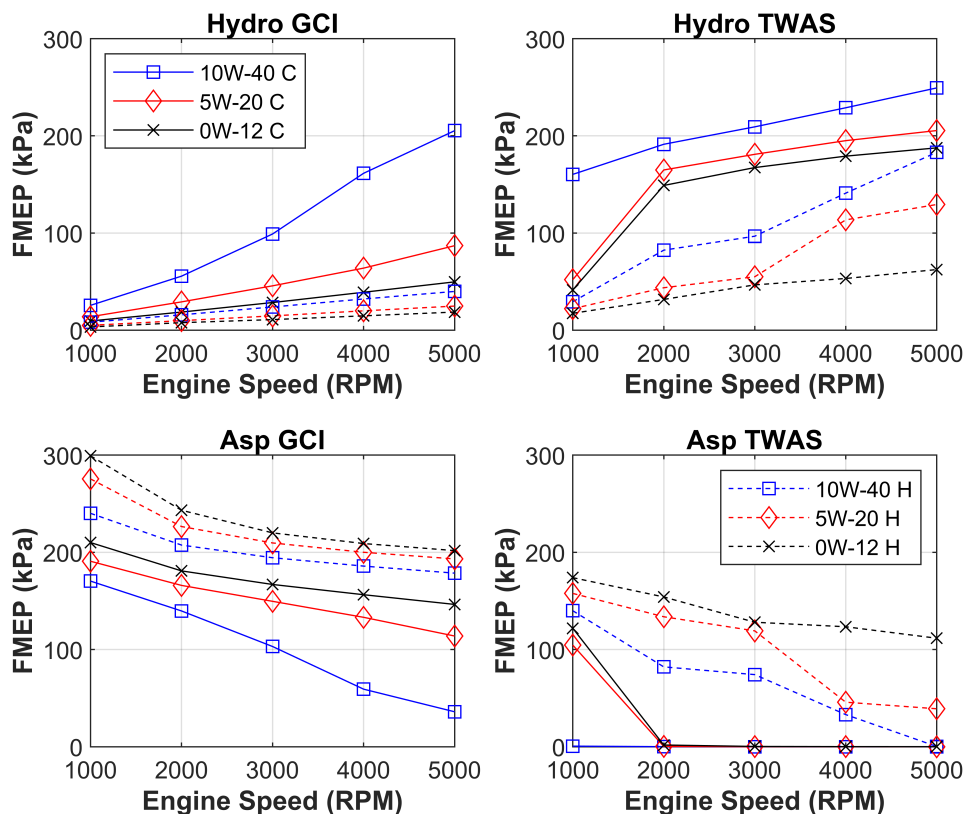


Figure 5.22: Friction losses in piston-ring assembly.

and different operating temperatures, it has been calculated how much friction is reduced by the usage of LVEO. Figure 5.24 shows the FMEP in piston skirt under cold and hot engine conditions.

5.3.2.3 Journal bearings

Although the major treatment to reduce friction has been given to the piston-ring by reducing the surface finish and viscosity in the oil, this section will look at the savings produced in the bearings, both main bearings and con-rod bearings. Due to the nature of their work, bearings work in a hydrodynamic regime, therefore, the immediate solution to reduce their contribution to friction is to reduce the viscosity of the oil

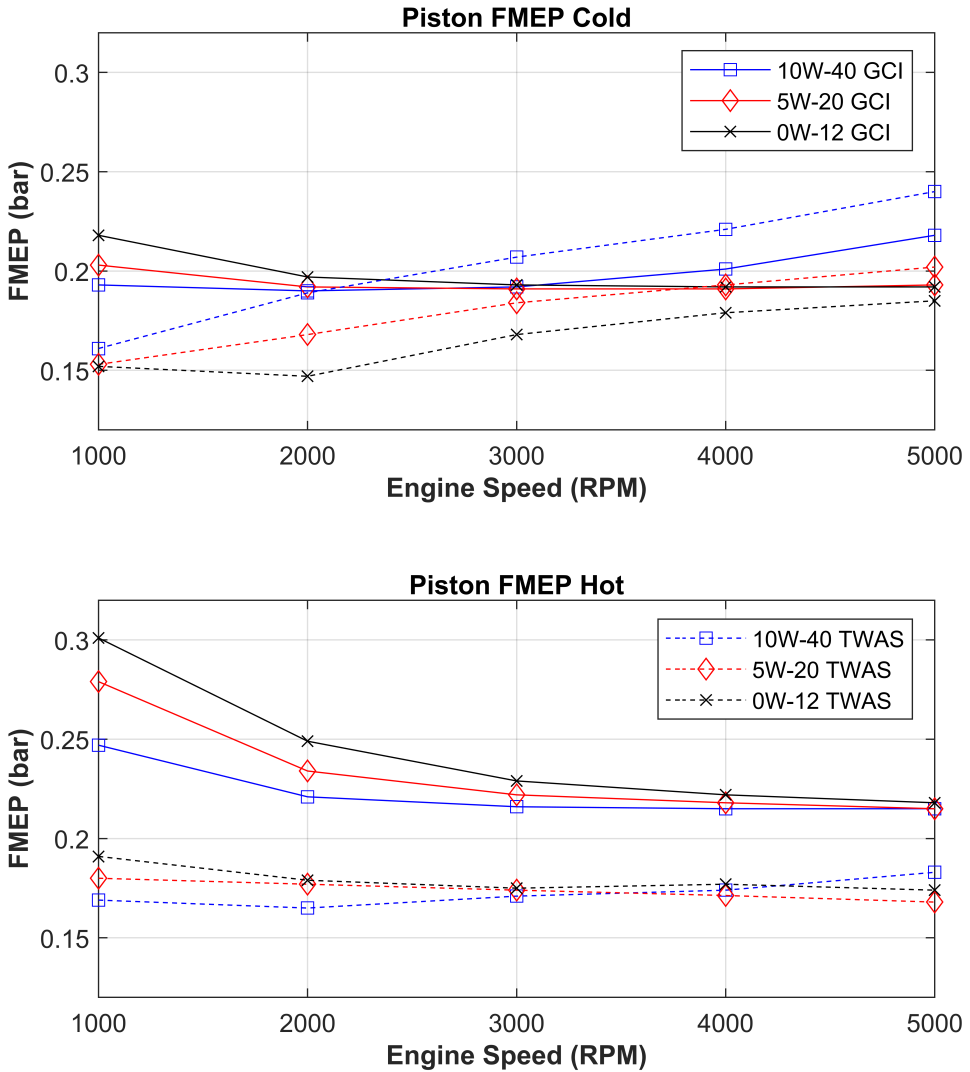


Figure 5.23: Total friction losses in piston-ring assembly.

being used. Therefore, for the three oils discussed in this chapter, the friction calculation for engine bearings has been launched.

In Figure 5.25, the frictional force for the conrod bearings and main bearings is shown. As discussed in the previous chapter and shown in

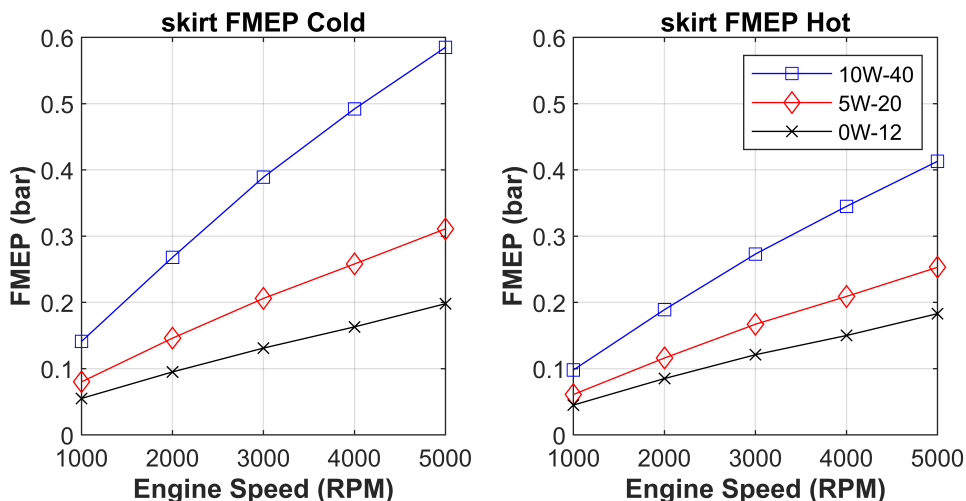
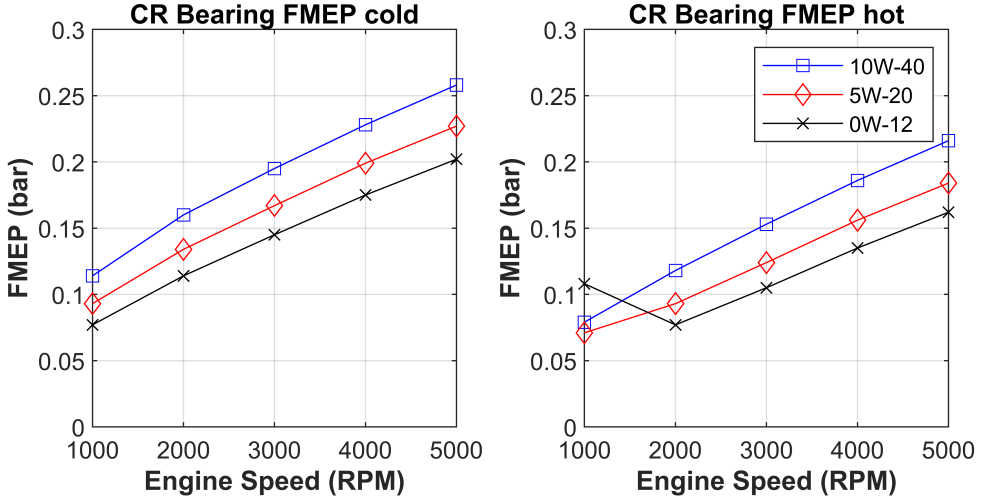


Figure 5.24: Total friction losses in piston-skirt.

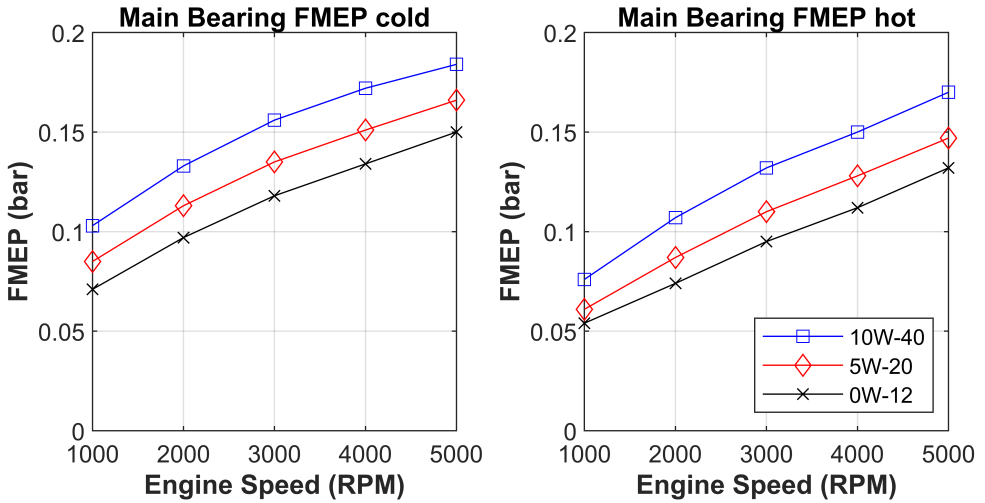
this figure, decreasing the oil viscosity leads to a direct saving in bearing friction, since the hydrodynamic regime is decreased. However, there is the case in which the oil viscosity has decreased so much that, for conrod bearing, the mixed regime is appearing. This condition, if it takes into account the rotational speed of an engine when it is hot during a real driving cycle, is not a very frequent point, however, the fact of starting to enter in mixed regime makes that the wear in the bearings could occur. At this point, a good solution to decrease the appearance of bearing wear would be adding Antiwear and Extreme Pressure engine oils additives. However, for the rest of the speeds, friction savings are obtained and will have an impact on fuel consumption.

5.3.2.4 Camshaft

In the camshaft, the effect of reducing oil viscosity has the opposite effect to that found in bearings. According to Stribeck, and because the camshaft mostly operates in mixed/boundary conditions, reducing viscosity increases friction loss. However, in figure 5.26, when the engine is in low temperature conditions and the oil viscosity is high, the tendency in the camshaft is to have a mixed/hydrodynamic regime. Under the



(a) Connecting-rod bearings



(b) Main bearings

Figure 5.25: Engine bearings FMEP.

same operating conditions, if the viscosity is decreased, the friction at low speed increases as the oil film decreases and, therefore, asperity losses come into play. This effect is more noticeable when the engine is in hot conditions, as the oil viscosity is even lower and friction losses increase due to the large asperity component present in the cam-follower contact. Therefore, to decrease friction in this tribological pair, it is advisable to add friction modifiers to decrease the boundary friction coefficient.

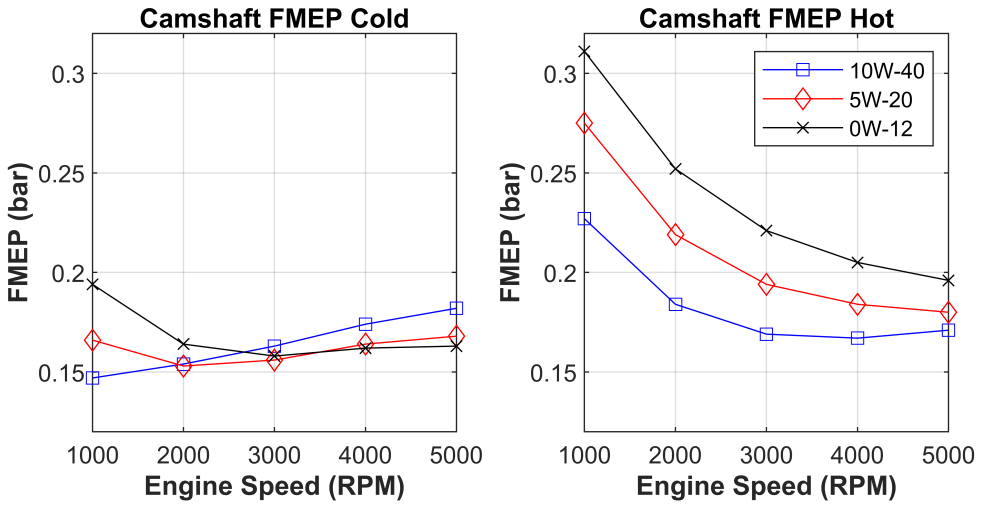


Figure 5.26: Total friction losses in camshaft.

5.3.2.5 Friction saving in the engine

After performing the component-by-component analysis, the aim is to estimate how much fuel consumption savings would be achieved by the different strategies carried out, namely the use of low-viscosity lubricants and the fitting of low-roughness surface finishing. For the estimation of fuel consumption savings the following expression has been used:

$$\Delta BSFC (\%) = \frac{\Delta FMEP}{IMEP} \cdot 100 \tag{5.2}$$

Where $\Delta BSFC$ is the fuel savings obtained from the strategies installed in the engine. $\Delta FMEP$ is the difference between the friction

mean effective pressure obtained in the different configuration and $IMEP$ is the indicated mean effective pressure at which the engine is working. This methodology has been used in different research works [4, 5]. From this expression, an estimate of the fuel consumption savings produced by different surface finishes and different low viscosity oils has been calculated. First, a pairwise comparison has been made with the fuel consumption that would be obtained by changing only the surface finish of the cylinder. Figure 5.27 shows the results obtained.

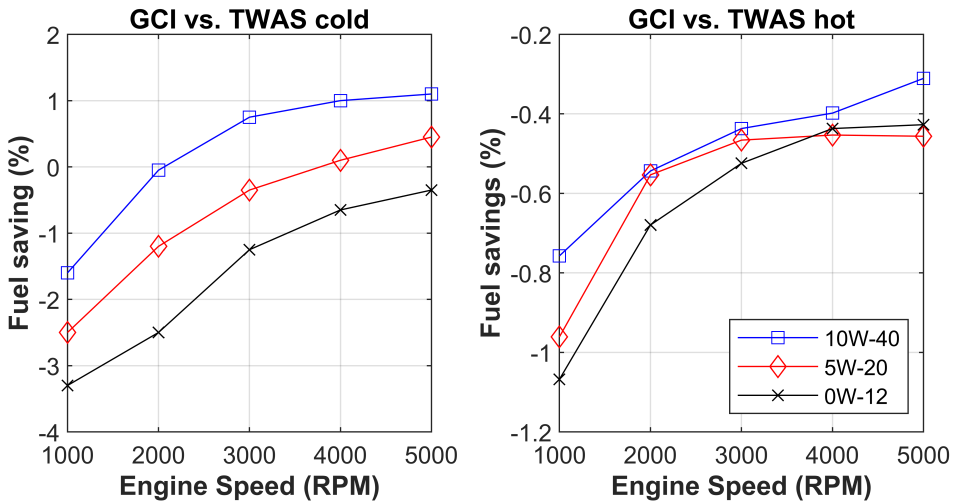


Figure 5.27: Fuel saving obtained from the cylinder surfaces.

On the one hand, the greatest fuel savings are estimated at low engine speed, as this is where the greatest amount of frictional losses occur due to the greater presence of asperity forces. As the engine speed increases, the hydrodynamic part has a higher weight and the fuel consumption savings are lower and it becomes counterproductive to install TWAS, especially for 10W-40 oil, due to the appearance of viscous forces. On the other hand, in high temperature conditions where the viscosity of the oil is lower, fuel consumption is reduced, but not sufficiently because even with a smoother surface finishing, asperity forces still appear at both low and high engine speed. However, in this case, as the conditions are hot, the viscosity of the oils is lower and savings are achieved throughout the engine speed.

In addition to the comparison shown above, another benchmark has been taken for the estimation of fuel consumption. This time, it has been considered that the engine is initially installed with GCI and 10W-40 oil, from there the savings in fuel consumption produced have been compared, showing the benefits of installing TWAS surface finish at the same time as using LVEO oil. Therefore, figure 5.28 shows the comparison.

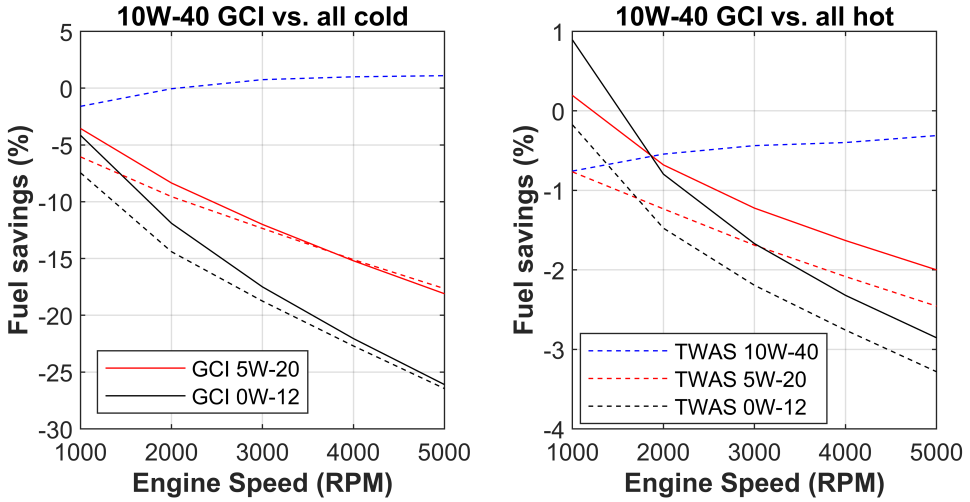


Figure 5.28: Fuel saving obtained from the cylinder surfaces.

The dashed line indicates that the surface finish is TWAS. In cold conditions, installing the surface finishing has a greater weight in reducing the frictional losses due to roughness, typical at low speeds. As the engine speed increases, the benefit of using the surface finishing decreases, except for the 0W-12 oil, where the viscosity decreases and not enough hydrodynamic force is created to increase friction losses. On the other hand, in hot conditions, simply by reducing the viscosity of the oil, it penalizes the frictional losses as lowering the viscosity leads to more frictional forces due to roughness, which is reduced by installing the TWAS finishing. In hot conditions, the increase in speed does not imply an increase in the overall frictional forces due to the increase in hydrodynamic force, as the lower viscosity per temperature means that the asperity frictional force continues to predominate. In general, the

savings in hot conditions can be around 3 % and in cold conditions, due to the difference in viscosity and surface finishes, in the order of 10 %.

5.4 Conclusions

In this chapter it has been studied how to reduce the friction force in internal combustion engines in two ways:

- First of all, rheologically optimized low-viscosity oils were used. In the first study, it has been observed that reducing the oil viscosity can have an impact on reducing fuel consumption, especially if the engine works under hydrodynamic operating conditions, i.e. at low load and high engine speed. Savings have mainly been achieved in the engine skirt and bearings, where the lubrication regime is hydrodynamic. For the piston ring assembly, the use of low viscosity oils penalizes fuel consumption, as they are designed to work in a mixed lubrication regime. As it has been seen, this phenomenon can be reduced by reducing the surface finish of the cylinder. Finally, in the camshaft, lowering the viscosity implies an increase in FMEP, especially in the cam-roller contact. If the surface finish of the cam is polished, so in order to reduce friction and increase engine efficiency, it would be optimal to add friction modifiers that reduce the boundary friction coefficient.
- On the other hand, the use of different surface finishes of the liner has been studied. The purpose of reducing the surface roughness of the liner is to reduce friction losses due to asperity and to ensure that the friction is as hydrodynamic as possible in the piston ring assembly. Thus, the second step would be the usage of LVEO oils to reduce viscous friction and obtain great savings in fuel consumption. Such strategies have been carried out, achieving estimated fuel consumption savings in the order of 10% in cold operating conditions and up to 3% in hot operating conditions. This optimized solution would be a step to optimize the ICE when it is operating in an electrified powertrain. The operation oil temperature of ICE when it is included in an electrified powertrain

decrease up to 20°C, this situation lead to use a less roughness coated bored in conjunction with LVEO.

In order to optimize friction losses, it is not only necessary to use a low-viscosity oil, because from this point of view the cost of installation in relation to the benefit obtained is high, but also the surface finish of the cylinder must be taken into account, as there are losses due to roughness. Furthermore, to reduce friction in the cam-roller assembly, the addition of friction modifiers would reduce friction and thus increase engine performance.

Bibliography

- [1] Tormos B., Pla B., Bastidas S., Ramírez L. and Pérez T. “Fuel economy optimization from the interaction between engine oil and driving conditions”. *Tribology International*, Vol. 138, pp. 263–270, 2019.
- [2] Lizarraga-Garcia E., Davenport T., Carden P., de Vries A., Cakebread S., Remmert S. and Mainwaring R. “Lubricant Impact on Friction by Engine Component: A Motored Friction Tear Down Assessment of a Production 3.6 L Engine”. *SAE Technical Paper*, n° 2019-01-2239, 2019.
- [3] Sander D., Allmaier H., Knauder C. and Strömstedt F. “Potentials and Risks of Reducing Friction with Future Ultra-low-viscosity Engine Oils”. *MTZ worldwide*, Vol. 79 n° 12, pp. 20–27, 2018.
- [4] Tomanik E., Profito F., Sheets B. and Souza R. “Combined lubricant - surface system approach for potential passenger car CO2 reduction on piston-ring-cylinder bore assembly”. *Tribology International*, Vol. 149 n° July, pp. 1–12, 2020.
- [5] Zhmud B., Tomanik E., Grabon W., Schorr D. and Brodmann B. “Optimizing the Piston/Bore Tribology: The Role of Surface Specifications, Ring Pack, and Lubricant”. *SAE Technical Papers*, n° 2020-01-2167, pp. 1–8, 2020.
- [6] Shayler P., Leong D. and Murphy M. “Contributions to engine friction during cold, low speed running and the dependence on oil viscosity”. *SAE Technical Papers*, n° 2005-01-1654, 2005.
- [7] Zhmud B., Tomanik E., Jimenez-Reyes A., Profito F. and Tormos B. “Powertrain Friction Reduction by Synergistic Optimization of Cylinder Bore Surface and Lubricant - Part 2: Engine Tribology Simulations and Tests”. *SAE Technical Paper Series*, Vol. 1, pp. 1–14, 2021.

Chapter 6

Conclusions and future works

Contents

6.1	Introduction	173
6.2	Conclusions	173
6.3	Future works	175

6.1 Introduction

In this chapter, the main conclusions obtained from the doctoral thesis will be presented, which are in line with the objectives described in chapter 1. Thus, after showing the results of chapter 4 and 5, the conclusions obtained will be introduced, as well as the future work to be carried out for the continuation of the study of friction in reciprocating internal combustion engines, with or without hybrid architecture.

6.2 Conclusions

The first two objectives of the doctoral thesis are linked to the development of models to quantify the friction losses produced by friction in each of the tribological components. Firstly, a stationary model was created in order to obtain technical parameters specific to tribology, which are difficult to obtain in experimental applications. Secondly, a transient model was carried out to quantify the energy dissipated by friction in each of the components in real driving cycles. Thus, the following conclusions can be drawn from the first part:

- In reciprocating internal combustion engines, all three lubrication regimes are present, hydrodynamic, mixed and boundary, predominating the mixed lubrication regime.
- Friction losses account for 60% for the piston assembly, 17% bearings, 13% auxiliaries and 10% camshaft on average.
- The predominant lubrication regime in the piston assembly is mixed, in bearings mainly hydrodynamic and mixed/boundary in the camshaft. Different strategies have to be implemented to reduce friction in these elements. This statement is given when the engine is in warm up condition. For a relative short journey (less than 10 km) the engine is not fully warmed up and must surely the lubrication condition tend to be more hydrodynamic.
- As predicted in the stationary model, the most frictional energy is consumed in the piston-ring assembly, followed by the engine bearings, auxiliaries and camshaft.

- In a real driving and WLTC cycle, the engine mainly operates at half load and at medium speed, being neither very hydrodynamic nor very mixed/boundary in terms of friction. Moreover, if the start of the cycle is at ambient condition, the trend of the friction is being dominated by hydrodynamic regime.
- In order to remove the dependence of friction losses on temperature and to avoid thermal inertia heating, the developed model should start under hot conditions. However, an adjustment to the friction in hot condition was performed to consider the dependence of friction losses with temperature.

After an analysis of the mechanical friction losses in each of the components, two strategies for the reduction of friction in internal combustion engines have been developed. Firstly, different low-viscosity oils were tested to reduce hydrodynamic friction losses and, subsequently, cylinders with different surface finishes were tested to reduce asperity losses, from which the following conclusions were obtained:

- The use of low viscosity oils is a good strategy for optimizing mechanical losses, due to their low cost of implementation in the engine. The greatest benefit in terms of friction reduction is obtained in the bearings and piston skirt where friction savings were up to 18% in comparison with a recommended oil OEM.
- In the piston ring and camshaft assembly, using LVEO, friction is penalized, but depending on the operating point of the engine, benefits of up to 6% in terms of FMEP are obtained. However, the predominant lubrication regime is mixed.
- After performing a WLTC homologation cycle with the different oils, savings of up to 1.0% are obtained for low viscosity oils compared to a 5W-30 reference. The main benefit was obtained at the beginning of the cycle in ambient temperature condition.
- Not only the use of low-viscosity oils is effective in increasing engine performance, it must also be combined with different cylinder surface finishes to reduce asperity losses. The combination of these two elements gives estimated results of up to 4% in fuel savings in

hot engine conditions and up to 15% in cold conditions, compared with a reference 10W-40.

- The combination of low-viscosity oils with surface finishes has been shown to be the best combination from the point of view of increasing engine performance through tribology for vehicles with hybrid architecture, as the oil temperature is, on average, substantially lower on a WLTC type-approval cycle.

6.3 Future works

This doctoral thesis has provided an increase in the knowledge of tribology in reciprocating internal combustion engines, establishing the knowledge base. After the completion of the doctoral thesis, there are several future works that can be carried out and that serve as a continuation of this field of research. Broadly speaking, there are two main avenues for further research in tribology, on the one hand, from the point of view of cylinder surface finishes and, on the other hand, from the point of view of rheologically optimized oils, so the following points are proposed as possible future work to be carried out:

- To adapt the developed Diesel engine model to a gasoline engine, in such a way that it serves to understand the tribology in this engine architecture. Gasoline engines are the most used in hybrid vehicles and, based on it, to know the operating points and optimize the oil rheologically through the shear rate to obtain an optimal engine performance from the point of view of the lubricant.
- Once the model has been realized, the next natural step would be to evaluate a hybrid architecture vehicle in real driving cycles. In such a way, through the working points of the engine in the cycle, useful information is obtained to optimize the oil rheologically, adding additives that improve the viscosity index.
- Carry out experimental tests to verify the predictions of the simulation model and quantify the actual fuel savings produced, so that the model can be validated and contrasted.

- On the other hand, to carry out theoretical studies with different surface finishes to reduce friction by asperity in the engine, as well as to combine this strategy with that of low viscosity oils to optimize fuel consumption.
- Finally, once the different surface finishes have been studied and combined with different rheologically optimized oils, they must be installed in a real combustion engine with hybrid application and studying the main advantages of using this two technologies in an real hybrid engine. The combination of this technologies together with the vehicle electrification would help to reduce the fuel consumption and, consequently, the CO_2 emitted to the atmosphere.

Bibliography

Ai X., Cheng H., Hua D., Moteki K. and Aoyama S.

A finite element analysis of dynamically loaded journal bearings in mixed lubrication.
Tribology Transactions, Vol. 41 n° 2, pp. 273–281, jan 1998. (cited in p. 49)

Akalin O. and Newaz G.

Piston Ring-Cylinder Bore Friction Modeling in Mixed Lubrication Regime: Part I Analytical Results.
Journal of Tribology, Vol. 123, pp. 211–218, Jan 2001.

Allmaier H., Sander D. and Reich F.

Simulating friction power losses in automotive journal bearings.
Procedia Engineering, Vol. 68, pp. 49–55, jan 2013. (cited in p. 49)

American Petroleum Institute.

Annex E - API Base oil interchangeability guidelines for passenger car motor oils and Diesel engine oils.
2019. (cited in p. 27)

American Society for Testing Material.

Designation D341-20: Standard Practice for Viscosity Temperature Equations and Charts for Liquid Petroleum or Hydrocarbon Products.
2020. (cited in p. 29)

Barus C.

Isothermals, isopiestic and isometrics relative to viscosity.
American Journal of Science, Vol. s3-45 n° 266, pp. 87–96, 1893. (cited in p. 30)

Beaman J.

Thermohydrodynamic analysis of laminar incompressible journal bearings.
Tribology Transactions, Vol. 29 n° 2, pp. 141–150, 1986. (cited in p. 50)

Booker F.

Dynamically loaded journal bearings: Mobility method of solution.
Journal of Fluids Engineering, Transactions of the ASME, Vol. 87 n° 3, pp. 537–546, sep 1965. (cited in p. 49)

Booker J.

Dynamically-Loaded Journal Bearings: Numerical Application of the Mobility Method.

Journal of Lubrication Technology, Vol. 93 n° 1, pp. 168, 1971. (cited in p. 49)

Carden P., Pisani C., Laine E., Field I., Devine M., Schoeni A. and Beyer P.

Calculation of crank train friction in a heavy duty truck engine and comparison with measured data.

Proceedings of the Institution of Mechanical Engineers, Part J: Journal of Engineering Tribology, Vol. 227, pp. 168–184, 2013. (cited in p. 35)

Carreño Arango R.

A comprehensive methodology to analyse the Global Energy Balance in Reciprocating Internal Combustion Engines.

Universitat Politècnica de València, 2016. (cited in pp. vii, 70, 71, 88, 89)

Chamani H., Karimaei H., Bahrami M. and Mirsalim S.

Thermo-elasto-hydrodynamic (TEHD) analysis of oil film lubrication in big end bearing of a diesel engine.

Journal of Computational and Applied Research in Mechanical Engineering, Vol. 5, pp. 13–24, 2015. (cited in p. 50)

Checo H., Ausas R., Jai M., Cadalen J., Choukroun F. and Buscaglia G.

Moving textures: Simulation of a ring sliding on a textured liner.

Tribology International, Vol. 72, pp. 131–142, apr 2014. (cited in p. 45)

Chen H., Li Y. and Tian T.

A novel approach to model the lubrication and friction between the twin-land oil control ring and liner with consideration of micro structure of the liner surface finish in internal combustion engines.

SAE Technical Papers, n° 2008-01-1613, 2008. (cited in pp. 25, 35, 103)

Cheng C., Kharazmi A., Schock H., Wineland R. and Brombolich L.

Three-dimensional piston ring-cylinder bore contact modeling.

Journal of Engineering for Gas Turbines and Power, Vol. 137 n° 11, nov 2015.

(cited in p. 46)

Cho S. H., Ahn S. T. and Kim Y. H.

A simple model to estimate the impact force induced by piston slap.

Journal of Sound and Vibration, Vol. 255 n° 2, pp. 229–242, aug 2003.

(cited in p. 34)

Cross M.

Rheology of non-Newtonian fluids: A new flow equation for pseudoplastic systems.

Journal of Colloid Science, Vol. 20 n° 5, pp. 417–437, 1965. (cited in p. 31)

Delprete C. and Razavykia A.

Piston ring-liner lubrication and tribological performance evaluation: A review.

Proceedings of the Institution of Mechanical Engineers, Part J: Journal of Engineering Tribology, Vol. 232 n° 2, pp. 193–209, feb 2018.

Dhingra R. and Das S.

Life cycle energy and environmental evaluation of downsized vs. lightweight material automotive engines.

Journal of Cleaner Production, Vol. 85, pp. 347–358, 2014. (cited in p. 19)

Dobrica M. and Fillon M.

Encyclopedia of Tribology.

Encyclopedia of Tribology, n° 2001, pp. 2284–2291, 2013. (cited in p. 24)

Dowson D. and Higginson G.

Elasto-Hydrodynamic Lubrication.
1977.

(cited in p. 51)

Dyson A.

Kinematics and wear patterns of cam and finger follower automotive valve gear.

Tribology International, Vol. 13 n° 3, pp. 121–132, jun 1980. (cited in p. 51)

Dyson A. and Naylor H.

Application of the Flash Temperature Concept to Cam and Tappet Wear Problems.

Proceedings of the Institution of Mechanical Engineers: Automobile Division, Vol. 14 n° 1, pp. 255–280, jan 1960. (cited in p. 50)

Erdemir A. and Holmberg K.

Energy consumption due to friction in motored vehicles and low-friction coatings to reduce it.

Coating Technology for Vehicle Applications, Vol. 47, pp. 1–24, jan 2015.

(cited in p. 5)

European Union.

REGULATION (EU) 2019/ 631 OF THE EUROPEAN PARLIAMENT AND OF THE COUNCIL - of 17 April 2019 - setting CO₂ emission performance standards for new passenger cars and for new light commercial vehicles, and repealing Regulations (EC) No 443 / 2009 and (EU) No 510 / 2011.

2019.

(cited in p. 8)

Fernández Feria R. and Ortega Casanova J.

Mecánica de fluidos. Notas de clase: Teoría, problemas y prácticas.

Universidad de Málaga, 2014.

(cited in p. 89)

Ferreira R., Martins J., Carvalho O., Sobral L., Carvalho S. and Silva F.

Tribological solutions for engine piston ring surfaces: an overview on the materials and manufacturing.

Materials and Manufacturing Processes, Vol. 35 n° 5, pp. 498–520, apr 2020.

(cited in pp. vi, 34, 35)

Forero J., Ochoa G. and Alvarado W.

Study of the Piston Secondary Movement on the Tribological Performance of a Single Cylinder Low-Displacement Diesel Engine.

Lubricants, Vol. 8 n° 11, pp. 97, oct 2020.

(cited in p. 48)

Funk T., Ehnis H., Kuenzel R. and Bargende M.

Validity of a Steady-State Friction Model for Determining CO_2 Emissions in Transient Driving Cycles.

SAE Technical Paper, n° 2019-24-0054, 2019.

(cited in p. 125)

Galindo J., Serrano J. R., Climent H. and Varnier O.

Impact of two-stage turbocharging architectures on pumping losses of automotive engines based on an analytical model.

Energy Conversion and Management, Vol. 51 n° 10, pp. 1958–1969, 2010.

(cited in p. 19)

GmbH Mahle.

Pistons and engine testing.

(cited in p. 36)

Goenka P.

Analytical Curve Fits for Solution Parameters of Dynamically Loaded.

Journal of Tribology, Vol. 106 n° 83, pp. 421–427, 1984.

(cited in p. 49)

Gopi E., Saleem M., Chandan S. and Nema A.

Thermal and static analysis of engine piston rings.

International Journal of Ambient Energy, 2019.

(cited in p. 46)

Gore M., Theaker M., Howell-Smith S., Rahnejat H. and King P.

Direct measurement of piston friction of internal-combustion engines using the floating-liner principle.

Proceedings of the Institution of Mechanical Engineers, Part D: Journal of Automobile Engineering, Vol. 228 n° 3, pp. 344–354, feb 2014.

(cited in p. 41)

Greenwood J. and Tripp J.

The contact of two nominally flat rough surfaces.

Proceedings of the Institution of Mechanical Engineers, Vol. 185, pp. 625–633, 1970.

(cited in pp. 42, 76)

Grützmacher P., Profito F. and Rosenkranz A.

Multi-scale surface texturing in tribology-current knowledge and future perspectives.

Lubricants, Vol. 7 n° 11, 2019.

(cited in pp. 10, 45)

Gu C. and Zhang D.

Modeling and prediction of the running-in behavior of the piston ring pack system based on the stochastic surface roughness.

Proceedings of the Institution of Mechanical Engineers, Part J: Journal of Engineering Tribology, Vol. 233 n° 12, pp. 1857–1877, dec 2019.

(cited in p. 25)

Guo J., Zhang W. and D.Zou.

Investigation of dynamic characteristics of a valve train system.

Mechanism and Machine Theory, Vol. 46, pp. 1950–1969, 2011.

(cited in p. 87)

H. Chen.

Modeling the Lubrication of the Piston Ring Pack in Internal Combustion Engines Using the Deterministic Method.

Massachusetts Institute of Technology, 2009.

(cited in pp. 25, 45)

- Habchi W., Eyheramendy D., Vergne P. and Morales-Espejel G.**
A full-system approach of the elastohydrodynamic line-point contact problem.
Journal of Tribology, Vol. 130 n° 2, pp. 1–10, apr 2008. (cited in p. 51)
- Hardy B. and Doubleday I.**
Boundary lubrication. The paraffin series.
Proceedings of the Royal Society of London. Series A, Containing Papers of a Mathematical and Physical Character, Vol. 100 n° 707, pp. 550–574, 1922.
(cited in p. 25)
- Hertz H.**
Über die Berührung fester elastischer Körper (On the contact of elastic solids).
Journal für die reine und angewandte Mathematik, Vol. 92, pp. 156–171, 1882.
(cited in p. 85)
- Heywood J.B.**
Internal combustion engine fundamentals.
Mc Graw-Hill series in mechanical engineering. McGraw-Hill, New York/etc, 1988.
(cited in pp. 9, 33)
- Hoag K. and Dondlinger B.**
Cranktrain Crankshafts, Connecting Rods, and Flywheel.
2016. (cited in p. 38)
- Holmberg K., Andersson P. and Erdemir A.**
Global energy consumption due to friction in passenger cars.
Tribology International, Vol. 47, pp. 221–234, mar 2012. (cited in pp. vi, 8, 20, 41)
- Holmberg K., Andersson P., Nylund N., Mäkelä K. and Erdemir A.**
Global energy consumption due to friction in trucks and buses.
Tribology International, Vol. 78, pp. 94–114, 2014. (cited in pp. vi, 7)
- Holmberg K. and Erdemir A.**
Influence of tribology on global energy consumption, costs and emissions.
Friction, Vol. 5, pp. 263–284, 2017. (cited in pp. xi, 3, 4)
- Holmberg K. and Erdemir A.**
The impact of tribology on energy use and CO_2 emission globally and in combustion engine and electric cars.
Tribology International, Vol. 135, pp. 389–396, jul 2019. (cited in p. 20)
- Holmberg K., Kivikytö-Reponen P., Härkisaari P., Valtonen K. and Erdemir A.**
Global energy consumption due to friction and wear in the mining industry.
Tribology International, Vol. 115, pp. 116–139, 2017. (cited in p. 3)
- Holmberg K., Siilasto R., Laitinen T., Andersson P. and Jäsberg A.**
Global energy consumption due to friction in paper machines.
Tribology International, Vol. 62, pp. 58–77, 2013. (cited in p. 3)

Hooker J. N.

Optimal driving for single-vehicle fuel economy.

Transportation Research Part A: General, Vol. 22 n° 3, pp. 183–201, 1988.

(cited in p. 19)

Houpert L.

New results of traction force calculations in elasto-hydrodynamic contacts.

Journal of Tribology, Vol. 107 n° 2, pp. 241–245, 1985.

(cited in p. 30)

Hutchings I. and Shipway P.

Lubricants and Lubrication.

In *Tribology. Friction and Wear of Engineering Materials*, pp. 79–105. 2016.

(cited in p. 28)

Hutchings I. and Shipway P.

Friction and Wear of Engineering Materials.

2017.

(cited in p. 21)

International Energy Agency.

Energy consumption in transport in IEA countries.

2018.

(cited in pp. vi, 6)

International Energy Agency.

Statistics report World Energy Balances.

2020.

(cited in pp. vi, 5)

Johansson S., Nilsson P., Ohlsson R. and Rosen B.

Experimental friction evaluation of cylinder liner piston ring contact.

Wear, Vol. 271, pp. 625–633, Jun 2011.

(cited in p. 79)

Jost H. P.

Lubrication (tribology) education and research. A report on the present position and the industry's needs. London, UK: Department of Education and Science.

1966.

(cited in p. 3)

Jost H. P.

Tribology - Origin and future.

Wear, Vol. 136, pp. 1–17, 1990.

(cited in p. 3)

Jost H. P. and Schofield J.

Energy saving through tribology: A techno - economic study.

Proceedings - Institution of Mechanical Engineers, Vol. 195, pp. 151–173, 1981.

(cited in p. 3)

Kälvelid F.

Numerical Modeling of Plain Journal Bearings within a Heavy-Duty Engine Oil System using GT-SUITE.

2016.

(cited in pp. vii, 50)

Kano M.

Diamond-Like Carbon Coating Applied to Automotive Engine Components.

Tribology Online, Vol. 9 n° 3, pp. 135–142, 2014.

(cited in p. 26)

Khonsari M. and Wang H.

On the fluid-solid interaction in reference to thermoelastohydrodynamic analysis of journal bearings.

Journal of Tribology, Vol. 113 n° 2, pp. 398–404, apr 1991. (cited in p. 50)

Kirner C., Halbhuber J., Uhlig B., Oliva A., Graf S. and Wachtmeister G.

Experimental and simulative research advances in the piston assembly of an internal combustion engine.

Tribology International, Vol. 99, pp. 159–168, jul 2016. (cited in p. 46)

Knauder C., Allmaier H., Sander D. and Sams T.

Investigations of the Friction Losses of Different Engine Concepts. Part 1: A Combined Approach for Applying Subassembly-Resolved Friction Loss Analysis on a Modern Passenger-Car Diesel Engine.

Lubricants, Vol. 7 n° 5, pp. 39, apr 2019. (cited in p. 41)

Knauder C., Allmaier H., Sander D. and Sams T.

Investigations of the Friction Losses of Different Engine Concepts. Part 2: Sub-Assembly Resolved Friction Loss Comparison of Three Engines.

Lubricants, Vol. 7 n° 12, pp. 105, nov 2019. (cited in p. 41)

Kobayashi S., Plotkin S. and Ribeiro S. K.

Energy efficiency technologies for road vehicles.

Energy Efficiency, Vol. 2 n° 2, pp. 125–137, jan 2009. (cited in p. 19)

Krishnanl A.

Simulation of an engine friction strip test.

Chalmers University, 2014. (cited in p. 36)

Kushwaha M. and Rahnejat H.

Transient elastohydrodynamic lubrication of finite line conjunction of cam to follower concentrated contact.

Journal of Physics D: Applied Physics, Vol. 35 n° 21, pp. 2872–2890, nov 2002. (cited in p. 51)

LaBouff G. and Booker J.

Dynamically Loaded Journal Bearings: A Finite Element Treatment for Rigid and Elastic Surfaces.

Journal of Tribology, Vol. 107 n° 4, pp. 505–513, oct 1985. (cited in p. 49)

Li Y., Chen H. and Tian T.

A deterministic model for lubricant transport within complex geometry under sliding contact and its application in the interaction between the oil control ring and rough liner in internal combustion engines.

SAE Technical Papers, n° 2008-01-1615, 2008. (cited in pp. 25, 45)

Liu H., Han L. and Cao Y.

Improving transmission efficiency and reducing energy consumption with automotive continuously variable transmission: A model prediction comprehensive optimization approach.

Applied Energy, Vol. 274, 2020. (cited in p. 19)

Lizarraga-Garcia E., Davenport T., Carden P., de Vries A., Cakebread S., Remmert S. and Mainwaring R.

Lubricant Impact on Friction by Engine Component: A Motored Friction Tear Down Assessment of a Production 3.6 L Engine.

SAE Technical Paper, n° 2019-01-2239, 2019. (cited in p. 141)

Luján J. M., Climent H., Novella R. and Rivas-Perea M.

Influence of a low pressure EGR loop on a gasoline turbocharged direct injection engine.

Applied Thermal Engineering, Vol. 89, pp. 432–443, 2015. (cited in p. 19)

Macián V., Tormos B., Ruíz S. and Ramírez L.

Potential of low viscosity oils to reduce CO2 emissions and fuel consumption of urban buses fleets.

Transportation Research Part D: Transport and Environment, Vol. 39, pp. 76–88, 2015. (cited in p. 19)

Mahmoud K., Knaus O., Parikyan T., Offner G. and Sklepik S.

An integrated model for the performance of piston ring pack in internal combustion engines.

Proceedings of the Institution of Mechanical Engineers, Part K: Journal of Multi-body Dynamics, Vol. 232 n° 3, pp. 371–384, sep 2018.

Marx N., Fernández L., Barceló F. and Spikes H.

Shear Thinning and Hydrodynamic Friction of Viscosity Modifier-Containing Oils. Part I: Shear Thinning Behaviour.

Tribology Letters, Vol. 66, 2018. (cited in p. 32)

Mayet C., Welles J., Bouscayrol A., Hofman T. and Lemaire-Semail B.

Influence of a CVT on the fuel consumption of a parallel medium-duty electric hybrid truck.

Mathematics and Computers in Simulation, Vol. 158, pp. 120–129, 2019. (cited in p. 19)

Meng F., Wang X., Li T. and Chen Y.

Influence of cylinder liner vibration on lateral motion and tribological behaviors for piston in internal combustion engine.

Proceedings of the Institution of Mechanical Engineers, Part J: Journal of Engineering Tribology, Vol. 229 n° 2, pp. 151–167, feb 2015. (cited in p. 47)

Meng X., Ning L., Xie Y. and Wong V.

Effects of the connecting-rod-related design parameters on the piston dynamics and the skirt-liner lubrication.

Proceedings of the Institution of Mechanical Engineers, Part D: Journal of Automobile Engineering, Vol. 227 n° 6, pp. 885–898, jun 2013. (cited in p. 48)

Moes H.

Optimum similarity Analysis with applications to Elastohydrodynamic Lubrication.

Wear, Vol. 159, pp. 57–66, 1992. (cited in p. 87)

Mufti R. and Priest M.

Theoretical and experimental evaluation of engine bearing performance.

Proceedings of the Institution of Mechanical Engineers, Part J: Journal of Engineering Tribology, Vol. 223 n° 4, pp. 629–644, 2009. (cited in p. 37)

Mufti R. A., Priest M. and Chittenden R. J.

Analysis of piston assembly friction using the indicated mean effective pressure experimental method to validate mathematical models.

Proceedings of the Institution of Mechanical Engineers, Part D: Journal of Automobile Engineering, Vol. 222, pp. 1441–1457, 2008. (cited in p. 35)

Nagano Y., Ito A., Okamoto D. and Yamasaka K.

A study on the feature of several types of floating liner devices for piston friction measurement.

SAE Technical Papers, n° 2019-01-0177, apr 2019. (cited in p. 41)

National Research Council of Canada: Associate Committee on Tribology.

A strategy for tribology in Canada: enhancing reliability and efficiency through the reduction of wear and friction.

1986. (cited in p. 3)

Ning L., Meng X. and Xie Y.

Incorporation of deformation in a lubrication analysis for automotive piston skirt-liner system.

Proceedings of the Institution of Mechanical Engineers, Part J: Journal of Engineering Tribology, Vol. 227 n° 6, pp. 654–670, jun 2013. (cited in p. 48)

Orgeldinger C. and Tremmel S.

Understanding Friction in Cam-Tappet Contacts: An Application-Oriented Time-Dependent Simulation Approach Considering Surface Asperities and Edge Effects.

Lubricants, Vol. 9, Nov 2021. (cited in p. 79)

Patir N. and Cheng H.

An Average Flow Model for Determining Effects of Three-Dimensional Roughness on Partial Hydrodynamic Lubrication.

Journal of Tribology, Vol. 100, pp. 12–17, 1978. (cited in pp. 25, 43, 75)

Patir N. and Cheng H.

Application of Average Flow Model to Lubrication Between Rough Sliding Surfaces.

Journal of Lubrication Technology, Vol. 101 n° 2, pp. 220–229, 1979. (cited in pp. 25, 43, 75)

Payri F. and Desantes J. M.

Motores de Combustión Interna Alternativos, volume 66.

Reverté S.A., 2011. (cited in p. 21)

Pelosi M. and Ivantysynova M.

Heat transfer and thermal elastic deformation analysis on the Piston-Cylinder interface of axial piston machines.

Journal of Tribology, Vol. 134 n° 4, oct 2012. (cited in p. 48)

- Phillips C., McQueen J., Gao H., Stockwell R., Hardy B. and Graham M.**
Design considerations in formulating gasoline engine lubricants for improving engine fuel economy and wear resistance part I: Base oils and additives.
SAE Technical Papers, n° 2007-01-4143, 2007. (cited in p. 41)
- Pinkus O. and Wilcock D.F.**
Strategy for energy conservation through tribology.
1977. (cited in p. 3)
- Piqueras P., Sanchis E. J., Herreros J. M. and Tsolakis A.**
Evaluating the oxidation kinetic parameters of gasoline direct injection soot from thermogravimetric analysis experiments.
Chemical Engineering Science, 2021. (cited in p. 19)
- Priest M., Dowson D. and Taylor C. M.**
Predictive wear modelling of lubricated piston rings in a diesel engine.
Wear, Vol. 231, pp. 89–101, 1999. (cited in p. 76)
- Priest M. and Taylor C. M.**
Automobile engine tribology - approaching the surface.
Wear, Vol. 241 n° 2, pp. 193–203, jul 2000. (cited in p. 34)
- Profito F., Tomanik E. and Zachariadis D.**
Effect of cylinder liner wear on the mixed lubrication regime of TLOCs.
Tribology International, Vol. 93, pp. 723–732, 2016.
(cited in pp. vii, 25, 45, 46, 76)
- Rahnejat H.**
Tribology and Dynamics of Engine and Powertrain: Fundamentals, Applications and Future Trends.
2010. (cited in pp. vi, 34, 38, 40)
- Rahnejat H., Offner G., Knaus O., Turnbull R., Bewsher S., Mohammadpour M. and Rahmani R.**
Effect of cylinder de-activation on the tribological performance of compression ring conjunction.
Proceedings of the Institution of Mechanical Engineers, Part J: Journal of Engineering Tribology, Vol. 231 n° 8, pp. 997–1006, 2017. (cited in p. 25)
- Raimondi A. A. and Boyd J.**
A Solution for the Finite Journal Bearing and its Application to Analysis and Design: I.
ASLE Transactions, Vol. 1, pp. 159–174, 1958. (cited in p. 83)
- Ramírez L.**
Contribution to the assessment of the potential of low viscosity engine oils to reduce ICE fuel consumption and CO₂ emissions.
Universitat Politècnica de València, 2016. (cited in pp. 26, 29)
- Rao T., Rani A., Nagarajan T. and Hashim F.**
Analysis of slider and journal bearing using partially textured slip surface.
Tribology International, Vol. 56, pp. 121–128, dec 2012. (cited in p. 37)

Reynolds O.

IV. On the Theory of Lubrication and its Application to Mr. Beauchamps Tower's Experiments, including an Experimental Determination of the Viscosity of Olive Oil. *Philosophical Transactions*, pp. 157–234, 1886. (cited in p. 23)

Roelands C.

Correlational aspects of the viscosity-temperature-pressure relationship of lubricants oils. 1966. (cited in pp. 30, 87)

Sagawa T., Nakano S., Shouganji I., Okuda S. and Nakajo T.

MR20DD Motoring Fuel Economy Test for 0W-12 and 0W-8 Low Viscosity Engine Oil. *SAE Technical Papers*, n° 2019-01-2295, 2019. (cited in p. 26)

Salvador Iborra J.

A Contribution to the Global Modeling of Heat Transfer Processes in Diesel Engines. Universitat Politècnica de València, 2020. (cited in p. 73)

Sander D., Allmaier H., Knauder C. and Strömstedt F.

Potentials and Risks of Reducing Friction with Future Ultra-low-viscosity Engine Oils. *MTZ worldwide*, Vol. 79 n° 12, pp. 20–27, 2018. (cited in p. 141)

Sander D., Allmaier H., Pribsch H., Reich F., Witt M., Füllenbach T., Skiadas A., Brouwer L. and Schwarze H.

Impact of high pressure and shear thinning on journal bearing friction. *Tribology International*, Vol. 81, pp. 29–37, 2015. (cited in pp. vi, 31, 99)

Sgroi M., Asti M., Gili F., Deorsola F., Bensaid S., Fino D., Kraft G., Garcia I. and Dassenoy F.

Engine bench and road testing of an engine oil containing MoS₂ particles as nano-additive for friction reduction. *Tribology International*, Vol. 105, pp. 317–325, 2017. (cited in p. 26)

Shayler P., Leong D. and Murphy M.

Contributions to engine friction during cold, low speed running and the dependence on oil viscosity. *SAE Technical Papers*, n° 2005-01-1654, 2005. (cited in p. 149)

Shirzadegan M., Almqvist A. and Larsson R.

Fully coupled EHL model for simulation of finite length line cam-roller follower contacts. *Tribology International*, Vol. 103, pp. 584–598, nov 2016. (cited in p. 51)

Shu J., Fu J., Zhao D., Liu J., Ma Y., Deng B., Zeng D., Liu J. and Zhang Y.

Numerical investigation on the effects of valve timing on in-cylinder flow, combustion and emission performance of a diesel ignition natural gas engine through computational fluid dynamics. *Energy Conversion and Management*, Vol. 198, pp. 111786, 2019. (cited in p. 19)

Souchet D., Hoang L. and Bonneau D.

Thermoelastohydrodynamic lubrication for the connecting rod big-end bearing under dynamic loading.

Proceedings of the Institution of Mechanical Engineers, Part J: Journal of Engineering Tribology, Vol. 218 n° 5, pp. 451–464, may 2004. (cited in p. 50)

Staron J. and Willermet P.

An analysis of valve train friction in terms of lubrication principles.

SAE Technical Papers, 1983. (cited in p. 51)

Stribeck R.

Die wesentlichen Eigenschaften der Gleit- und Rollenlager.

1902. (cited in p. 22)

Tabata H., Kaneko N. and Mihara Y.

Improvement in Accuracy of Piston frictional force measurement using floating liner engine.

Tribology Online, Vol. 12 n° 3, pp. 141–146, jul 2017. (cited in p. 41)

Tan Y. and Ripin M.

Technique to determine instantaneous piston skirt friction during piston slap.

Tribology International, Vol. 74, pp. 145–153, jun 2014. (cited in p. 47)

Taylor C. M.

Engine Tribology.

Elsevier, 1993. (cited in p. 83)

Taylor R. I. and De Kraker B. R.

Shear rates in engines and implications for lubricant design.

Proceedings of the Institution of Mechanical Engineers, Part J: Journal of Engineering Tribology, Vol. 231, pp. 1106–1116, 2017. (cited in pp. 31, 99)

Taylor R. I., Morgan N., Mainwaring R. and Davenport T.

How much mixed/boundary friction is there in an engine and where is it?

Proceedings of the Institution of Mechanical Engineers, Part J: Journal of Engineering Tribology, Vol. 234, pp. 1563–1579, 10 2020. (cited in p. 35)

Teodorescu M., Balakrishnan S. and Rahnejat H.

Integrated tribological analysis within a multi- physics approach to system dynamics.

Tribology and Interface Engineering Series, Vol. 48, pp. 725–737, jan 2005. (cited in p. 51)

Teodorescu M., Kushwaha M., Rahnejat H. and Taraza D.

Elastodynamic transient analysis of a four-cylinder valvetrain system with camshaft flexibility.

Proceedings of the Institution of Mechanical Engineers, Part K: Journal of Multi-body Dynamics, Vol. 219 n° 1, pp. 13–25, mar 2005. (cited in p. 51)

Teodorescu M., Taraza D., Henenin Naeim A. and W.Bryzik.

Simplified Elasto-Hydrodynamic Friction Model of the Cam-Tappet Contact.

SAE Technical Paper, n° 2003-01-0985, 2003. (cited in p. 86)

Tian T.

Dynamic behaviours of piston rings and their practical impact. Part 2: Oil transport, friction and wear of ring/liner interface and the effects of piston and ring dynamics. *Proceedings of the Institution of Mechanical Engineers, Part J: Journal of Engineering Tribology*, Vol. 216 n° 4, pp. 229–248, apr 2002. (cited in p. 46)

Tian T., Wong V. and Heywood J.

A piston ring-pack film thickness and friction model for multigrade oils and rough surfaces. *SAE Technical Papers*, 1996. (cited in p. 41)

Tomanik E., Chacon H. and G.Teixeira.

A simple numerical procedure to calculate the input data of Greenwood-Williamson model of asperity contact for actual engineering surfaces. *Tribological Research and Design for Engineering Systems*, pp. 205–215, 2003. (cited in p. 77)

Tomanik E., Fujita H., Sato S., Paes E., Galvao C. and Morais P.

Investigation of PVD piston ring coatings with different lubricant formulations. *ASME 2017 Internal Combustion Engine Division Fall Technical Conference, ICEF 2017*, Vol. 2, pp. 1–10, 2017. (cited in p. 26)

Tomanik E., Profito F., Sheets B. and Souza R.

Combined lubricant - surface system approach for potential passenger car CO2 reduction on piston-ring-cylinder bore assembly. *Tribology International*, Vol. 149 n° July, pp. 1–12, 2020. (cited in pp. 34, 75, 141, 166)

Tormos B., Martín J., Carreño R. and Ramírez L.

A general model to evaluate mechanical losses and auxiliary energy consumption in reciprocating internal combustion engines. *Tribology International*, Vol. 123, pp. 161–179, jul 2018. (cited in p. 87)

Tormos B., Pla B., Bastidas S., Ramírez L. and Pérez T.

Fuel economy optimization from the interaction between engine oil and driving conditions. *Tribology International*, Vol. 138, pp. 263–270, 2019. (cited in pp. 19, 92, 141)

Tower B.

First Report on Friction Experiments. *Proceedings of the Institution of Mechanical Engineers*, Vol. 35 n° 1, pp. 29–35, 1884. (cited in p. 23)

Tower B.

Second Report on Friction Experiments. *Proceedings of the Institution of Mechanical Engineers*, Vol. 36 n° 1, pp. 58–70, 1885. (cited in p. 23)

Tribology Institution of the Chinese Mechanical Engineering Society.

An investigation on the application of tribology in China. 1986. (cited in p. 3)

Tung S. and McMillan L.

Automotive tribology overview of current advances and challenges for the future.
Tribology International, Vol. 37 n° 7, pp. 517–536, jul 2004. (cited in p. 39)

Turnbull R., Dolatabadi N., Rahmani R. and Rahnejat H.

An assessment of gas power leakage and frictional losses from the top compression ring of internal combustion engines.
Tribology International, Vol. 142, pp. 105991, feb 2020. (cited in p. 46)

Vaezipour A., Rakotonirainy A. and Haworth N.

Reviewing In-vehicle Systems to Improve Fuel Efficiency and Road Safety.
Procedia Manufacturing, Vol. 3, pp. 3192–3199, 2015. (cited in p. 19)

Vakis A., Yastrebov V., Scheibert J., Nicola L., Dini D., Minfray C., Almqvist A., Paggi M., Lee S., Limbert G., Molinari J., Anciaux C., Aghababaei R., Echeverri Restrepo S., Papangelo A., Cammarata A., Nicolini P., Putignano C., Carbone G., Stupkiewicz S., Lengiewicz J., Costagliola G., Bosia F., Guarino R., Pugno N., Müser M. and Ciavarella M.

Modeling and simulation in tribology across scales: An overview.
Tribology International, Vol. 125, pp. 169–199, 2018. (cited in p. 23)

Van der Tempel L., Moes H. and Bosma R.

Numerical simulation of dynamically loaded flexible short journal bearings.
Journal of Tribology, Vol. 107 n° 3, pp. 396–401, jul 1985. (cited in p. 49)

Wang Y. and Wang Q. J.

Lubrication Regimes.
2013. (cited in pp. vi, 21, 23)

Wolff A.

Numerical Analysis of the System Piston-Ring-Cylinder of an Automotive IC Engine.
SAE Technical Papers, n° 2020-01-2160, sep 2020.

Wong V. W. and Tung S.

Overview of automotive engine friction and reduction trends - Effects of surface, material, and lubricant-additive technologies.
Friction, Vol. 4 n° 1, pp. 1–28, mar 2016. (cited in p. 41)

World Energy Council.

Global Transport Scenarios 2050.
2011. (cited in pp. vi, 5)

Wu W., Wang J. and Venner C.

Thermal Elastohydrodynamic Lubrication of an Optimized Cam-Tappet Pair in Smooth Contact.
Journal of Tribology, Vol. 138 n° 2, apr 2016. (cited in p. 51)

Yamamoto K., Hiramatsu T., Hanamura R., Moriizumi Y. and Heiden S.

The Study of Friction Modifiers to Improve Fuel Economy for WLTP with Low and Ultra-Low Viscosity Engine Oil.
SAE Technical Papers, n° 2019-01-2205, 2019. (cited in p. 26)

Zammit J. P., McGhee M. J., Shayler P. and Pegg I.

Benefits of cylinder deactivation on a diesel engine and restrictions due to low boost.
Internal Combustion Engines: Performance, Fuel Economy and Emissions, pp. 95–108, 2013. (cited in p. 19)

Zhao J., Xi Q., Wang S. and Wang S.

Improving the partial-load fuel economy of 4-cylinder SI engines by combining variable valve timing and cylinder-deactivation through double intake manifolds.
Applied Thermal Engineering, Vol. 141, pp. 245–256, 2018. (cited in p. 19)

Zhmud B., Tomanik E., Grabon W., Schorr D. and Brodmann B.

Optimizing the Piston/Bore Tribology: The Role of Surface Specifications, Ring Pack, and Lubricant.
SAE Technical Papers, n° 2020-01-2167, pp. 1–8, 2020. (cited in pp. 26, 141, 166)

Zhmud B., Tomanik E., Jimenez-Reyes A., Profito F. and Tormos B.

Powertrain Friction Reduction by Synergistic Optimization of Cylinder Bore Surface and Lubricant - Part 2: Engine Tribology Simulations and Tests.
SAE Technical Paper Series, Vol. 1, pp. 1–14, 2021. (cited in pp. xii, 160)

Zhu D. and Ren N.

Roughness Effect on Elastohydrodynamic Lubrication.
In *Encyclopedia of Tribology*, pp. 2955–2967. 2013. (cited in pp. vii, 45)

Zhu Dong and Wang Q. Jane.

On the λ ratio range of mixed lubrication.
Proceedings of the Institution of Mechanical Engineers, Part J: Journal of Engineering Tribology, Vol. 226 n° 12, pp. 1010–1022, 2012. (cited in p. 104)